Design and Development of a Multi-Functional Rotational Speed Measurement System for Investigation of Influential Factors

Behrad Rajabzadeh

Thesis submitted for the fulfillment of the requirements for the degree of

Master of Applied Research

Victoria University, Melbourne, Australia,

Institute for Sustainable Industries & Liveable Cities (ISILC)

July 2025

Abstract

In this research, a unique, novel, state-of-the-art hybrid encoder system (The Validist Encoder) is fully designed, developed and implemented for rotational speed measurements. Revolutions per minute (RPM) measurements are crucial for the proper functionality of many devices used in the industry and consumer sectors. Precision is highly valued, whether it is a wind turbine or a motor propeller. This becomes more important in sensitive applications that require high accuracy, while there are factors present influencing the system's measurement. An autonomous electrical vehicle (AEV) is a good example of this. Speed measurements in AEVs are critical since a simple error can cause catastrophic incidents. AEV's speed measurement can require measurement of the rotational speed of the shafts and parts engaged in the rotation of the vehicle's wheels, and the utilized measurement system will be exposed to various influential factors, including vibrations, temperature changes, magnetic fields, etc, while the AEV is operating. This research develops a rotational speed measurement system that can utilize different sensors and methods, providing a platform that is suitable for the examination of different methods, sensors and components in various conditions and situations for a side-by-side comparison of them while allowing investigation of the effects of influential factors on each, to select the best solution for the desired application based on an informed decision. The system comprises several apparatus and two main parts: a specifically designed electronic circuit and a special 3D-printed disk. These two main parts can interact with each other for high-speed rotation tests, while each part can be used individually for experiments. After design, simulations and development, the system is utilized in a high-speed rotation setup and several additional experimentations. Rotational speed measurement methods are not perfect as they generate false results when they are affected by influential factors related to the physics of their operational basis. Among several methods available, there are two mainstream methods used worldwide. The system designed in this research is a beneficial tool for conducting practical experiments. These experiments can be conducted focusing on simulating certain specific conditions in the laboratory environment that occur in situations where these devices are deployed, while being able to observe the functionality, output, and shortfalls for both measurement methods. With the data achieved from this system in the experiments, modifications, improvements, and system developments will be easier, while the costs will be reduced. The developed system is a novel solution practical for use in various applications where false readings are essentially avoided.

Declaration of Authenticity

I, Behrad Rajabzadeh, declare that the Master of Applied Research thesis entitled "Design and Development of a Multi-Functional Rotational Speed Measurement System for Investigation of Influential Factors" is no more than 50,000 words in length including quotes and exclusive of tables, figures, appendices, bibliography, references and footnotes. This thesis contains no material that has been submitted previously, in whole or in part, for the award of any other academic degree or diploma. Except where otherwise indicated, this thesis is my own work.

I have conducted my research in alignment with the Australian Code for the Responsible Conduct of Research and Victoria University's Higher Degree by Research Policy and Procedures.

Signature   Behrad Rajabzadeh   Date   11th of July 2025

Acknowledgments

This research journey would not have started if it weren't for my supervisors, Professor **A**khtar **K**alam and Professor **A**ladin **Z**ayegh, who have supported me, given me hope, and shown me the way to follow, as a bright star in a dark sky would have shown.

This journey, however, would not have been continued without the blessful presence of Professors **J**ohn **P**rice, **R**andall **R**obinson and **S**tephen **G**ray.

I also want to thank my dear friend **M**ohsen for his positivity and technical help in structrual designs, Professor **A**nthony **W**att for sharing his percise research ideology, technical officer **M**iroslav **R**adev for his technical guidance, and **M**ousa, a true engineer, whose online shared designs, knowledge, and vision significantly influenced my engineering prespective, enabling me to enhance my designs and ideas furthermore. The designs in this project would not be as improved as they are now if they were not for his shared works. I want to thank all my friends for their support throughout these times.

In addition, I would like to individually thank a prior friend of mine who turned bitterness into delightness for a time during my difficult stay in Melbourne.

The last but the exact opposite of least, I want to thank my mom, my dad and my little brother for all the positive impacts they have had on me… enabling me to move forward to this point.

There are, of course, many others whom I'm willing to appreciate for what they have done for me. It may not be feasible to name them all; however, I want to tell them all guilelessly: Thank you.

List of Publications

1. Rajabzadeh, B., Kalam, A. and Salehi, A., 2024, "A Grid Configuration to Use Solar Electricity 24 Hours a Day Without Energy Storage", pages 1-10 (Volume 1), **Innovations in Electrical and Electronics Engineering. ICEEE 2024. Lecture Notes in Electrical Engineering, vol 1295. Springer.**

2. Ishkanian, J. A. Harb, H. and Rajabzadeh, B., 2025, "Sensor Cost-Effectiveness in Machine Learning Based Preventive Maintenance Applied to Three-Phase Induction Motors", pages 629-652 (Volume 2), **Innovations in Electrical and Electronics Engineering. ICEEE 2024. Lecture Notes in Electrical Engineering, vol 1295. Springer.**

Table of Contents

List of Figures

List of Tables

List of Abbreviations

ABS   Acrylonitrile Butadiene Styrene

AC   Alternating Current

AEV   Autonomous Electric Vehicle

BDHD   Energy product (magnetic materials)

BOP   Magnetic Operating Point

BR   Residual Induction

BRP   Magnetic Release Point

CAD   Computer-Aided Design

CMOS   Complementary Metal-Oxide-Semiconductor

DC   Direct Current

DFM   Design for Manufacturability

EMF   Electromotive Force

EMI   Electromagnetic Interference

ENIG   Electroless Nickel Immersion Gold

EV   Electric Vehicle

FR   Flame Retardant

GND   Ground

HC   Coercive Force

IC   Integrated Circuit

IPC   Institute for Printed Circuits

IR   Infrared

LED   Light Emitting Diode

MMPA   Magnetic Materials Producers Association

MR   Magnetoresistive

NAND   NOT-AND (logic gate)

NI   National Instruments

NPN   Negative-Positive-Negative transistor

PA   Polyamide (Nylon)

PCB   Printed Circuit Board

PWM   Pulse Width Modulation

QSR   Quick Support Removal

RC   Resistor-Capacitor (circuit)

RMS   Root Mean Square

RPM   Revolutions Per Minute

SMD   Surface Mount Device

SMT   Surface Mount Technology

TC   Temperature Coefficient

TG   Glass Transition Temperature

TI   Texas Instruments

USB   Universal Serial Bus

VCC   Voltage Common Collector (referring to positive supply voltage)

VFD   Variable Frequency Drive

VH   Hall Voltage

VSS   Ground reference voltage

Chapter 1 : Introduction

Shafts, wheels, and gears are commonly used in various machinery and devices. The rotational speed of these parts is constantly measured as it is crucial to the functionality of these devices. This can be for purposes of control, predictive maintenance, optimization, etc. Wherever this is required, different solutions are available for engineers. Among these solutions two non-contact methods have been the most common. As technological advancements continue to shape the landscape of modern society, the demand for precision and durability becomes increasingly paramount making the process of choosing the best method even more important. For instance, electric vehicles (EVs) are widely acknowledged as the future of transportation and are integral to sustainability plans. To align with established targets, it is imperative that EVs function with the utmost reliability. However, the existing methods that can be employed for measuring speed and distance in EVs (based on rotational speed measurements) can face limitations in terms of accuracy and reliability. This is primarily owing to the influence of several factors, wherein EVs alone can include:

- Magnetic interference and external Magnetic fields
- The EV's various components
- The power system
- The high-voltage EV propulsion
- The EV's powertrain
- The electric motor
- Vibrations and physical stress
- Temperature
- Optical noise, optical exposure and external light sources
- Water exposure
- Exposure to external particles (dust, as example)

- Exposure to external Ferromagnetic materials including ferromagnetic dust/powder and Ferrofluids.

The decision to choose the best solution for each specific application is usually accompanied by a tremendous amount of uncertainty since each method has its pros and cons. Furthermore, malfunctions in the speed and distance measurements of autonomous vehicles can have catastrophic consequences. As such, it is imperative to conduct a thorough investigation of the existing methods considering the influential factors and making the necessary changes to help the development of better-performing designs. This has resulted in many designers not being able to choose the best option at the prototyping stages and a lot of cost can be incurred for changing the method used while approaching the final stages of product development. This may even lead to problematic performance of the developed devices after implementation and during usage. In contrast with this matter, there have not been many studies practically comparing different available methods through experiments to act as a guide for design engineers, enabling them to choose the best option. This is mainly because there is currently no proper platform for utilizing different methods easily while comparing them side-by-side to help with an informed decision. By better understanding each method's behavior in the presence of the influential factors that they may get exposed to, the accuracy of the system will be improved while the costs are minimized. This requires a system that can utilize different methods and can be used at different speeds, easily applicable to different setups. The effects of the influential factors should be minimal on other parts of the system so that the effects can be better studied on the sensor and the method itself. For the best observation and precise measurement, the system should be able to provide information about the number of rotations and exposures in addition to rotational speed and revolutions per minute (RPM) values. However, there is a need for such a system as flexibility, adaptability and ease of use are not offered and thus the investigation of operational conditions to better understand

the system's behavior is not often achieved until the last stages of the product development and sometimes even after operation.

Currently, rotational speed measurement systems are integrated into the devices they are being used in, making them dependent on the motherdevice in many aspects including the power supply and the rotating parts that interact with the measurement system. They are also usually designed only to work with a specific type of sensor. Regarding adaptability, currently, there is no system that can easily be put into different conditions for various required experiments to undergo temperature changes, noise exposures, vibrations, etc. While there may be a chance to conduct some experiments on the existing rotational speed measurement systems, the effort and the cost will be tremendously high and the whole process will be time-consuming and will require the collaboration of many individuals with different specialties. Such collaborations will be associated with many limitations and challenges as well.

This research is going to fully develop a system that includes an electronic circuit, a rotating interactive disk and some other apparatus (Figure 1.1) enabling research and investigation of different methods and sensors. The unit will be able to adapt and be used in many operational conditions while providing high precision and accuracy in collecting information and data regarding all the tests and experiments that are conducted with it. Since many applications will require measuring very high rotational speeds, one of the objectives will be for the system to withstand fast rotation speeds. Consequently, for testing, a high-speed setup should also be introduced enabling proper research and investigation in the future, where needed. The developed system will be beneficial to researchers, designers and industries to thoroughly and precisely study the characteristics of the shortfalls associated with the main existing rotational speed measurement methods enabling them to understand the nature of the shortfalls by conducting experiments that can simulate the specific conditions and factors.
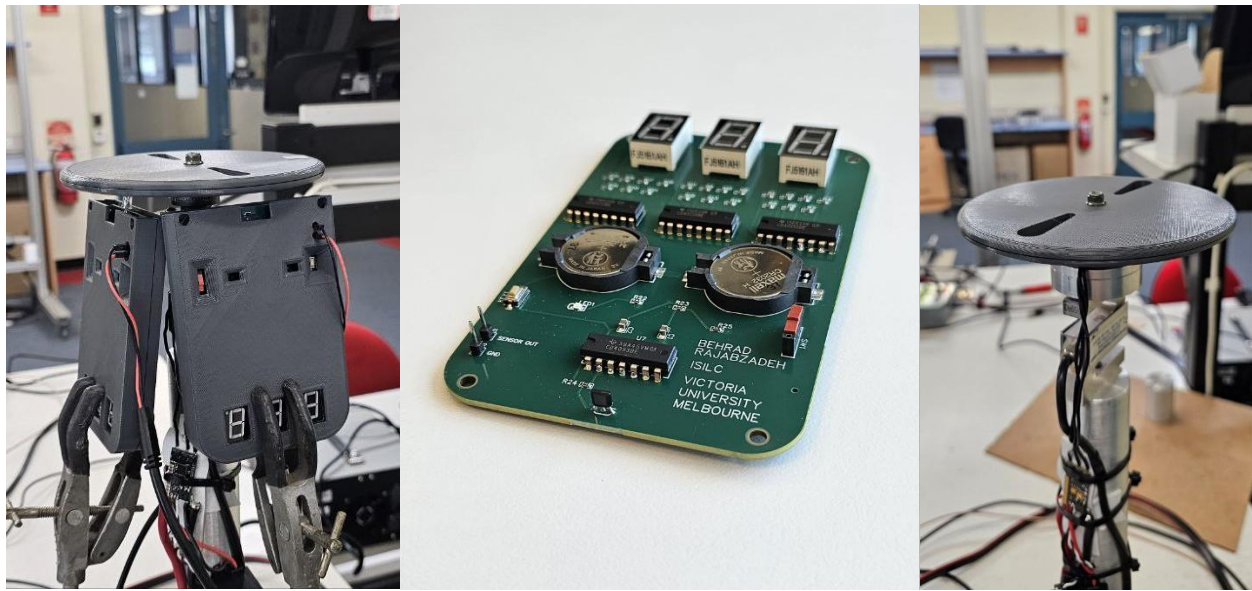
Figure 1.1. Developed system apparatus.

1.1 Methodology and Conceptual Framework

This research mainly deploys a positivist/postpositivist view since it focuses on achieving high precision. Considering the types of data being collected for the project, the used methods are mostly quantitative [1]. However, the overall approach is a mixed method to achieve nuanced details.

This research mainly follows an engineering design and development approach involving conceptualization, prototyping and testing.

This involves the design and development of two main parts:

- A circuit Board with different functions for related observation, studying, testing, investigation and data collection, and

- A Disk designed with mechanical modeling and simulation, made and utilized to support the needed characteristics required for rotation tests, while enduring high-speed rotations.

The circuit is developed using a 6-layer printed circuit board (PCB) with a mix of surface mount and through-hole components, Designed by EasyEDA online software with many measures in

mind for proper signal integrity. There are several measures for data collection as well, including a fast response LED indicator, sensor ground and output pins and a three-digit number display (Figure 1.1). The outputs are designed to be connected to an oscilloscope for analysis. The circuit is tested on a series of experiments including a High-speed setup utilizing two different sensors. The sensors mounted on the electronic circuit are a KingBright phototransistor and a Texas Instruments Hall effect sensor and a disk interacts with both these sensors. With the specefic design of the circuit, he two types of sensors used on the board can be changed and installed easily without any need for modifying any other part of the circuit or components. The design also includes an independent onboard power supply system enabling the board to operate on its own. The characteristics and other details of this circuit are tested and discussed in Chapter 3.

The disk is developed with lightness, thinness and structural durability in mind. The disk was used in a high-speed setup which spun at a rate of around 10,000 RPM without any sign of collapse. The simulation for structural analysis of the disk was done by ANSYS and the primary model was developed by using the online CAD software ONSHAPE. The design consisted of two halves, the top part and the bottom, both 3D printed individually. Additional information regarding the disk are presented in Chapter 4.

The high-speed setup uses a drone motor with a specific driver circuit. The speed of the motor was adjustable by changing an input voltage signal in the driver circuit. The input voltage signal was set by using a National Instruments data acquisition unit connected to a Windows PC. The experiments that were conducted using the proposed and developed apparatus are provided in Chapter 5. Generally, experimental apparatus is mainly used in three forms of experiments:

1. Misdetection of exposure tests while there is no real exposure
2. Undetected exposure tests
3. Variable speed rotation tests: The Disk is connected to the highspeed motor with the speed being controlled by the driver.

1.2 Occupational Health and Safety Risks

This project involves practical laboratory work. Common safety practices were considered in Laboratory practices. Safety equipment was used where necessary. The experiments were conducted with the equipments available in J.L Kepert's Building laboratory spaces (Victoria University Footscray Park campus, Building D).

Online Health, Safety and Wellbeing Awareness training has been completed

1.3 Ethical Considerations

This research process does not study any human participants.

1.4 Scope and Limitations

This research project develops an advanced rotational speed measurement system from the very beginning of the process, almost from scratch, and briefly examines its functionality. This system and the setup used are also a great platform for the precise investigation of sensors, related methods and applications. However, this project does not include using the system for these investigations.

1.5 Significance

A multi-functional, state-of-the-art, novel hybrid encoder system is fully designed, developed, and implemented in this project. The designs and the developed systems, other than being a platform enabling researchers and engineers to properly analyze different kinds of sensors for individual applications, are **fully functional** with detailed documented specifications for design and

components utilized **that can be used in the industry, automation and medical applications**.
The designed system can provide highly accurate RPM measurements in sensitive applications.
Based on the application and usage, the device can be set to avoid false readings.

This is accompanied by a series of tests that the system and the designs have undergone.

1.6 Thesis Structure

This thesis consists of six main chapters.

Chapter 1 discusses the Introductory details of the project while including preliminary information such as context, objectives, significance and methodology.

Chapter 2 initiates with the inclusion of background information about sensor systems, showcasing some gathered data about sensors while focusing on two sensor types used commonly for rotational speed measurement systems, concluding with literature studies.

Chapter 3 Chapter 3 focuses on the electronic circuit designed and developed for this project.

Chapter 4 details the process behind the development of the high-speed disk that interacts with the electronic circuit developed in the previous chapter.

Chapter 5 includes details about a high-speed test setup, demonstrating the system performance, with some other experiments conducted on the developments of this project.

Chapter 6 concludes the project and proposes future work.

Chapter 2 : Background and Literature

A sensor is generally known to be a device that can convert a physical phenomenon into a processable, understandable, and measurable electrical signal. This means that sensors are a part of the interface between the actual physical world and the operational devices, including computers and many other technologies. On the other hand, an actuator is the exact opposite, which converts electrical signals into physical phenomena [2].

2.1 Sensor Systems

The use of sensors is now a crucial part of many advanced products as they improve the performance of these devices. In the digital world, microprocessors are heavily dependent on sensors, and without electrical inputs from the sensors, they cannot receive the necessary information for proper operation [2].

There are many characteristics in a sensor, which are essential to understand the sensor. Some significant ones are sensitivity, range, accuracy and output noise. Each sensor has a transfer function that shows the relationship between the physical input parameter and the sensor's signal output. A graph might be provided to visualize the transfer function better. Sensitivity is usually known as the relationship between the input and the output in the form of a ratio between changes in the output and input. For instance, a thermometer would be considered sensitive if a slight temperature change would significantly change the voltage output [2]. Usually, a high sensitivity is desirable, but it is also more challenging to achieve. All sensors produce noise on their output signal. This can heavily impact the function and performance of the sensors. The response time, also known as the sensor's bandwidth, is also significant in sensors. It can be defined as the delay a sensor has in generating the change in its output signal when a physical signal changes.

The way different sensors work may not be similar at all. For instance, some may be passive and

others active. Some may need additional amplification while other sensor types may directly produce output signals that can be processed or used. For example, Hall effect sensors usually need strong amplification and filters to create an output that is readable/usable by other devices since the Hall effect changes are very faint.

It is also necessary to mention that, precisely speaking, a sensor is a device that reacts to a physical stimulus by an electrical signal, while a transducer converts one type of energy into another one [2]. For ease of understanding, these two terms (sensor and transducer) will be used interchangeably in this thesis.

Sensors are usually accompanied by some circuits associated with them. The design and characteristics of these circuits are based on several factors but the most important one is their activeness or passiveness. A passive sensor generates its own electrical output without requiring an external voltage or current. Active sensors usually require a current running through them to operate. However, there is no clear demarcation between active and passive sensors, and based on the associated circuits, a sensor can be considered active in one situation and passive in another. Table 2.1 highlights some of the typical sensors and their industry classification.

Table 2.1. Sensors and the industry classifications [2].

PROPERTY	SENSOR	ACTIVE/PASSIVE
Temperature	Thermocouple	Passive
	Silicon	Active
	RTD	Active
	Thermistor	Active
Force/Pressure	Strain Gage	Active
	Piezoelectric	Passive
Acceleration	Accelerometer	Active
Position	LVDT	Active
Light Intensity	Photodiode	Passive

Whether a sensor is active or passive, since the output voltage and current are very small, external circuitry is required. Due to this, a whole class of circuits has been formed which are commonly known as signal conditioning circuits [2].

One of the primary sensing techniques used in rotational speed measurement devices is the Hall effect.

2.2 The Hall Effect

To better understand the methods used in odometry and other related techniques, the basis of the devices used are discussed. The Hall effect is named after Edwin Hall who discovered it when he was a Doctoral student in Baltimore in 1879. Despite being known for more than a century the first practical use was in the 1950s. In 1968, it was used to introduce the first solid keyboard and since then the applications have been numerous [3]. Each Hall effect sensor has a Hall element, which is usually a thin sheet of a conductive or semiconductive material. When a conductor (or semiconductor) that is carrying current is exposed to a magnetic field, a voltage will be induced perpendicular to the flow of the current and the field. This phenomenon is known as the Hall effect, which is shown in Figure 2.1 [3].
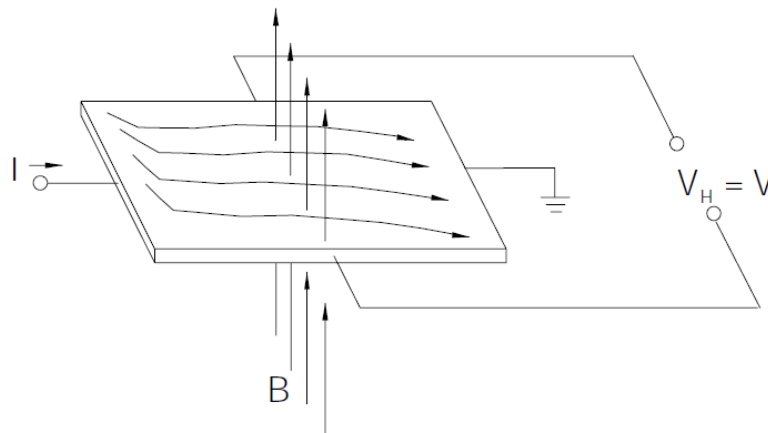
Figure 2.1. The Hall effect illustration. Current I, Magnetic field B and Voltage V are shown [3].

The value of the Hall voltage (V_H) is related to the current and the magnetic field ($V_H \propto IB$). Through this, the magnetic field can be sensed. To do so, strong signal conditioning is required as the value of the Hall voltage is usually very small and unusable as a direct output for most applications. The amount of Hall voltage present depends on many factors in practical applications. The size of the conducting material and the material type are among these. However, generally, it is considered a low-level signal on the order of around 30 µV while being exposed to a magnetic field with the magnitude of one Gauss. Usually, different types of amplifiers are integrated with the Hall element on the chips. Figure 2.2 shows the transfer function of a general-use analog Hall effect sensor.
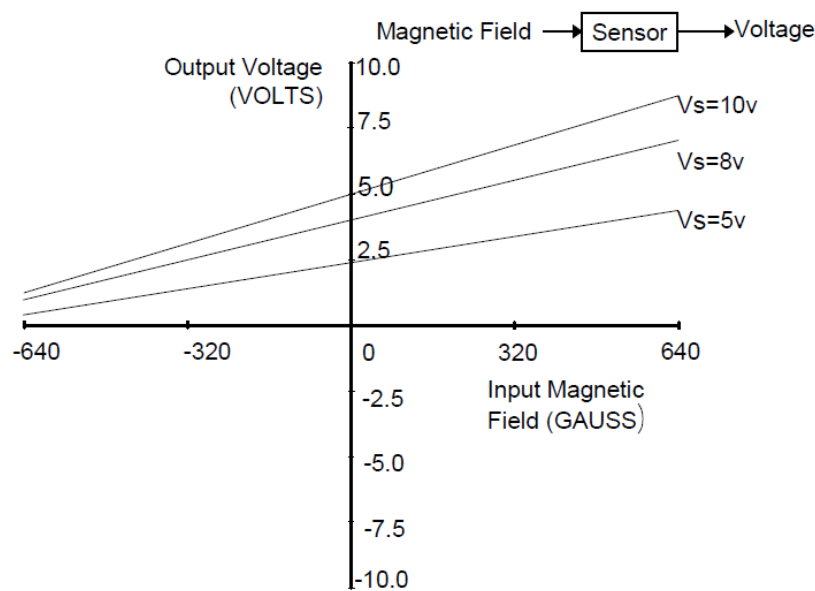
Figure 2.2. The relationship between magnetic field input (gauss) and voltage output of an analog Hall effect sensor made by Honeywell [3].

The transfer function of the digital output sensors is ideally rectangular (Figure 2.3) as they have only two states: ON or OFF.
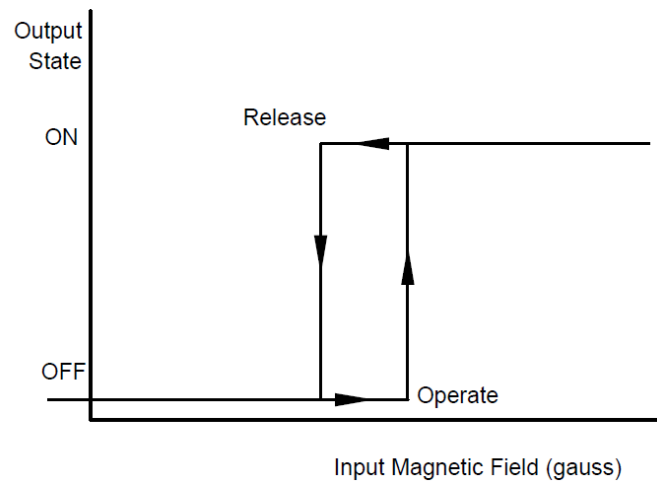
Figure 2.3. The transfer function of a digital output sensor by Honeywell [3].

It is worth noting that the resistance of the Hall element can also be changed while exposed to magnetic fields which can be used for magnetic sensing. In this case, this type of magnetic sensor is called Magnetoresistor. The type of material used as the Hall element in these sensors is very important and research is being done regarding this. Table 2.2 shows the comparison of these technologies.

Table 2.2. Magnetoresistive and Hall effect [3].

	Hall effect	Magnetoresistive (MR)
Process Technology	Silicon IC	NiFe Thin Film
Sensitivity	10uv/v/g	2 mv/v/g
Saturation Field	None	10 - 100g
Linearity	< 1%	$COS^2 \Theta$
Sensitive Axis	Perpendicular to plane of chip	Parallel to plane of chip
Output for Constant Field	Yes	Yes

Several materials can be used for Hall effect sensors, but silicon has a huge advantage as the signal conditioning circuits can be easily integrated on the same chip through common semiconductor manufacturing processes including CMOS.

2.2.1 Permanent Magnets in Hall Effect Systems

Considerations regarding the magnets being used in Hall effect systems are extremely important. Figure 2.4 illustrates a general configuration of the Hall effect systems. Magnet materials, Demagnetization and related information should be considered and utilized.
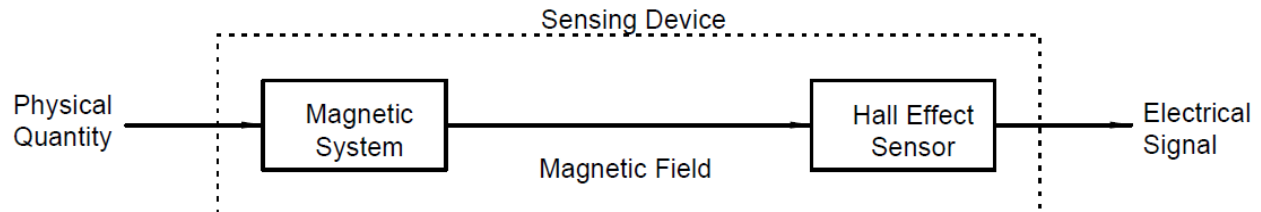
Figure 2.4. General magnetic Hall effect sensor diagram [3].

Almost all of the Hall effect systems use a magnet in their setup. The way the magnet is utilized may be different in every system. Generally, what is important is the flux of the magnet. The magnetic flux is stronger near the poles of the magnet and gradually reduces as the distance increases. An illustration of conceptual magnetic flux is shown in Figure 2.5.
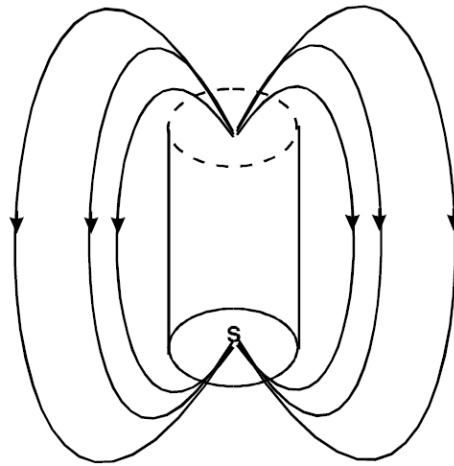
Figure 2.5. Magnetic lines of flux (by Honeywell [3])

The flux density is also affected by many other factors. The cross-sectional area, the shape of the magnet, the material, and the substance obstacles in the path of the flux are among these. The path of the flux as shown in Figure 2.5 is considered to be from the north pole of the magnet to the

13

south pole. At a distance ' d ' from the north pole of a magnet, the field is proportional to $\frac{1}{d^2}$. The position of the south pole is also important as it affects the field near the north pole. The geometry of the magnet also plays a role and in linear shapes, the distance of the poles from each other can alter the path that the flux should travel meaning that with a bigger length in a linear magnet, a weaker field would result. This is one of the logics behind the U-shaped magnets.

The material of the magnet is one of the most important factors in field strength and affectability. The original magnets were from iron oxides that were magnetized by lightning. These magnets were Lodestones. Although iron is a major ferromagnetic material it lacks many properties for industrial use. This resulted in the development of the first material specifically for permanent magnets in the 19th century. This is supposed to be one of the first attempts to achieve stable metallurgically and magnetically stable materials. One of these materials is **Alnico** which is an aluminum-nickel-cobalt alloy [3].

Nowadays, there are several options available to choose from when it comes to the magnet material. These include Alnico, which was discussed and is simply manufactured by pressing metal powders into the desired shape and then heating it up. This process is commonly referred to as sintering and for Alnico results in magnetic material with good uniform flux patterns and distribution while maintaining mechanical properties. One of the other options is **Indox** ®. While Indox is manufactured in a way very similar to Alnico, it has a different chemical composition with poor heat and electricity conduction. Indox, also will not change much in regard to magnetic characteristics while exposed to shock, vibration and stress. **Lodex** ® is another option and the main difference it has compared to the other two materials is that it is a single-domain material. The magnetic domains inside the magnets are the cause of any magnetic fields. While some magnets have multiple locked-in magnetic domains, others like Lodex can be single-domained. The last material that is worth mentioning is **Rare Earth**. A rare earth magnet includes a

composition of rare earth elements and is considerably stronger than the other aforementioned magnets. To better understand the types of magnets and to compare them, it is essential to understand the terms and properties associated and used when describing a magnet:

- Br: Residual Induction. Can be considered the flux intensity.

- Hc: This can be described as the resistance of a material to demagnetization.

- BDHD: Energy product. The energy that a magnetic material can supply.

- (BDHD)max: The maximum energy that a magnetic material can supply.

- TC (Br): Reversible temperature coefficient of the residual induction.

Table 2.3 shows these Terms for each of the materials discussed earlier.

Table 2.3. Magnetic Materials Characteristics (By Honeywell [3], additionally color coded for rare earth magnets)

Material	Relative		(BDHD)MAX	Cost	Stability	BR TC (%/°C)
	BR	HC				
Alnico	High	Low	Med.	High	medium	-0.02
INDOX ®	Low	High	Low to Med.	Low	high	-0.2
Ferrite	Medium	Medium	Medium	Low	high	-0.04
Rare Earth	**High**	**Highest**	**Highest**	**Highest**	**high**	**-0.12**
NdFeB	High	High	High	Medium	High	-0.12

Where it is possible to ignore the cost, Rare Earth magnets seem to be the best option for a Hall Effect sensor system based on their characteristics. However, there are other factors that can influence the strength of a permanent magnet, these can include:

- Time
- Temperature
- Reluctance changes
- Adverse fields, and
- Mechanical stresses such as vibration and shock.

Modern magnetic materials usually will not be affected by time at <u>room temperature</u>. The temperature, however, plays a significant role with effects being categorized generally under three categories:

1. Metallurgical
2. Irreversible, and
3. Reversible.

Metallurgical changes caused by high temperatures can usually make unrecoverable changes in the flux, meaning that the remagnetization will not bring back the changes. This can vary significantly for different materials. As an example, commercially used Lodex can initiate Metallurgical changes at only 100°C while for some other ceramic materials, this can be around 10 times higher. Exposure to low or high temperatures can also cause **Irreversible** losses, which are defined as partial demagnetization.

These changes can be avoided by exposing the magnets to the temperatures they might get exposed to while magnetizing them. This will require several temperature cycles while the magnet is being magnetized in the magnetic circuit, a pure AC field, or on an assembly.

Reversible changes have also been visible in many magnetic materials and while these changes are not eliminated by the stabilization treatments, using temperature composition material in the magnet will reduce these effects. Speedometer magnets are usually compensated in all the aforementioned manners.

Reluctance changes are unrelated to the topic of demagnetization being investigated in this project

and are not discussed. Adverse fields, mechanical stresses and temperature changes will be observed through basic experiments in Chapter 5.

Magnetic Materials Producers Association (MMPA) in Chicago, USA, publishes standards for material, tests, and magnetization practices [3]. Magnetization methods introduced by MMPA are not within the scope of this project and is not reviewed nor analyzed. However, the following methods [3] are considered to be the most appropriate for commercial and industrial use:

1. Permanent magnet method (using the magnetization field of a permanent magnet)

2. DC Electro-coil method (using DC coils to produce magnetization fields)

3. Capacitor discharge method

4. One-half cycle method (simply using a half-wave for the magnetizing coil).

Optical sensing is the other sensing mechanism used commonly in rotational speed measurement systems.

2.3 Optical Sensors

Light detection is usually based on a quantum detector or a thermal detector device. This comes from the fact that any type of light is considered to be both a quantum and also mechanical phenomenon. Photons are considered to be the particles that light is made of in many modern and well-accepted theories. With a speed of $c = 3 \times 10^8$ m/s optical systems have become one of the main topics of extensive research. This has also caused the availability of a variety of affordable photosensors available commercially. The energy of a photon is the most important characteristic when it comes to detection and determines how the photon should be detected [2].

Quantum detectors have better performance compared to thermal detectors. The process that

makes quantum detectors work is based on absorbing a photon and liberating electrons with the energy that the absorbed photon was carrying. The quantum detectors will only accept allowed amounts of energy creating the concept of cutoff frequency and wavelength. The structure of these quantum devices and the exact process in which is responsible for creating the free electrons in these devices are complicated and beyond the scope of this project. However, in some cases, this will cause the device to have different cutoff frequencies at different locations of the device. There are two types of quantum photodetectors that are produced commercially:

- Photodiodes, and
- Phototransistors.

Photodiodes are made based on P-N junction methods. For photodetection, these diodes are biased in two different ways. One is commonly known as the photovoltaic mode and the other one is photoconductive. Both come with their own disadvantages and need to be set up for the operating mode with basic electronic elements such as resistors, capacitors and amplifiers. Phototransistors are also made using the bipolar junctions, but the accuracy is much higher compared to Photodiodes making them a better device when it comes to photo detection. In Phototransistors the current generated by the photons (also called the photocurrent) flows from the **base** to the **emitter** and a larger current is then flowed from the **collector** to the **emitter.** The collector-emitter current is much larger than the photocurrent. This is one of the primary reasons that a phototransistor can be much more sensitive than a photodiode. Phototransistors and photodiodes are usually most sensitive near the Infrared (IR) spectrum. This is simply because these devices are usually made from Silicon which has a solid bandgap energy. Figure 2.6 shows the spectral sensitivity of an NPN silicon chip phototransistor (AA3528P3S) made by Kingbright.
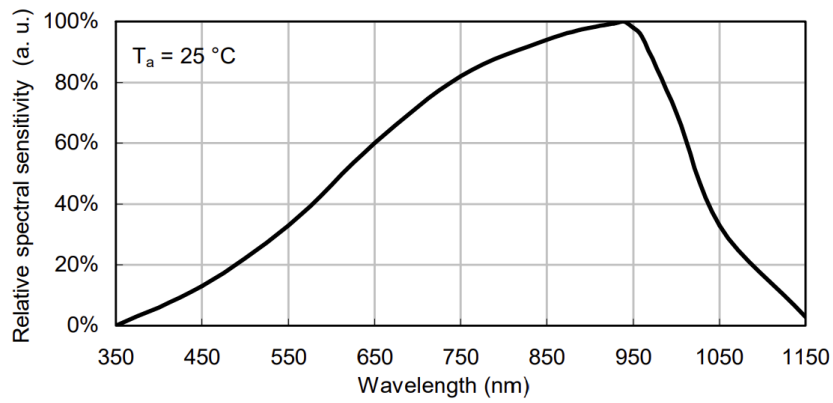
Figure 2.6. Relative spectral sensitivity vs. wavelength. (by Kingbright)

Although adjusting this sensitivity spectrum is neither easy nor simple, changing the material itself can be a solution since different materials have various Badgaps. Some of these bandgaps are shown in the Table 2.4.

Table 2.4. Different Bandgaps of Semiconductors [2].

Material	Bandgap (eV)
ZnS	3.6
CdS	2.41
CdSe	1.8
CdTe	1.5
Si	1.12
Ge	0.67
PbS	0.37
InAs	0.35
Te	0.33
PbTe	0.3
PbSe	0.27
InSb	0.18

Photosensors can be made from almost any of the materials shown in Table 2.4 The process of manufacturing is not as easy and not as available as Silicon and the availability and cost of such devices are not ideal at all. The other important consideration in photosensors is the thermal effect and behavior of the devices. There is a possibility of thermally generated carriers appearing in the system at certain temperatures. These carriers cannot be separated from the photocarriers and may introduce errors into the system. The change in temperature can also alter the bandgap. Silicon performs very well at room temperature but conversely, at higher temperatures, silicon photodetectors act strangely. This matter is usually even worse when it comes to other semiconductor materials, requiring a working temperature well below room temperature.

Among different materials investigated for this purpose, Mercury Cadmium Telluride has been found to be the best performer with a cutoff between 10 to 20 microns and has excellent characteristics for IR detection. This also comes with low dark current and low carrier scattering. However, it is very difficult to make and the process poses serious environmental hazards. It is also very hard to be bonded onto the silicon chips and the operational temperate for it should be less than 77K (-196.15 °C) [2]. Another option is InSb (Indium antimonide) which is fairly easier to manufacture but can not detect anything in 10–20 μm region and also requires an operating temperature of around 100K (-173.1°C) [2].

Thermal IR detectors are another set of options for detection applications but being very susceptible to temperature changes, they are not a good candidate for industrial nor commercial usage and generally speaking, there are not many choices of practical materials when it comes to functional IR detection other than Silicon.

2.4 Position and Rotation Sensors

Rotation Sensors can be considered position sensors that are used for rotary objects and systems. Within the technologies developed, there are two main categories employed:

- Contact sensors, and
- Non-contact sensors.

The popularity of the non-contact approaches is tremendous. This is because physical contact methods come with various downsides, such as wear and tear. However, since different applications will have different parameters and environments, many contact devices, for instance, Limit switches, are still used for some automation projects. One of the main reasons for utilizing a Limit switch is its capability to operate with minimum risk within explosive environments. There are many standards taken into account for these Limit switches and although explosion-proof versions may be costly, they may also be the only logical solution.

When it comes to the high-speed rotation, the benefits of contact methods for measuring position, motion and rotation start to fade. This is where non-contact technologies become mainstream. Some of the most non-contact technologies include:

- Magnetic Sensing
- Ultrasonic systems
- Optical sensing
- Proximity sensors.

Between these methods, Magnetic and optical systems have gained more popularity, since the other two (Ultrasonic and Proximity sensors) have certain downfalls when used in harsh environments. The downfalls of the Proximity sensors are related to the technology on which they are based. However, they also come with one big advantage: being able to sense/detect all materials. As an example, while Capacitive Proximity sensors can detect the proximity of all materials, Inductive sensors are usable for metals only. This advantage may not be desirable in

certain circumstances where there is a target and there are multiple objects that can be exposed to the Proximity sensor, causing measurement errors. The targeted object can be narrowed down better with the use of inductive sensors, which can detect all metals, or only the ferrous metals or only the non-ferrous metals. The Inductive Proximity switches usually use an oscillator coil as the basis of their function. When a metal object is close to this coil, eddy currents will be induced into the oscillator and the amplitude of the oscillator will change. This change will be used to create the final output of the sensor. Despite all the advantages the inductive proximity switches offer, they are nowhere near the Optical and Magnetic systems when a high-speed rotation is being measured.

The Ultrasonic sensors also have their own drawbacks when being used in industrial applications. These include extreme sensitivity to high temperatures and weakened target detection with slight surface misalignment. Limitations associated with the target size and deadzone of the ultrasonic devices are also among the reasons that they are not utilized as much as other devices in rotation speed measurements. Although each sensor comes with a datasheet and specification, the actual sensing range should be determined by conducting tests with the target that is going to be used with it. This also makes Ultrasonic sensors less reliable compared to their competitors.

However, there is still controversy when selecting a Magnetic or Optical system for rotational speed measurement applications. These methods both remain reliable for many applications to the point that designers sometimes have doubts about which one to use. Some design engineers simply prefer one over another only because they have more experience with one. Others may randomly choose one and observe if the system performs well in the end. Since this study focuses on these two methods, they have been discussed earlier in this chapter. As mentioned earlier, although Hall effect sensors are very dominant in magnetic sensing, the magneto-resistive (MR) devices are also an option available to design engineers. The main difference in MRs is the parameter they measure,

which is the direction of the magnetic field. This provides some advantages over just measuring the strength of a magnetic field, such as less sensitivity to the temperature changes of the environment, being less prone to errors caused by physical shock/vibrations and increased measurement distance. The MR sensors are not easy to manufacture since it is not possible to implement them in CMOS. Consequently, MR should be manufactured on separate silicon wafers. The Hall effect is easily implemented on CMOS, making it more ideal for mass usage.

Optical systems work based on the communication between an optical transmitter and a receiver. The transmitter and receiver could be on the same side or facing each other. By choosing the right wavelength and brightness, Optical sensors can detect all types of targets, whether it is transparent, shiny or a solid matt black. As light is the fastest matter in the universe, many optical systems offer a generous detection speed. However, this should not cause any misconceptions about the detection speed of the magnetic systems, as they also are measuring magnetic fields, which are part of electromagnetic waves, having a speed equal to the speed of light.

2.5 Literature Approaches and Studies

For shaft rotation measurements, one of the common apparatuses used to determine the shaft speed is a purely signal processing method implemented on a logical circuit, compatible only with certain types of electrical motors. Ramli et al. [4] discussed the use of adaptive filters for rotational speed estimation of sensorless DC motors with brushes. The proposed method in [5] is based on the fact that the rotational speeds of these kinds of motors are proportional to the frequency of the ripple component on the supply current of the motor. To obtain the fundamental frequency of the ripple current, adaptive line enhancers have been used, and to modify the results, low-pass filters have been implemented for the better estimation of the rotational speed of the motors. However, the

drawbacks of the proposed method are numerous. Modern motors used in EVs are complex and have several components that affect the supply current's characteristics including the ripple current without being related to the number of motor rotations [6], [7]. Subsequently, this method [4] only provides an estimation and thus is not reliable when high precision is needed. Considering these facts and noting that there are many rotating shafts that are not connected nor related to any DC motor, it can be concluded that this method [4] is not suitable enough for the applications that were explained earlier.

Nemec et al. [5] also investigated a similar method based on signal processing of current peaks related to DC motors. However, the commonly used approach is the use of a permanent magnet mounted to the motor's shaft and the detection of the rotation by sensing the magnetic field by the Hall effect sensor. This article [5] also includes useful information about the drawbacks related to the use of the Hall effect sensor for rotation measurement applications. It explains that the rotating magnet may cause electromagnetic noise and interference in nearby electronics and thus compromising the overall accuracy of the device. There are also problems associated with the presence of ferromagnetic dust that may pollute the magnet and affect the sensor's readings. Another approach [8] mentions that the back EMF can be proportional to the speed of the rotor (and the motor's shaft) when considering "$u_{bemf} = K_u\omega$" and Figure 2.7 provides the equivalent of the brushed DC motor (K_u is the back EMF constant and ω is the angular velocity).
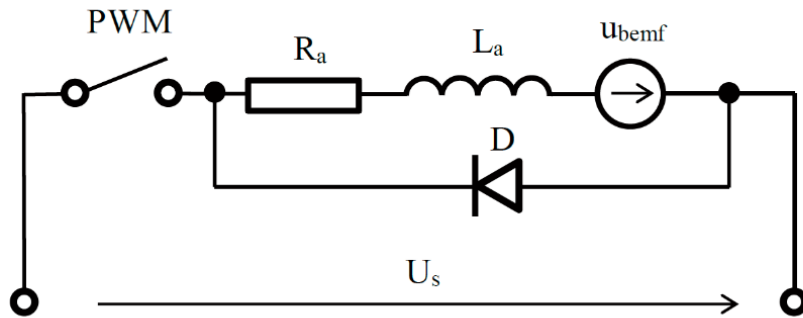
Figure 2.7 ; K_u is the constant of back EMF and ω is the current angular velocity of the rotor [8].

24

Combining these concepts Nemec et al. [5] propose an electronic odometer design that works on the primary concept of detecting the changes of the armature's impedance caused by the non-zero size of the commutator brushes as each brush shorts one or more winding coils for a while resulting in periodic changes in the motor's impedance and thus, creating spikes in the supply current. The proposed design also has several other drawbacks as the frequency of the Pulse width modulation (PWM) may also affect the detection in some instances. Using a combination of analog and digital filtering a sensor board prototype has been developed. The final results, however, are limited to a specific range of RPM. The results and the conclusions made in [5] are much more reliable compared to [8] since the proposed method was tested and verified using a hardware prototype.

A comparative study by Rapos et al. [8] investigates two majorly used methods in the industry. The study is based on the experiments conducted by Taylor [9] in the process of developing this thesis [9]. The two compared devices are the Hall effect sensor and the incremental encoder. The incremental encoder has been explained as a device that is comprised of three main parts:

1. A Stationary disc with some slits

2. A Rotating code wheel similar to the stationary disk regarding the configurations, and

3. A Light source.

The rotation of the shaft blocks and unblocks a photo detector from the light source, creating impulses that can be used to determine shaft speed. An example has been given of such a sensor, which is a quadrature incremental encoder with 360 pulses per revolution with three available recording channels for better determination of the shaft position. Between these three channels, two of them measure the impulses per revolution out of phase from one another while the third one counts full shaft rotations.

The application/function of the third channel is the most important one in this review [8] since it

provides an output similar to the Hall effect sensor. The testing equipment used in the study included an open loop controller connected to a motor, with the rotating shaft being used to test the encoder and the Hall effect sensor. The motor used in the experiment is an AC motor and the open loop controller is a Variable Frequency Drive (VFD). The generated data was collected by PXI6221 National Instruments dynamic signal acquisition card. The encoder used was an HS25 Incremental Optical Encoder from BEI Sensors. The summarized schematics of the testing setup can be seen in Figure 2.8.
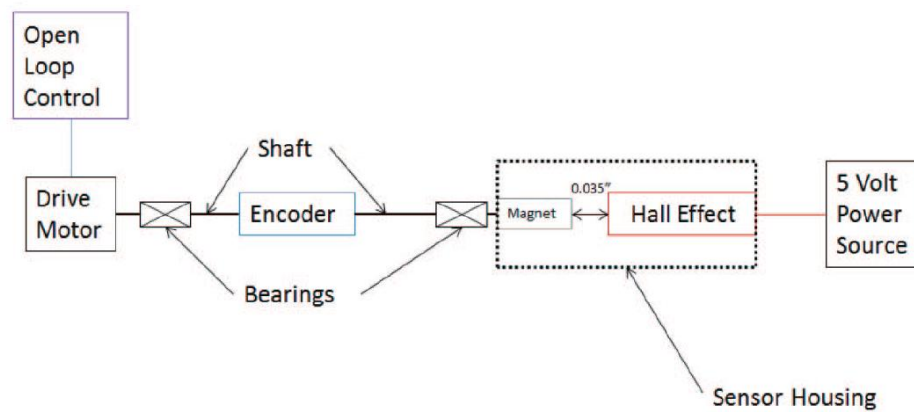
Figure 2.8: Schematic of the experimental apparatus [4]

However, the Hall effect sensor used and many of the characteristics of the permanent magnet accompanying the Hall effect sensor have not been identified. The experiment included testing the setup in a variety of configurations including varying speed, magnet size, magnet to sensor lateral distance, and exploration of sensor readability. Although magnet size is an important factor in the setup it would have been better to include the actual strength of the magnet by measuring the magnetic field and including the results in the form of the standard unit of Gauss. This missing information causes uncertainty regarding the results that have been generated on the mentioned configuration and thus is not discussed in this review. The experiment, however, generates valuable data in regard to the general comparison between the Hall effect sensor and the HS25

Incremental Optical Encoder in varying speeds that have been selected to simulate a range of operating conditions that would be found in typical industrial situations. The test was run to detect any sensor recording differences at different speeds. This involved running the setup from zero RPM to pre-selected speeds and then back to zero RPM using the manual and the automated controls. The results can be found in Figure 2.9.
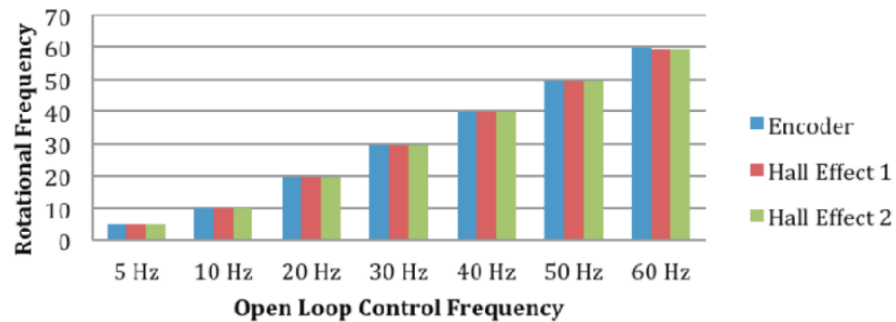
Figure 2.9: Displaying the rotational frequencies [4]

The results in the above Figure depict the preciseness of the encoder in measurements compared to the Hall effect sensor with obvious differences in 60Hz frequency. A chart to compare the deviation of the measurements has also been provided since the results were so close in magnitude when the frequency was below 60Hz. This illustration can be found in Figure 2.10.
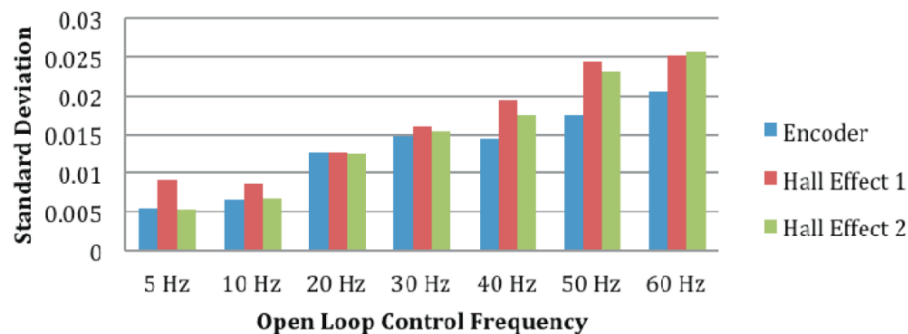
Figure 2.10: Displaying the standard deviations [4]

By further investigation of the experiment's data, it can be concluded that the difference does increase with rotational frequency. However, this variance was consistent and small (as a

percentage of the overall measured rotational speed). It was observed that as the speed of the shaft increases so does the standard deviation recorded by both the encoder and Hall effect sensor meaning that they both have noticeable errors in the measurement. The testing and the experiments do not go further to investigate the performance of these devices in regard to measurements while they are exposed to different kinds of noises and other similar conditions in specific circumstances. Any related noise can heavily impact the sensor's functionality and experiments to investigate the effect of these noises are essential to determine the performance and precision of the sensors in practical usage.

As reviewed, two of the most common rotational speed measurement systems are based on either the Hall effect sensors or optical detectors, being the backbones of the sensing systems in each method. To investigate these methods, it is essential to determine their performance and precision in practical usage of the application, and the solution is a platform that enables us to implement these two methods side by side for each specific sensor. Most immmportantly, it should be noted that as each method also has its unique downfalls, the need for a novel system remains extremly profound. The next three chapters will provide this platform in the form of a novel, multi-functional hybrid system, starting from the designs, continuing with the prototyping, and finalising with some tests and experiments to showcase the functionality of the developed systems.

Chapter 3 : Circuit Design and Manufacturing

3.1 Design and CAD

Since the main goal is to utilize two types of sensing methods (and the various sensors based on them) for investigation, the circuit and specifically the signal-generating segment, should be able to work with both sensor types without requiring any changes to other parts of the circuit board. Although this may look very challenging, it will become less difficult to achieve by choosing the right sensor range and designing the signal conditioning circuit with a proper technique, making it compatible with both technologies. To work with a variety of sensors, three input pins were located at the edge of the circuit board, as the order suggests:

1. A round 0.6mm power output connected to the supply voltage; this is required for sensors that need VCC for operation (Active sensors).
2. A second pin with the same dimensions, connected to the circuit's ground. Most sensors, whether they are switches or an analog output device, need a ground connection (GND).
3. The most important pin: the sensor's output.

These three pins located on the edge of the printed circuit board (PCB) shown in the CAD environment, are designed to utilize a vast number of optical and magnetic sensors. This will provide the necessary connections and appropriate exposure as shown in the Figure 3.1.
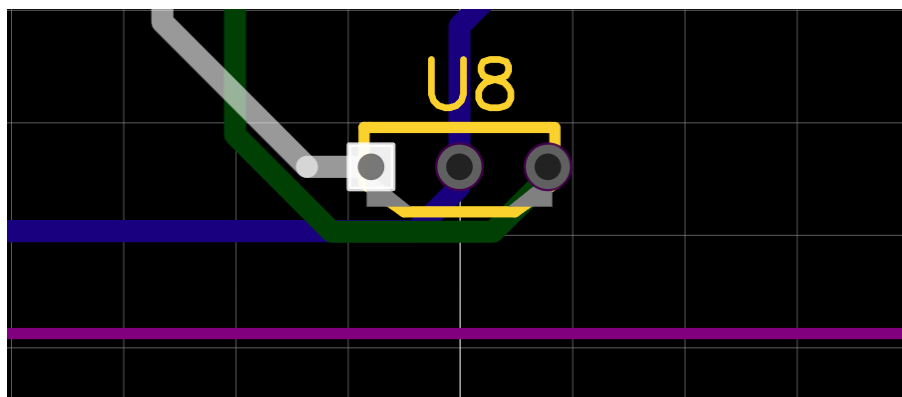
Figure 3.1. The purple line indicates the outline of the circuit board. The left pin is the sensor's output with a copper track connected to it on the top layer. The middle pin is the GND connected to a bottom track and the plain ground. The right pin is the VCC connected to a copper track in the Inner 2 layer.

Since the board is designed to act as an analysis platform, both the ground and the Sensor's output have been connected to gold-plated 2.54 mm single-row pin Headers for sampling, data collection and convenient oscilloscope monitoring as shown in Figure 3.2.
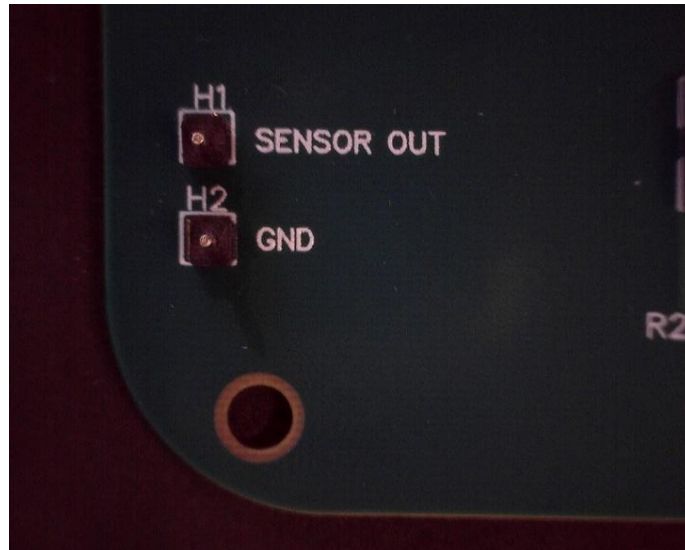
Figure 3.2. A close-up view of the Header pins on the actual board connected directly to the sensor.

Both the pins of the sensor and the head pins were distanced with appropriate clearance to retain signal integrity. 2 mm minimum clearance has been applied for each pin of the sensor. This is illustrated in Figure 3.3. This clearance has also been applied to all the tracks connected to these pins to prevent field and electrical interferences.
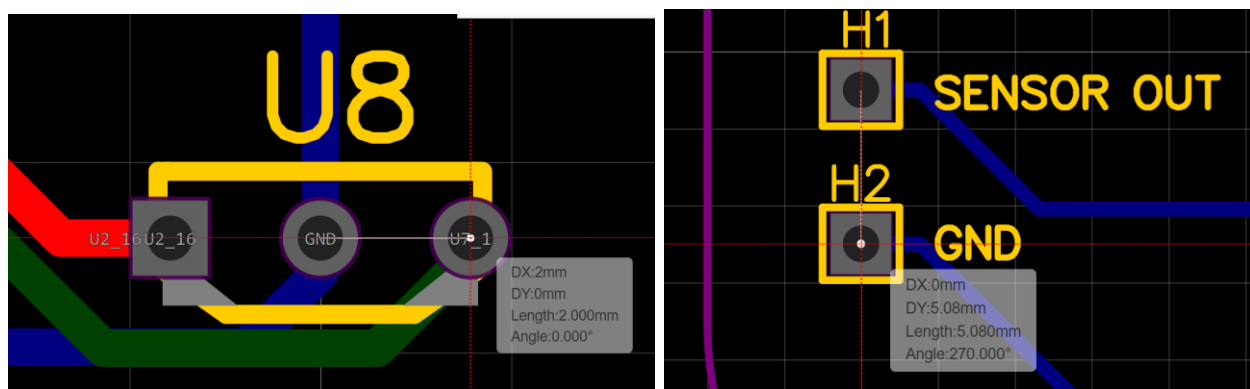
Figure 3.3. The clearance of the pins connected to the sensor.

In addition, a pull-up resistor with a nominal value of 10 kΩ is connected to the output to keep it high when the sensor is not detecting exposure, setting the default state of the sensing mechanism at a logical high and preventing any unwanted noise. For precise applications, it is essential to use a "pull" resistor to prevent the occurrence of the unpredictable (floating) states while the circuit is operating. To efficiently prevent the floating inputs, the location of the pull-up resistor and the sensor housing should be close. This can be shown in Figure 3.4.
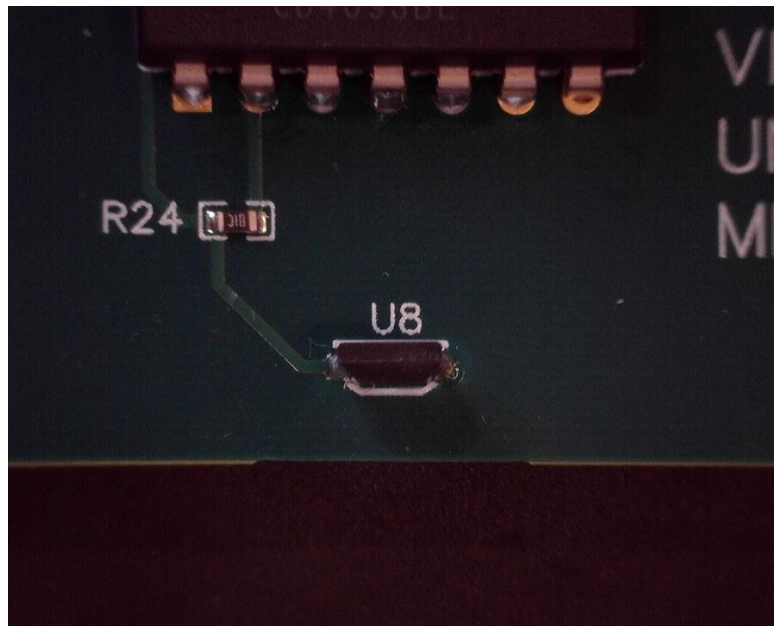
Figure 3.4. The actual position of the pull-up resistor (R24) and the sensor housing on the board. A Hall effect sensor is installed in the sensor area of the board, at the time this microscope shot was taken.

All the resistors used in this circuit, including the pull-up resistor, are surface mount Thick Film Chip Resistors made Uniroyal Electronics. The ratings of these resistors are as shown in Table 3.1.

Table 3.1. Pull-up Resistor Ratings [10].

Type	Max. Working Voltage	Max. Overload Voltage	Dielectric withstanding Voltage	Resistance Value of Jumper	Rated Current of Jumper	Max. Overload Current of Jumper	Operating Temperature
0603	75V	150V	300V	<50mΩ	1A	2A	-55℃~155℃

The rating curve of this type of resistor is also available in Figure 3.5. With an ambient temperature

of more than 70℃, the rated load will decrease; however, this will not impact the function of the

resistor for this specific setup till it reaches temperatures around 100℃.
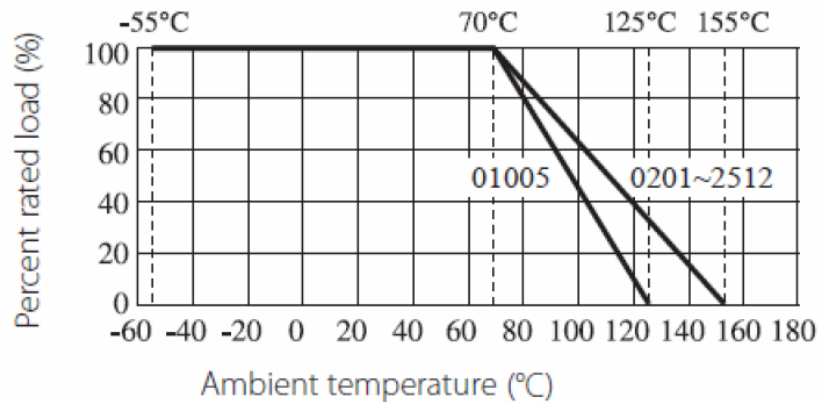
Figure 3.5. Rating curve of the Thick Film Chip Resistors used in the circuit [10].

The overload characteristic and the AC ratings of these resistors are not discussed here as the

circuit will not go above any of the limit thresholds of the direct current and the root mean square

(RMS) equivalent of the AC. The structure of these resistors is shown in Figure 3.6:

1. High purity Alumina substrate
2. Protective coating
3. Resistance element

4. Termination (Inner) Ni / Cr
5. Termination (Between) Ni Barrier
6. Termination (Outer) Sn
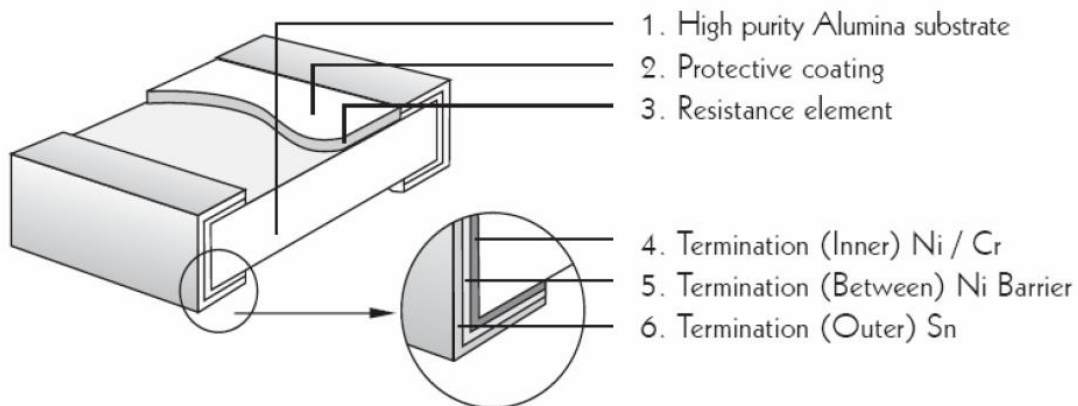
Figure 3.6. The structure of the Thick Film Chip Resistors used. [10]

The diagram of the sensing mechanism circuit is shown in Figure 3.7. U8 represents the sensor used. Other parts of the circuit are discussed in chapter 3.2 Subsystems and Components.
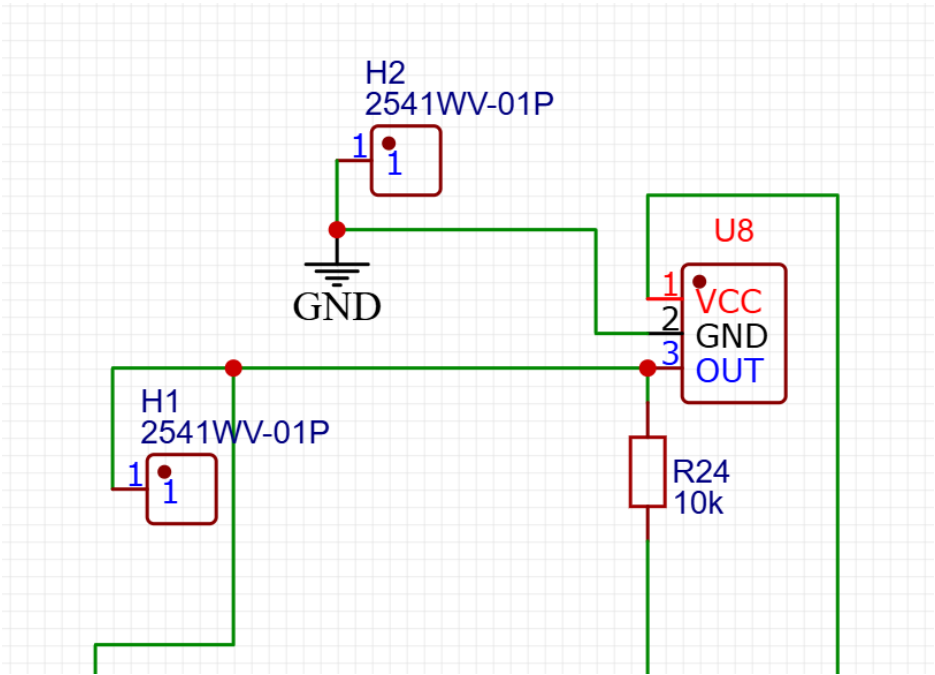
Figure 3.7. Circuit diagram of the sensing mechanism on the board.

The rules integrated with the design have been persistent with a minimum standard throughout the circuit. The primary design rules set can be shown in Figure 3.8.

Design Rule

Rule	Track Width (min)	Clearance (min)	Via Diameter (min)	Via Drill Diameter (min)	Track Length (max)
Default	0.5	0.7	0.8	0.4	

Figure 3.8. Primary circuit board design rules for tracks and vias.

As mentioned earlier, where necessary, the standards have been increased. As an example, the clearance between the pins of the sensor was 2 mm, which is 1.3 mm more than the primary minimum clearance of 0.7 mm in the design rule.

A total of 6 copper layers are used throughout the circuit board. The configuration can be seen in Figure 3.9.

No.	Display	Name	Type	Color
1	☑	TopLayer	Signal	#FF0000
2	☑	Inner1	Plane ⌄	#999966
3	☑	Inner2	Signal ⌄	#008000
4	☑	Inner3	Signal ⌄	#00FF00
5	☑	Inner4	Plane ⌄	#BC8E00
6	☑	BottomLayer	Signal	#0000FF

Figure 3.9. Circuit board copper Layers.

The use of 6-layer PCB technology increases the overall accuracy and the precision of the circuit. Two planes have been assigned to provide extra shielding for the critical signals, i.e., the sensor output. Being able to use six layers for the design also increased the routing efficiency, keeping the size of the board small while retaining signal integrity. The stackup used for the layers was SIG/PL/SIG/SIG/PL/SIG, starting from the top layer and ending with the bottom layer. The small size of the board is very desirable since, for many testing applications, limited space is available for implementation. The weight was also kept low by using the mentioned stackup. The utilization of two planes ensures minimal electromagnetic interference (EMI) on the board, enabling the users of the system to focus on the issues that only the sensor under analysis has been affected by, while increasing the precise performance of the system if used for a practical application.

The power delivery system of the board is explained in the next section, chapter 3.2.1 Onboard

Power Supply System. The existence of the plain ground assists better power delivery, decreasing the power disruptions and improving the overall performance

3.2 Subsystems and Components

Since the board is designed to work with as many sensors as possible, the output pin of the sensing mechanism (output of the sensor) is first directed into a Schmitt Trigger. The use of Schmitt Trigger is mostly essential for analogue sensors that produce curvy outputs and may also have noise within the produced signals. The digital sensors would not usually require a Schmitt Trigger for conditioning, especially the switching sensors as they come with internal circuitry implemented before the output, but to use one not only does it not interfere with their proper operation and functionality, but also ensures a noiseless signal even after long tracks since the tracks may pick up noises along the way.

The Schmitt Trigger used in the circuit is a Texas Instruments CMOS 2-input NAND CD4093BD. Inside, CD4093BD has four separate Schmitt Trigger circuits. On the board, CD4093BD is connected directly to the onboard power supply as it is an active component. The through-hole version of CD4093BD has been chosen to increase the impact resistance and durability of the board and lower the vulnerability to vibration and physical stresses. All the large or heavy components used on the board have been chosen from the through-hole options/version for this reason. CD4093BD has an operating temperature range of -55℃ to +125℃ [11]. The use of CD4093BD on the board is shown in Figure 3.10.
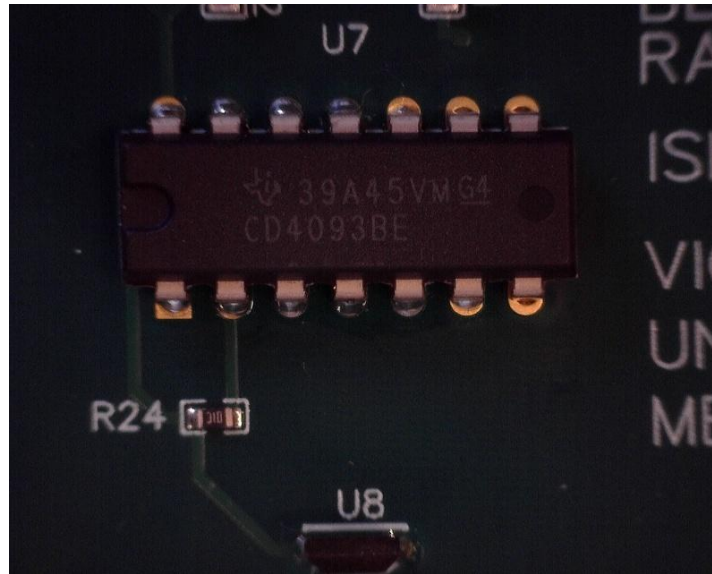
Figure 3.10. Microscopic view of CD4093BD (U7) on the circuit board.

3.2.1 Onboard Power Supply System

To improve the usage and practicality of the system, the circuit board has been designed with a reliable onboard power supply. The backbone of the power supply is a pair of CR2032H batteries. With two batteries connected in series, the total voltage across the terminals is 6V DC. The batteries are based on Manganese Dioxide–Li [12] made by Maxell. The operating temperature range is from –20°C to +85°C, which is among the best for a battery in this class. Each battery weighs around 3 grams, much lighter than many other batteries with the same technical specifications, and has an impressive compact package size, as shown in Figure 3.11.
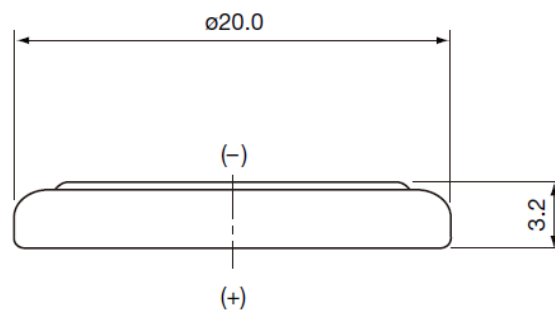
Figure 3.11. CR2032H battery dimensions [12].

Each with a nominal capacity of 240 mAh is an ideal option for long runs, and the general characteristics related to normal discharge and pulse discharge are outstanding. Figure 3.12 illustrates these characteristics, along with the discharge curves at different temperatures.
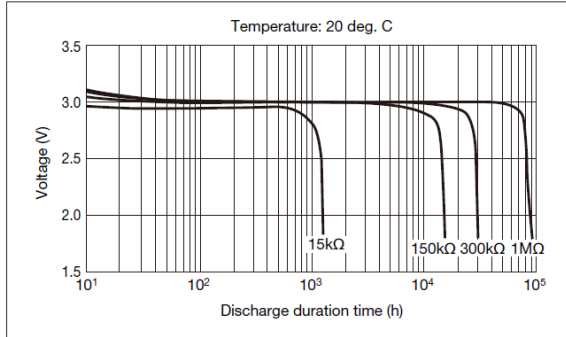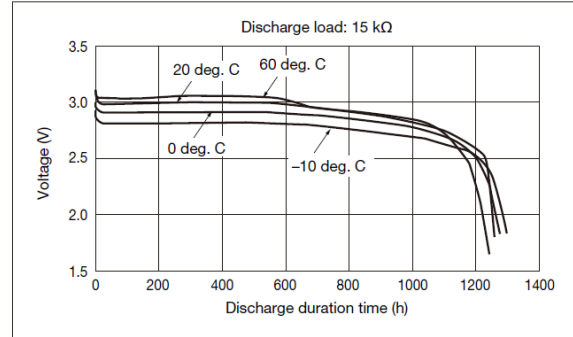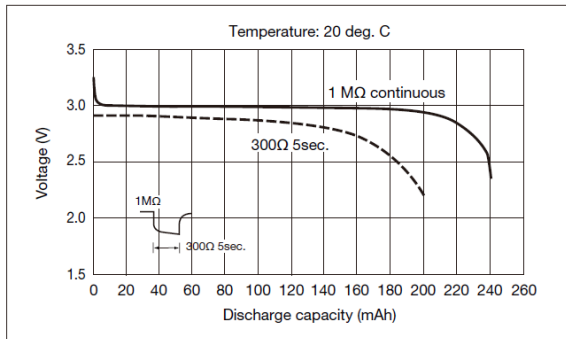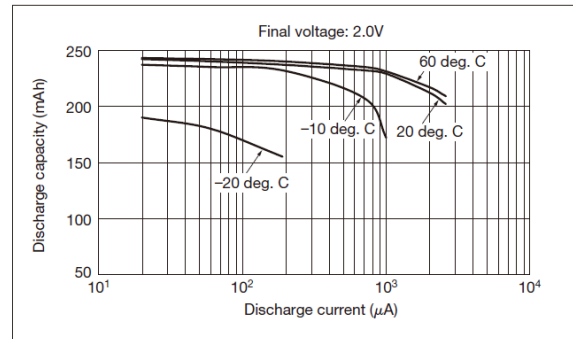
Figure 3.12. CR2032H characteristic graphs (Courtesy of Hitachi Maxell Energy [12].

Whilst the battery shows good performance over pulse discharges, the circuit's system needs extra support as it is used for high-speed rotation speed measurements, receiving many exposures in a very short period of time. This becomes an important aspect as the sensing mechanism is based on a high logical default mode. To enhance the power delivery to the system, decoupling capacitors have been utilized close to the batteries, the sensor location, and the Schmitt trigger integrated circuit (IC).

The use of capacitors in the power delivery system has various advantages from different aspects for the overall functionality of the circuit board. The capacitors used act as a semi-local power

source for high-consuming components and subsystems, which consume a large amount of power (current), and systems that work on high frequencies. This benefit comes from the capacitor's ability to discharge very quickly, providing instant power that the battery may not be able to provide by itself. While the current is provided to the device with increased consumption, the voltage will stay stabilised, and fewer fluctuations will appear on the power supply output and throughout the whole system as well. Other than the effects on the reliability by improving the power delivery, the use of decoupling capacitors will also reduce the overall noise in the system and improve the signal integrity.

In the circuit manufactured for this project, Multi-Layer Ceramic Capacitors were used. This is not only because of their superior technical performance over electrolytic capacitors, but also because of many other desirable functions and characteristics they have. This has been the primary reason for them being the reliable choice for high-end Automotive, Medical and Industrial electronics.

The unique technical design allows for very compact dimensions and package size while being manufactured in high capacities. The two 100μF Multilayer Ceramic Capacitors used on the circuit are made by the reputable manufacturer TAIYO YUDEN. Figure 3.13 shows the structure and dimensions of these capacitors. Use of these capacitors compared to other types will have numerous benefits for the circuit board's system from many aspects, including:

- Lighter weight
- Smaller size
- Higher performance
- Longer lifecycle
- Better thermal resistance
- Less susceptible to physical stress, etc.
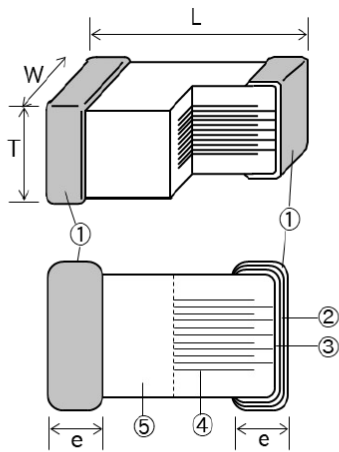
No.	Name	Material
①	Terminal Electrodes (Surface)	Sn Plating
②	Terminal Electrodes	Ni Plating
③	External Electrodes	Cu
④	Internal Electrodes	Ni
⑤	Dielectric	Barium titanate

Table 1: Dimensions

Dimension Code	Thickness Code	Dimension tolerance Code	Dimensions [mm]			
			L	W	T	e
21	G	B	2.0 +0.20/-0.00	1.25 +0.20/-0.00	1.25 +0.20/-0.00	0.50 ±0.25

Figure 3.13. Structure and Dimensions of the Multilayer Ceramic Capacitors used for manufacturing the circuit [13].

The location of the capacitors has been decided in a way that would create minimal physical distance between the power supply, sensing mechanism and the Schmitt Trigger IC as shown in Figure 3.14.
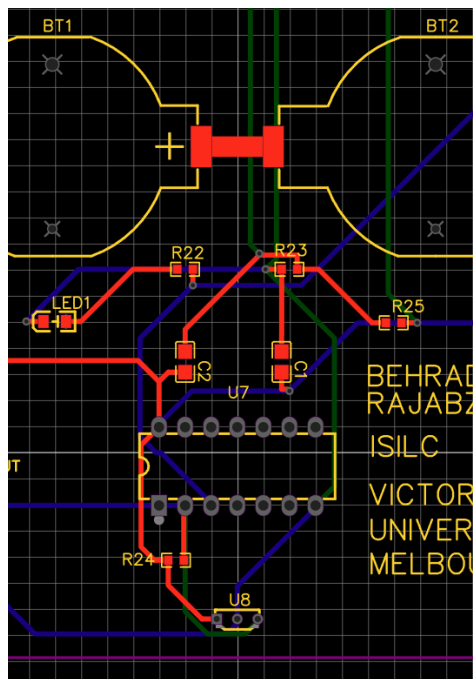
Figure 3.14. Relative location of the capacitors (C1 and C2) to the batteries (BT1-2) and the sensor.

Figure 3.15 shows the actual placement of the capacitors (C1 and C2) on the circuit board with a microscopic shot. A group of technicians from EasyEDA team, with their contact Haidy, provided their valuable help for the technical drawings of this part, specifically for this board.
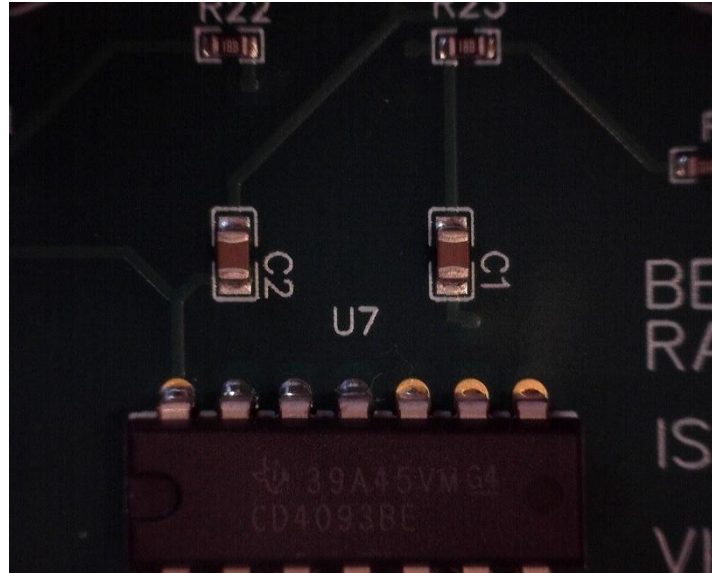
Figure 3.15. Capacitors on the circuit board.

To better understand the characteristics of this capacitor quantitatively and thus its suitability for this usage, some of the characteristics have been illustrated in Figure 3.16.
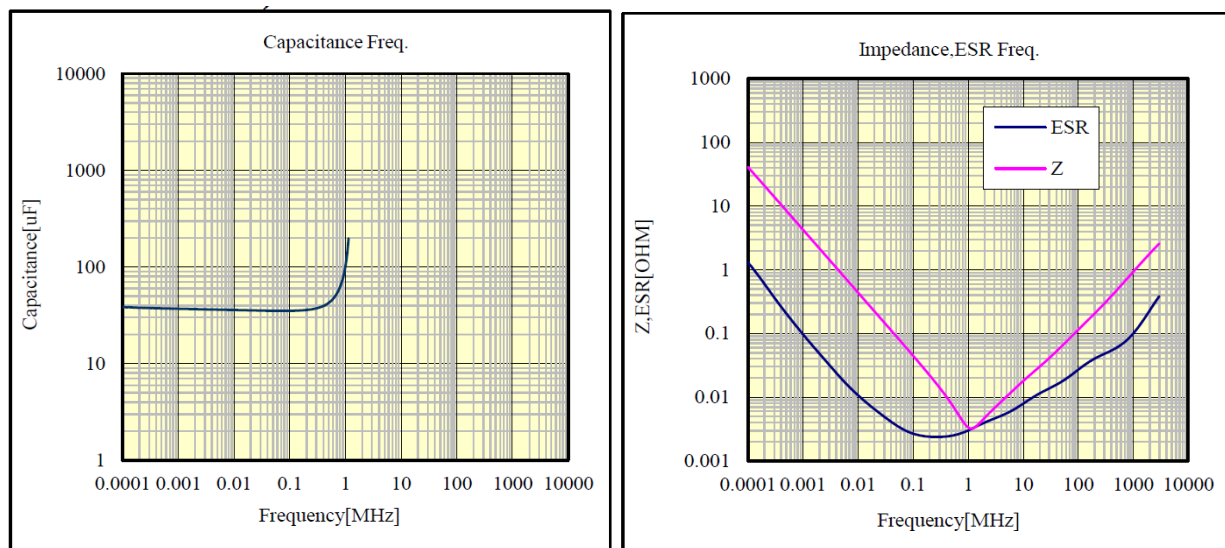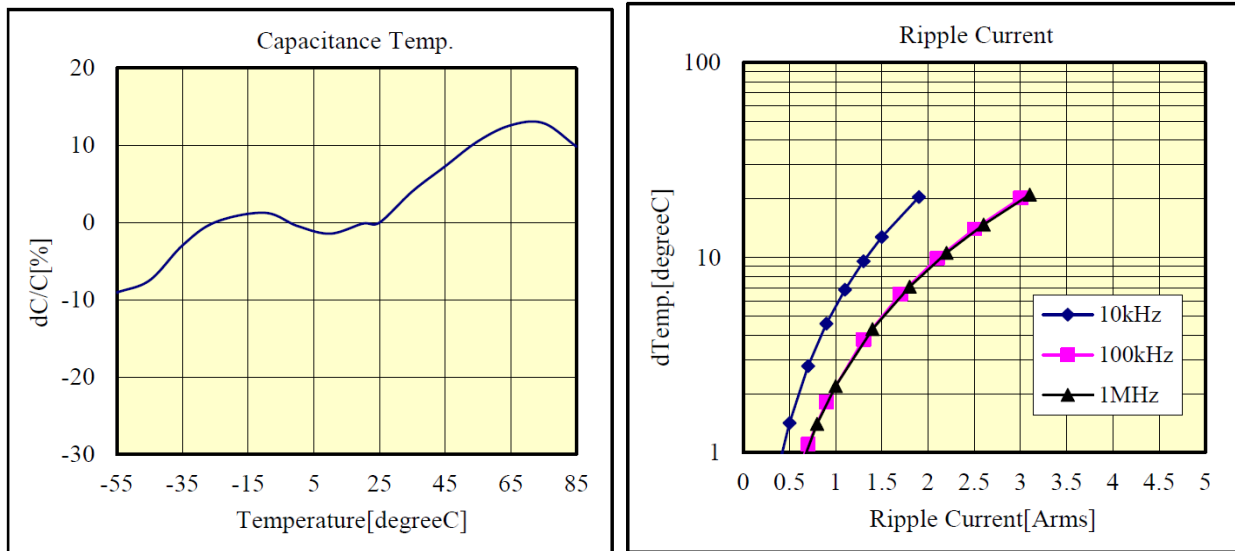
Figure 3.16. Characteristics of the capacitor used on the Board [13].

As seen in Figure 3.16, these capacitors are a very reliable choice for precision projects and high noise/stress environments. The information available on the datasheet suggests optimal layout on PCBs to minimize the effect of physical stress on the board as shown in Figure 3.17, which was considered for the design based on the final shape of the board and the board's physical characteristics.
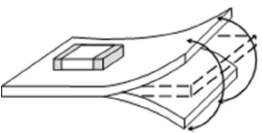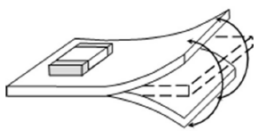
Figure 3.17. Capacitor layouts recommendation from TAIYO YUDEN [13].

The batteries are held in place by special plastic holders that offer a snug fit for CR2032 batteries. This comes with a consequence, as they come with a low life cycle. Due to the small size and the light weight, the surface mount option has been used without on the board and no issues were observed. This rigidity comes from the fact that these Liquid Crystal Polymer (LCP) battery holders have two posts supporting them from underneath over the board. The back side of the

battery holder used and the schematics are shown in Figure 3.18.
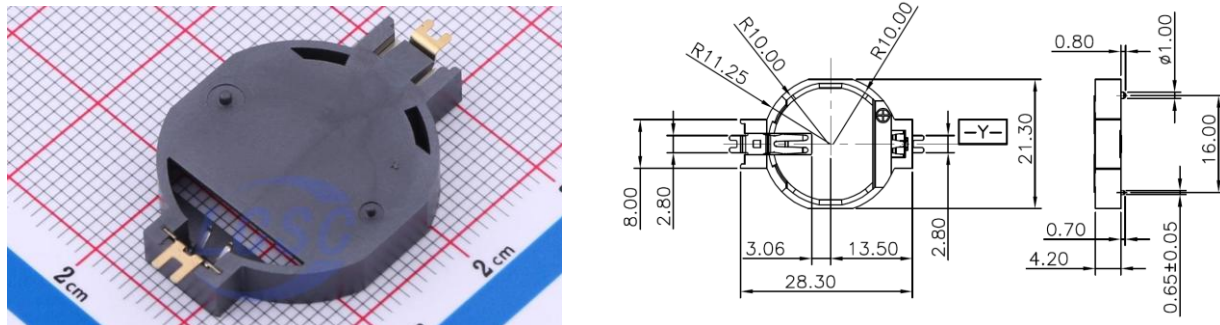
Figure 3.18. Back side of the LOTES battery holder with visible posts shown in the Left picture. Schematics of the holder on the right. (Photo from LCSC Electronics and schematics from [14]).

The track connecting the two batteries together has a width of 2 mm for efficient battery-to-battery current flow. The common ground of the series has a track width of 1 mm, and the positive terminal is connected directly to a switch with the same track width. Shown in Figure 3.19 is the second battery in series connection from the board.
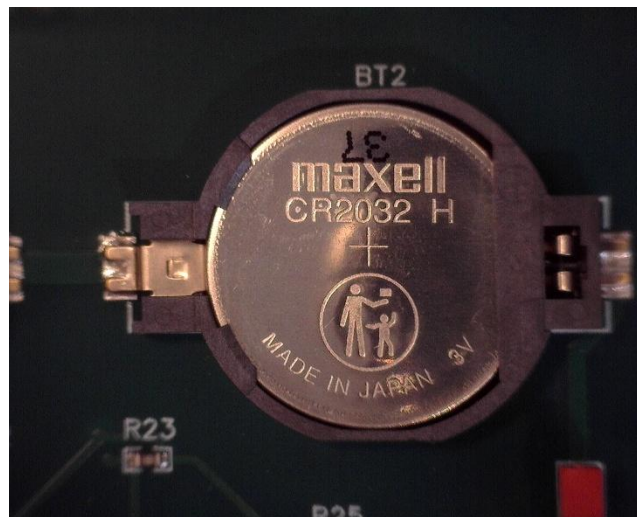
Figure 3.19. The battery with the holder on board. The track connecting the batteries can be seen on the left-hand side of the battery holder. The output is shown on the right-hand side of the battery going to the switch (the red component in the bottom right).

Using a switch is an important consideration for this circuit, with the presence of resetting ICs and high-capacity capacitors on the board. Before discussing the details of the switch, it should be

mentioned that the capacitors supporting the power supply system have been used with two resistors in a branch parallel with the batteries. In this branch, a high-value resistor is in parallel with one of the capacitors, followed by a 1.5 kΩ resistor in series with them and another 100µF capacitor parallel with all of them. This combination has several duties, and some are as follows:

1. Reducing the total inrush current at the time of startup in the system.

    Since the capacitors tend to draw vast amounts of current when they are first connected to the power supply, other parts of the circuit may experience fluctuations and voltage drop. This is because of the fast charging time of the capacitors.

2. Creating an RC filter for noise reduction through the system.

3. The resistor path acts as a way for slow discharge/bleed, maintaining the functionality of the capacitors and allowing a safe way of discharge when needed.

Other than the bleed mechanism available via the resistors connected to the capacitors, the switch itself has a specific configuration as shown in Figure 3.20.
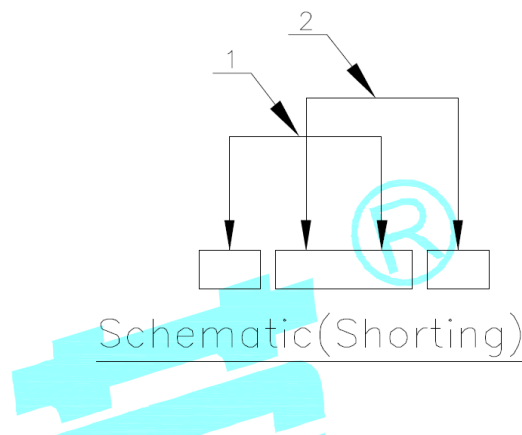
Figure 3.20. Shorting schematics of the main slide switch [15].

The shortings of the switch were used in such a way that when the device is turned off, the switch will connect the circuit to the ground. This will ensure a fresh start each time the system is turned on as all the ICs have been reset and the capacitors discharged when the system was shut down.

To improve the grounding process, the third pin of the switch was connected to the plain ground (plain GND) directly. The switch (SW1) on the board can be seen in Figure 3.21.

Figure 3.21. The slide switch on the board.

The switches used on the board are manufactured by Korean Hroparts. The slide switch features high voltage and current ratings, good insulation resistance, and high dielectric strength. The contacts are Gold (Au) plated, and silver (Ag) cladding has been used in some parts of the switch [15].

The only other switch used in the system is a "Push button" utilized for resetting a counter in the circuit. Although the function of this button is very simple, the complications caused by any malfunction can affect the function of the system heavily.

To prevent this, a very small and reliable button is used on the board. The schematic of this switch is shown in the Figure 3.22.
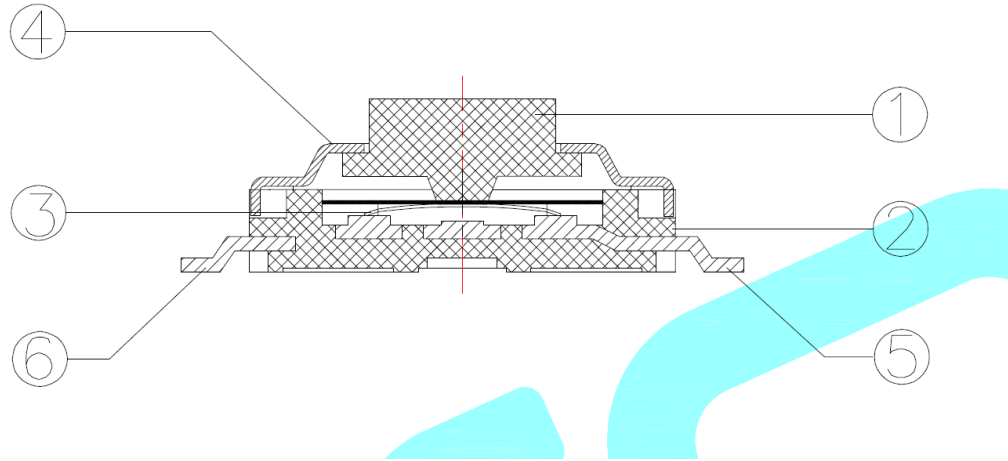
Figure 3.22. Schematics of the push button [16] .

Parts labeled as 5 and 6 are the terminals of the button, both made from brass and plated with silver (Ag). Part 1 is the keystoke with a dimension of 2.6 mm x 3.7 mm preventing accidental activation with 2.5 Newtons push force requirement. The distance between the PCB pins layout (which is connected to points 5 and 6) is more than 7 mm which ensures proper isolation of the ends. Part 3 is the contact, made from stainless steel and plated with Ag. This switch is also made by Korean Hroparts (HRO). It has a wide operating temperature range of -25℃ to +85℃ [16]. The picture of the switch on the board is shown in Figure 3.23.
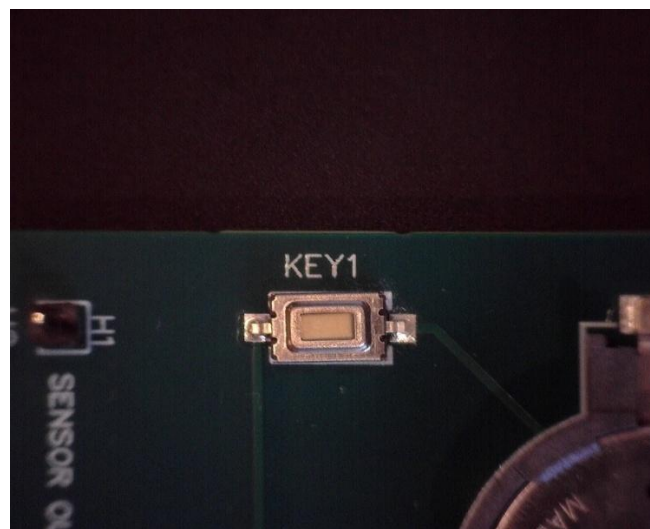
Figure 3.23. Microscopic shot of the push button used for resetting the counter on the board.

3.2.2 The Counter

The signal generated by the Schmitt trigger is shared in two paths. One of which is directed to a counter system with a 3-digit display on the board. The counter system consists of three separate decimal counters with dedicated ICs. These counters have been cascaded, forming a 3-digit decimal counter. The IC used is a   Texas   Instruments   (TI)   CD4011BE,   which   is multifunctional as it acts as both a counter and a 7-segment driver. The IC enables direct common cathode LED driving and cascading without the need for external/additional circuitry. The functional diagram of CD4011BE is shown in Figure 3.24.
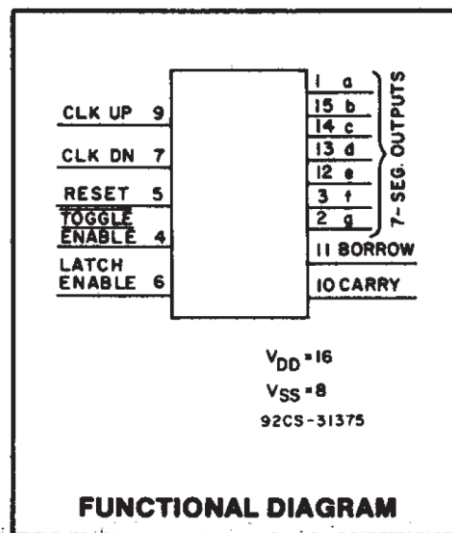
Figure 3.24. CD4011BE functional diagram [17]

The purpose of the counter in this system is to count and record the number of exposures made to the sensor used in the circuit. This will be used for several matters, including the recorded observation of false sensing and any missed sensing by the system and the sensor. This will also be utilized to record any per-exposure difference on two boards used with different sensors, different systems, or side-by-side comparisons. The track connecting the output of the Schmitt trigger to the counter system is shown in the Figure 3.25.
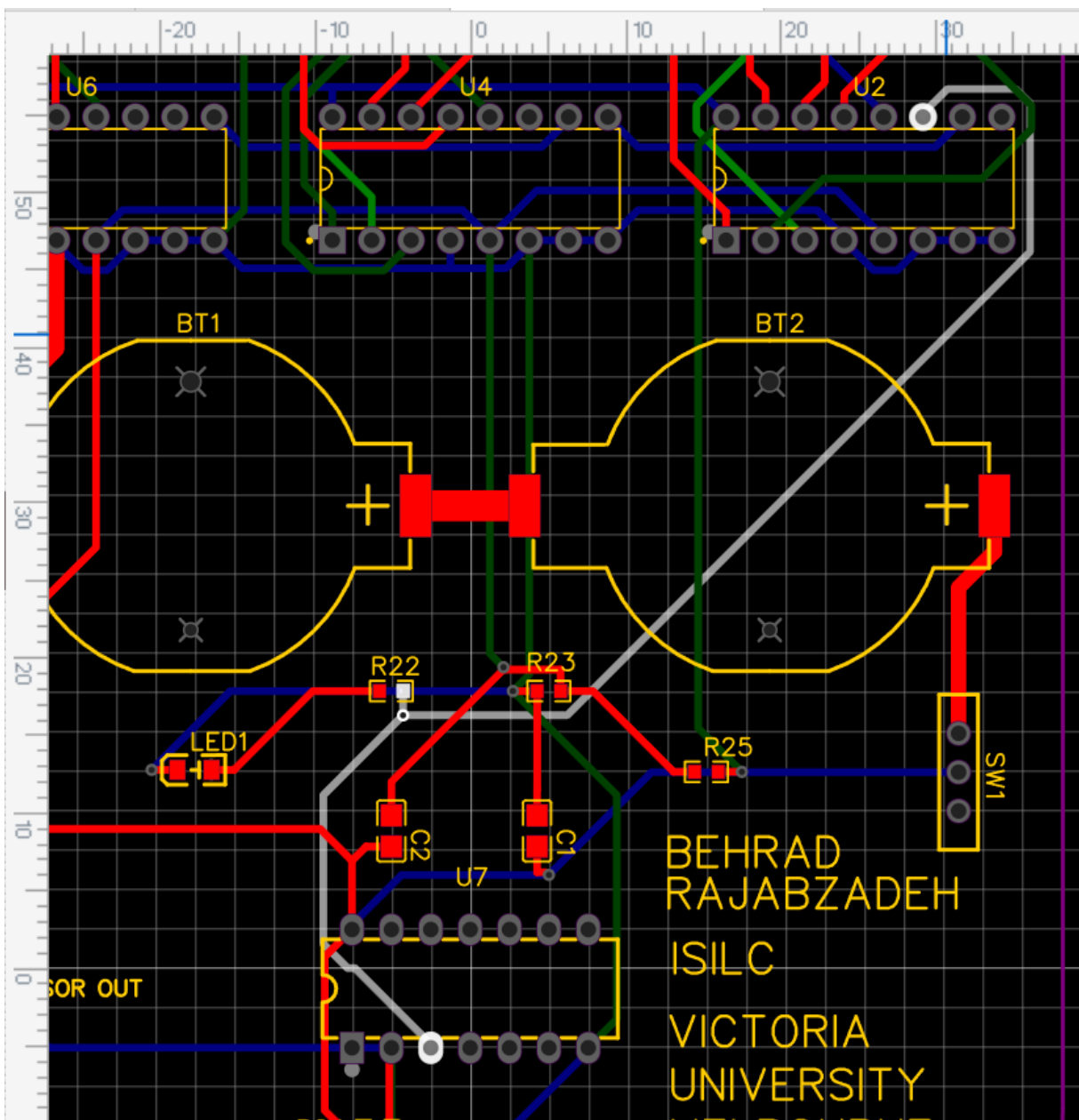
Figure 3.25. The white track shows the connection of the Schmitt trigger to the counter system.

This track was supposed to enter pin 9 of CD4011BE, which is assigned as Clock up. Because of

a design error, this track was connected to pin 11 (Borrow) of the counter IC. Since the track was

on the bottom layer, after manufacturing, the track was manually soldered to pin 9 as well. The

connection of the track to Borrow does not raise any issues with the function of the counter or any

parts of the system. In fact, this also increased the stability of the counting system with positive

support along the track and the Clock up pin. This is because of the default state of the borrow pin on CD4011BE. Borrow is set to default of logic 1 unless the counter changes from 0 to 9 [17] (which happens only on countdowns). Since this will not occur in this system, the Borrow is always a Logic 1 in this setup. To do this modification to the board, a small area of the track, close to pin 9, was unmasked and a solder connection was applied.

Inside CD4011BE, there is a Johnson counter connected to a Latch. The internal diagram of TI CD40110BE is shown in Figure 3.26.
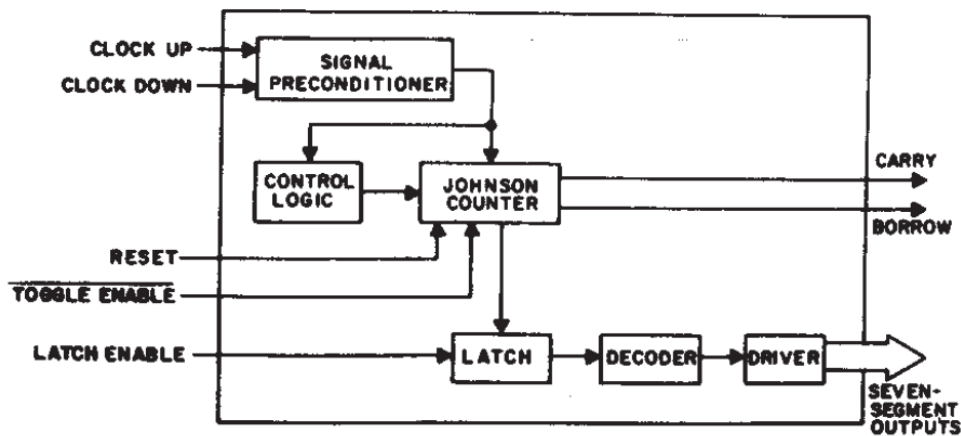
Figure 3.26. Internal diagram of Texas Instruments CD40110BE

The design of the circuit was primarily based on microcontrollers and, more specifically, on ATmega32. The reason behind the transition into the 4000 series CMOS was the simplicity and hence, fewer complications and errors being created in the system, making analysis and precision studies more efficient and focused. Subsequently, the performance of the chips is sufficient to support the proper functionality of the system. The disk interacting with this circuit produces two exposures per revolution on both magnetic and optical methods, generating signals well below the limit of the chips, even on high rotation speeds.

Pins 4, 6, 7 and 8, respectively, ttoggle enable, latch enable, clock down and VSS are connected directly to the ground (GND) on all three counter ICs. Pin 10 (Cary) is connected to the Clock up

(Pin 9) of the higher digit counter for cascading, except for the highest value digit in the counter. Pin 5, reset, is connected to the push button (KEY 1) in all counters. By pressing the push button, the reset pin in all counters will be connected to +6V, which acts as a logic 1 for CD401110BE and will reset all the counters and the respective 7-segments simultaneously. Whilst the push button is not activated, the reset pins are connected to the ground via the 1.5 kΩ resistor used in the power delivery system. This will ensure a Logic 0 across the reset pins at all other times. The push button will also get support from the capacitors used in the power supply when activated. Figure 3.27 shows the circuit diagram of the 3-Digit cascaded counter with the 7-Segments.
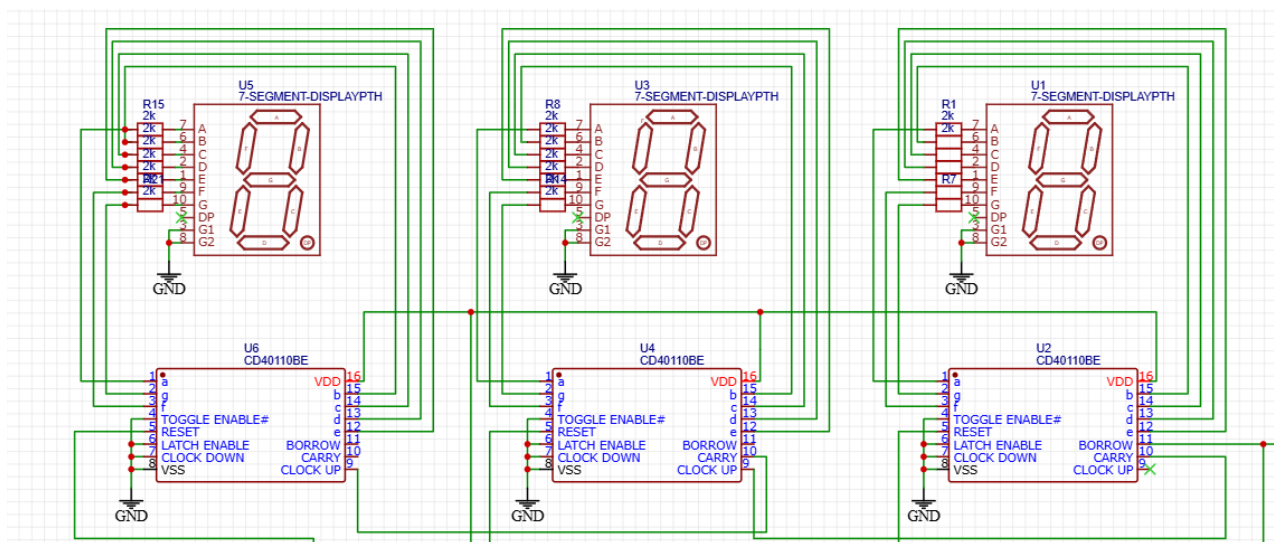
Figure 3.27. circuit diagram of the 3-digit cascaded counter with the 7-segments.

On the right side of Figure Above, it can be seen that the output of the Schmitt trigger entering the counter also goes through an additional path, which has the duty of indicating the presence of an exposure sensed by the sensor. This simple branch will be explained in the next section, chapter 3.2.3 Exposure Indicator, briefly.

7-Segments are fast and simple, with very low power consumption compared to other display methods. They have an operating temperature range similar to LEDs, which is much better when compared to other displays. They are also impact resistant. The &-segment used for this circuit is

comprised of Red LEDs that emit low-energy visible lights, having the least interference with any optical system that this circuit may be implemented on. 7-Segments do not react to vibrations and will not be affected by many influential factors that would disturb other types of displays. Both the 7-segments and the counter ICs are through-hole components. This has been selected because of their relatively large size and weight. While connecting the counter ICs with the 7-segments, 2 kΩ resistors have been used to limit the power consumption on the 7-segments and reduce their brightness. This will help with the power management of the board and reduce the amount of light emitted by the 7-segments to the ambient environment. The counter and more specifically the 7-segments are embedded at the farthest point from the sensor to lower the chance of any unwanted optical reflections and interference. Microscopic shots of the 7-segment, the limiting resistors and the counter IC on the board can be shown in Figures 3.28 – 3.30.
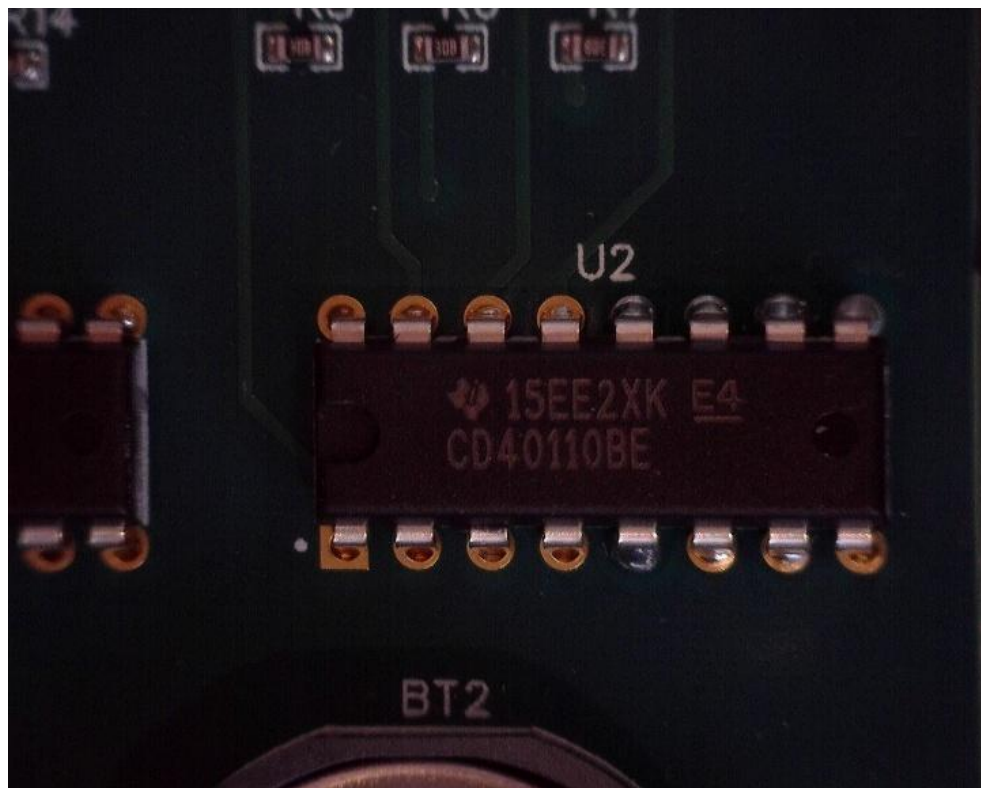
Figure 3.28. Counter IC of the first digit of the counter. Located on the right-hand side of the board.
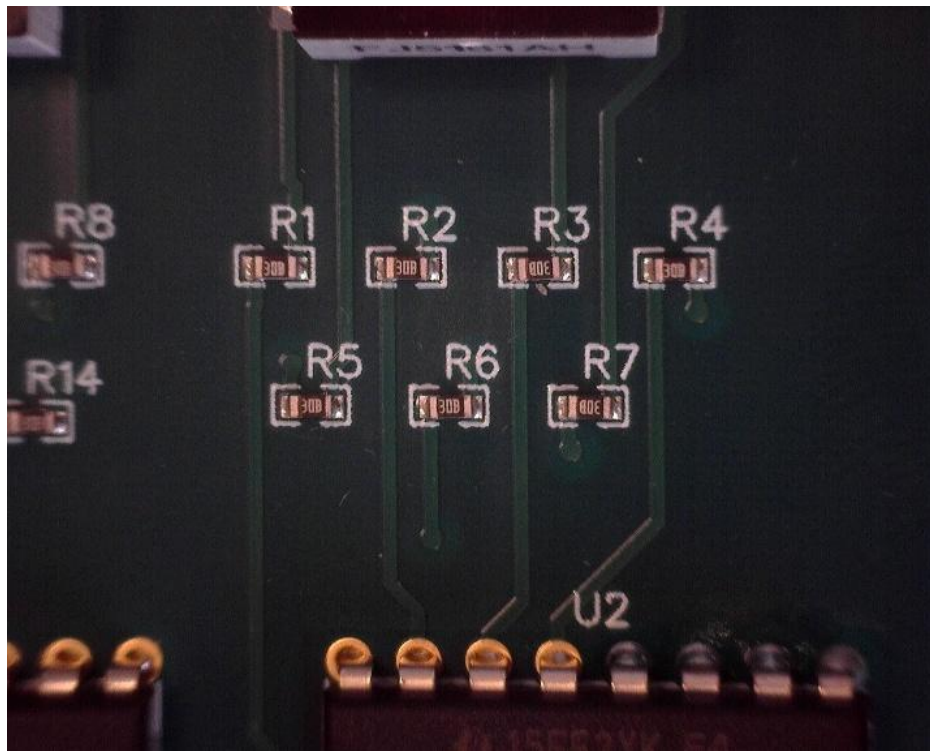
Figure 3.29. A set of current-limiting thick-film chip resistors, located on the tracks connecting the counter IC to the 7-segment.

Figure 3.30. The first digit of the counter shown by the respective 7-segment on the board

The track routing and the PCB layout of the counter system in the CAD environment are shown in Figure 3.31.
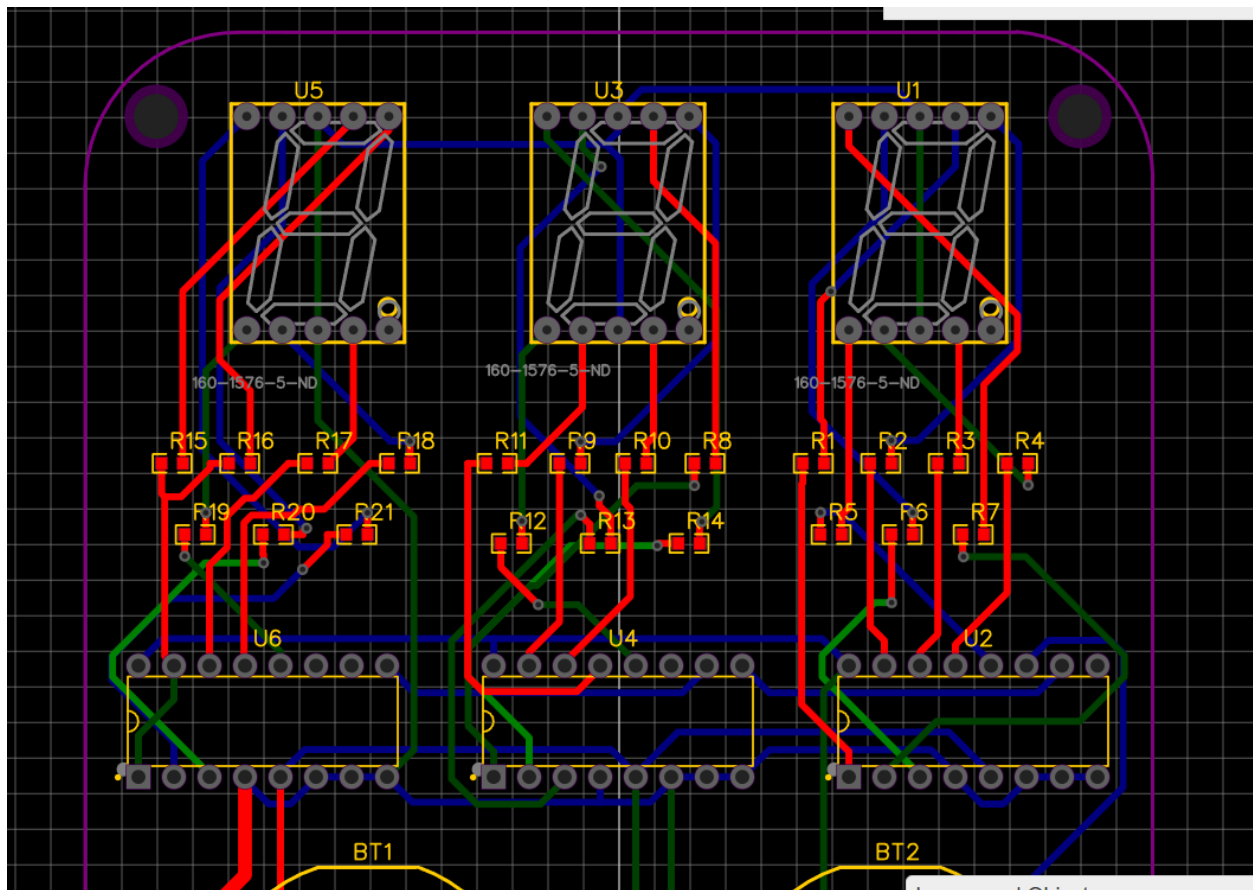
Figure 3.31. The counter components, Track routes and layouts shown within the boards outline.

The counter is the only part of the circuit that uses the Inner3 layer for route tracking. As mentioned earlier, the track connecting the output of the Schmitt trigger to the counter also has an extra branch. This happens closer to the Schmitt trigger IC and is the last circuit segment to be discussed. Figure 3.32 shows the track junction from the output of the Schmitt trigger IC.
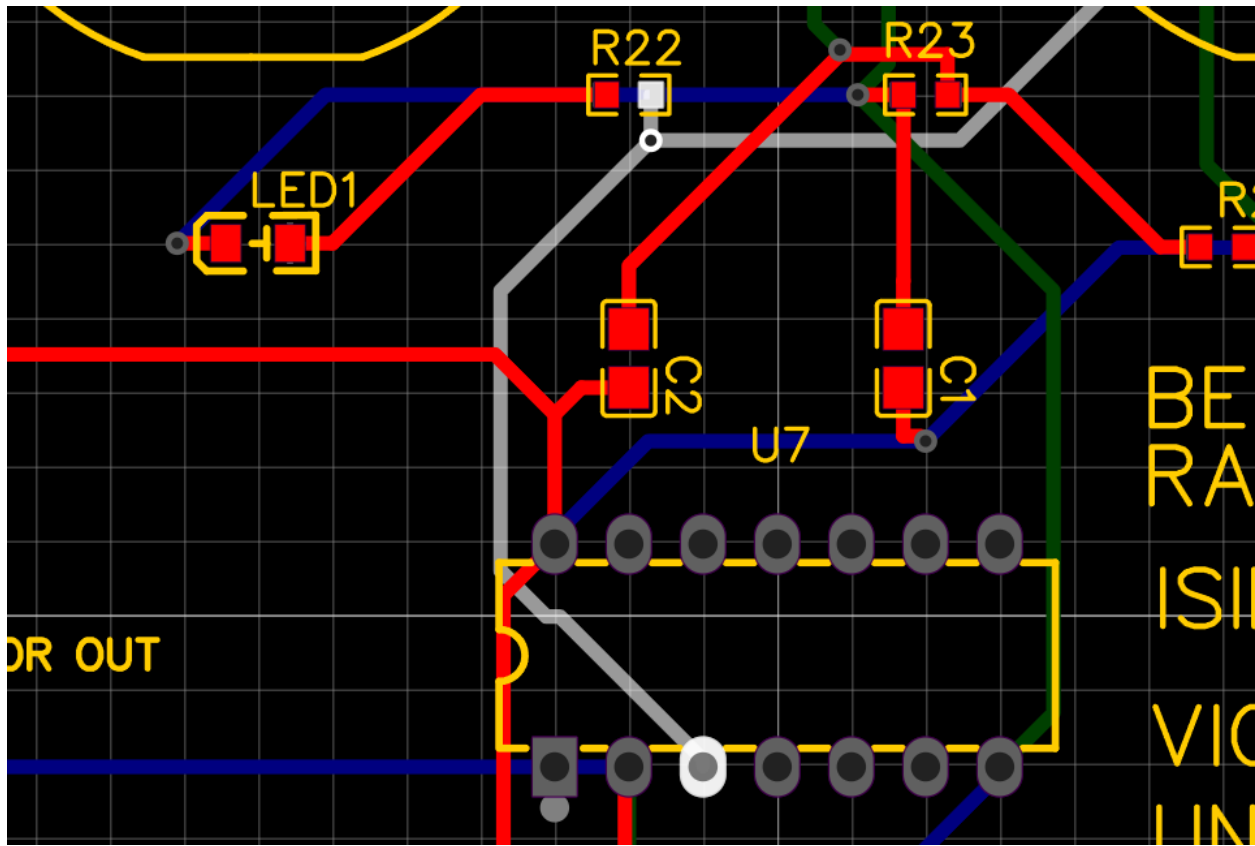
Figure 3.32. The Schmitt Trigger output track highlighted in white goes into two different paths.

As shown, the track has a junction created with a via that directs the signal in two different paths: up to R22 close to the via and right to the counter system. The path connected to R22 is responsible for the visual indication of exposures sensed by the circuit. Figure 3.33 shows a close-up view of the via used for branching the Schmitt trigger output into two different paths.
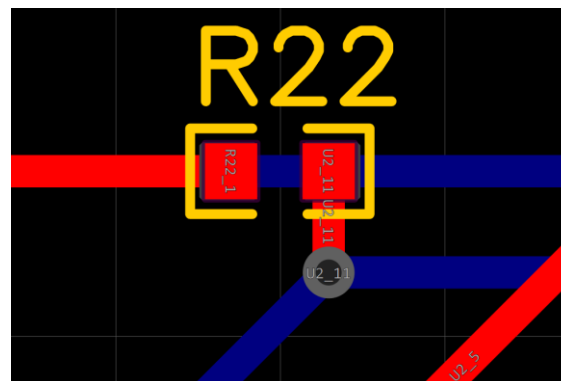
Figure 3.33. close-up view of the via used for branching of the Schmitt trigger output into two different paths.

53

3.2.3 Exposure Indicator

For analysis, it is essential to observe, record and know whether or not an exposure is sensed by the sensor and the system. The exposure indicator circuit is a system providing visual indication of exposures. The circuit is simply comprised of a resistor, an LED and a ground connection. The circuit diagram of this system is shown in Figure 3.34.
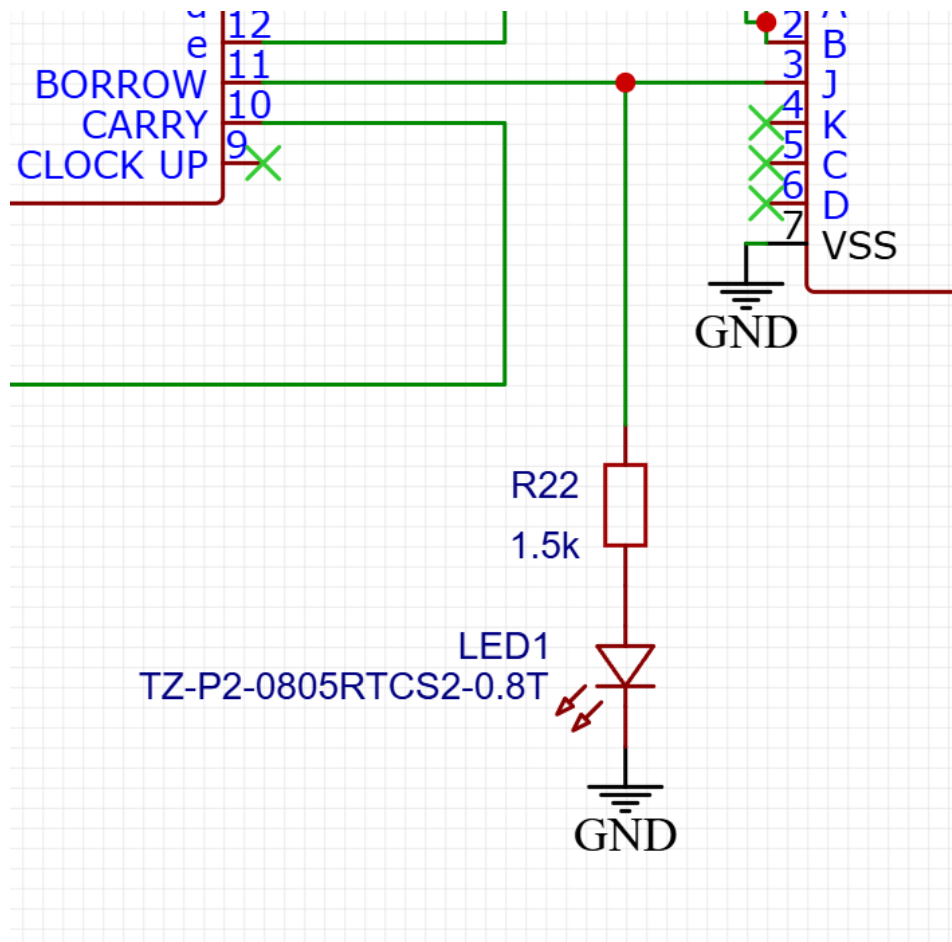
Figure 3.34. Exposure indicator's circuit diagram.

When the sensor senses an exposure powerful enough to activate the Schmitt Trigger, the signal generated will carry current into the path of the exposure indicator circuit, causing the LED to be lit. The illuminated LED of the exposure indicator circuit in the presence of an exposure can be seen in Figure 3.35.
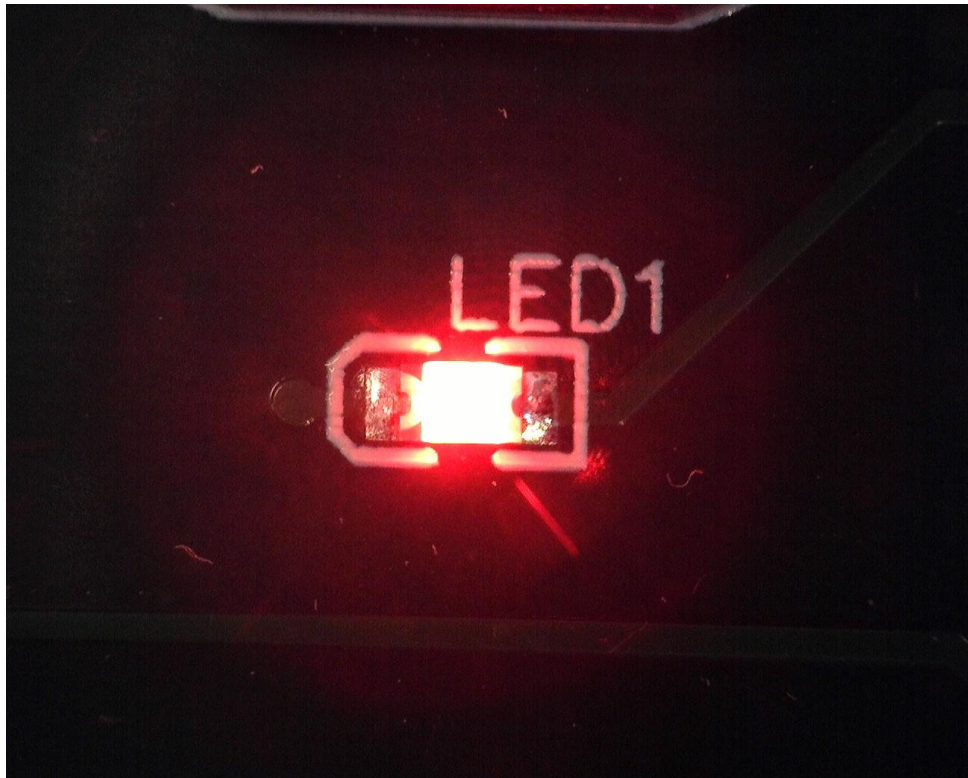
Figure 3.35. Microscopic shot from the board showing the illuminated LED of the exposure indicator circuit, in the presence of an exposure.

The LED used is a Red surface mount device (SMD) light made by TUOZHAN which can radiate accurately within the visible light wavelength as the graph shown in Figure 3.36.
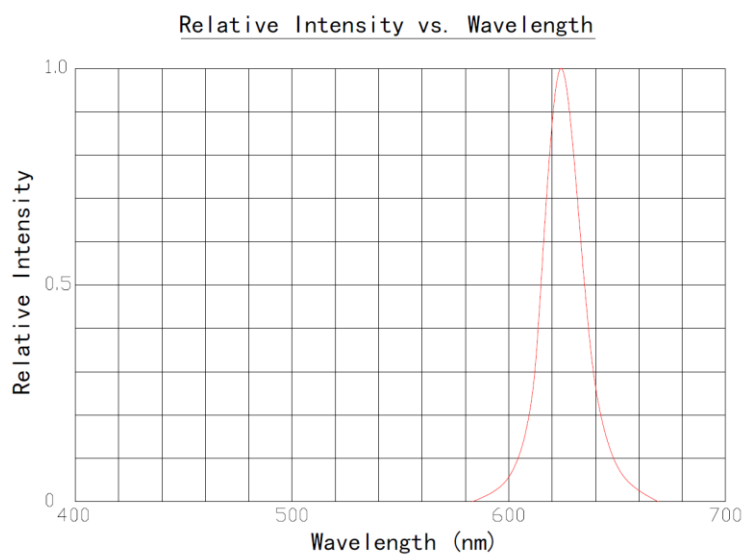
Figure 3.36. Relative Intensity vs. Wavelength graph of the exposure indicator circuit's LED.[18]

The LED used has proper tolerance toward temperature changes and these can be shown in Figure 3.37 and 3.38.
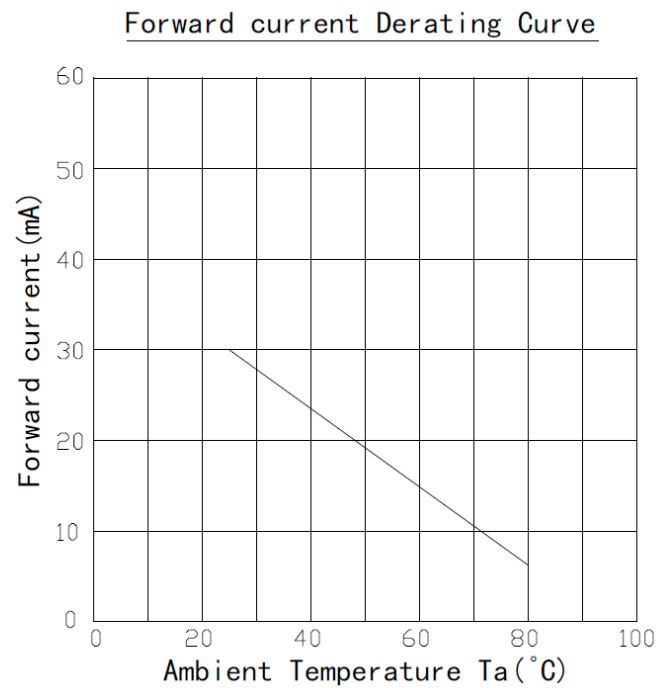
Figure 3.37. Forward current Derating Curve of the exposure indicator circuit's LED. [18]
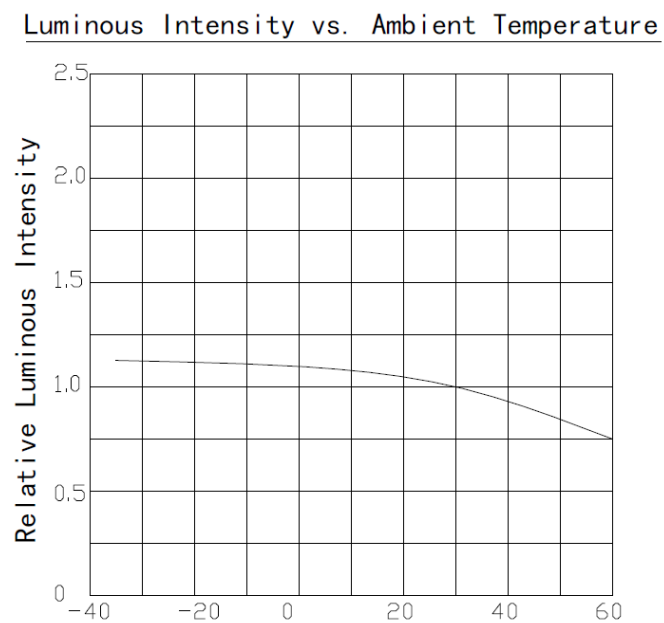
Figure 3.38. Luminous Intensity vs. Ambient Temperature of the exposure indicator circuit's LED.[18]

The light emitting diode performs well within a wide range of temperatures. The ambient radiation diagram of this LED is shown in Figure 3.39.
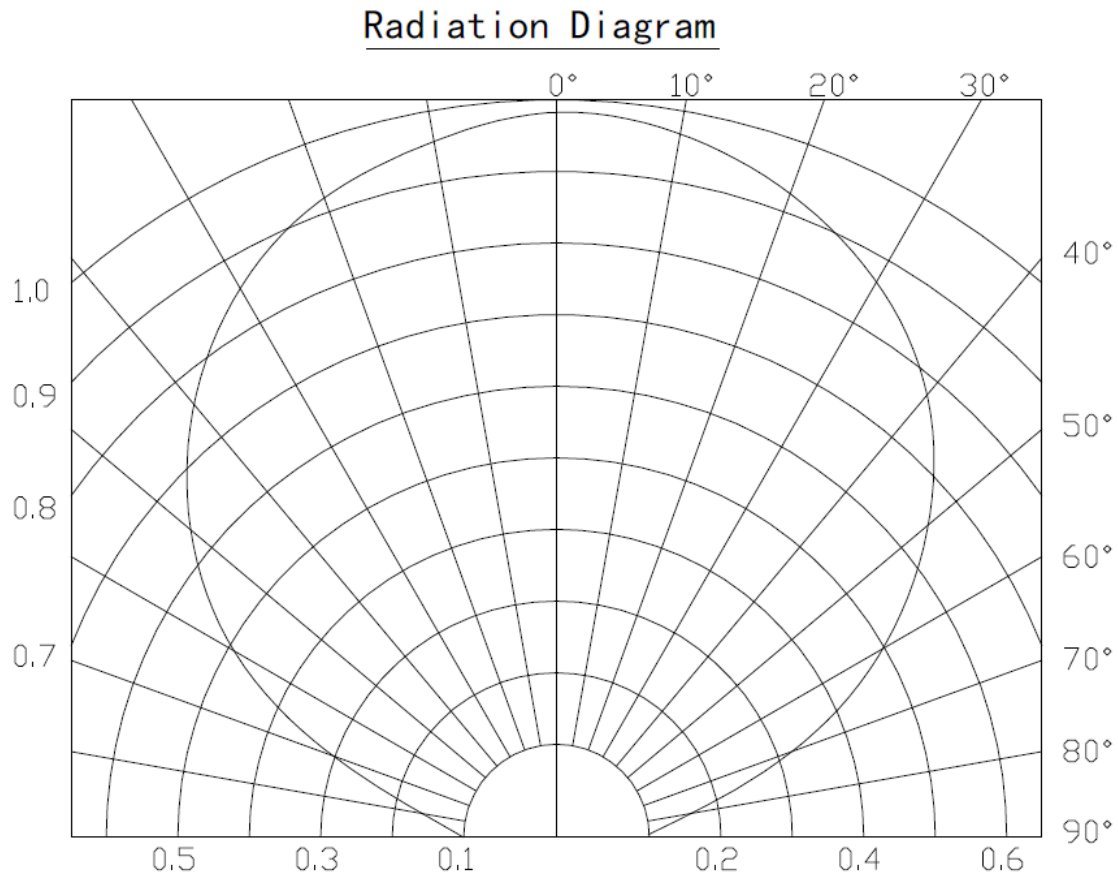
Figure 3.39. Radiation Diagram of the used LED. [18]

The light radiation, other than being within a very specific wavelength (from 600 nm to less than 700 nm), is also very discrete but broad in radiation angles. This is achieved by the transparent lens used on top of the LED as shown in Figure 3.40. This combination makes the device ideal for precision use as light pollution will be minimal, reducing optical disturbance while providing a wide visibility angle of 120°. The energy consumption of the device is also very low, approximately 60mW [18].
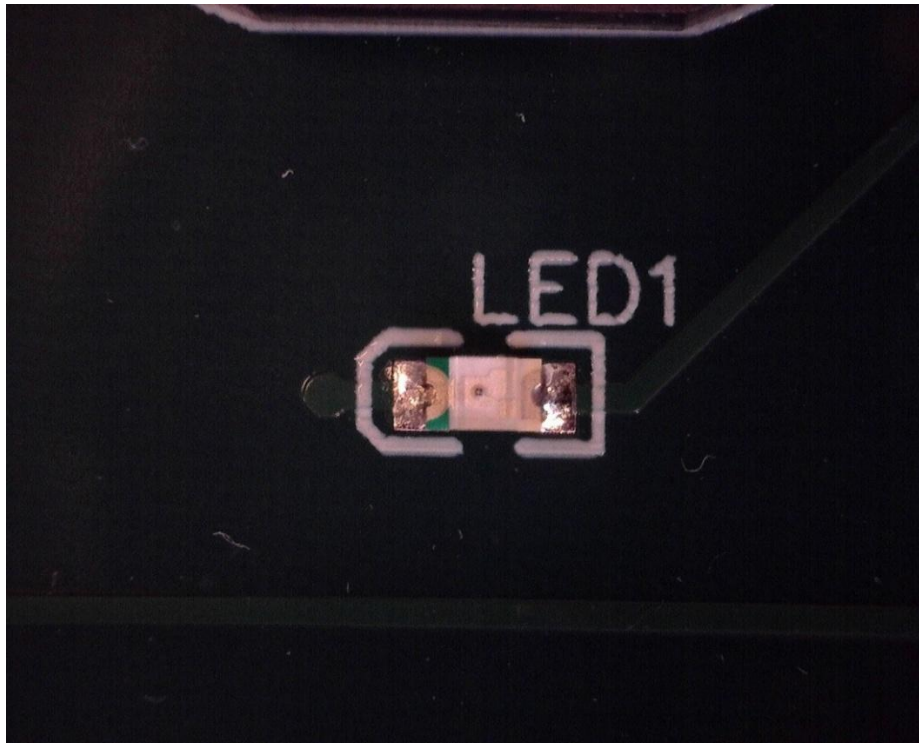
Figure 3.40. The microscopic shot of the LED on the board while not activated.

Many components and parts, including this LED on the board, use both a grounding track route and the ground plane for reliable operation.

The overall view of the designed board and the ground plane are shown in Figures 3.41 and 3.42.
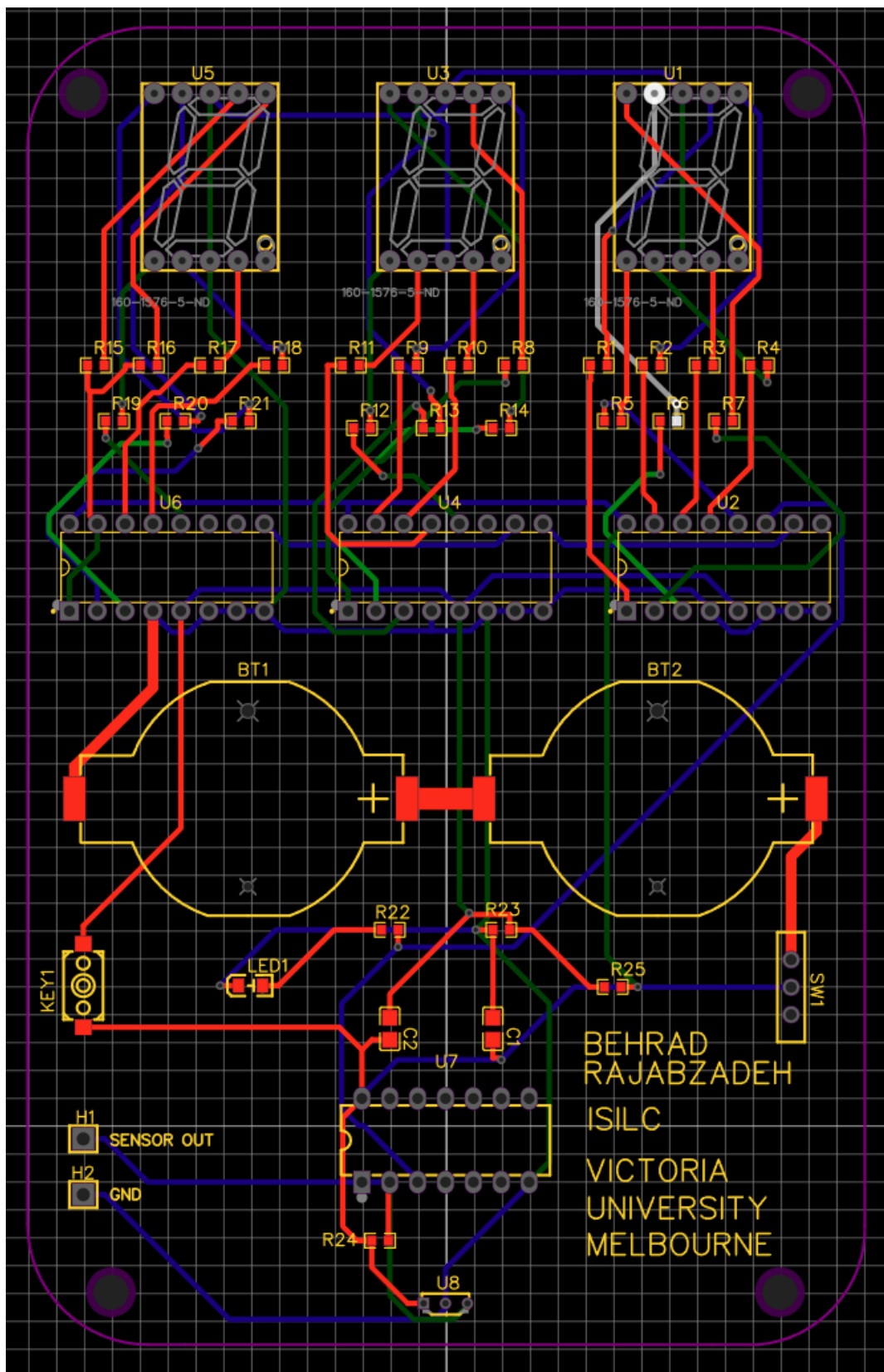
Figure 3.41. The overall view of the designed board.
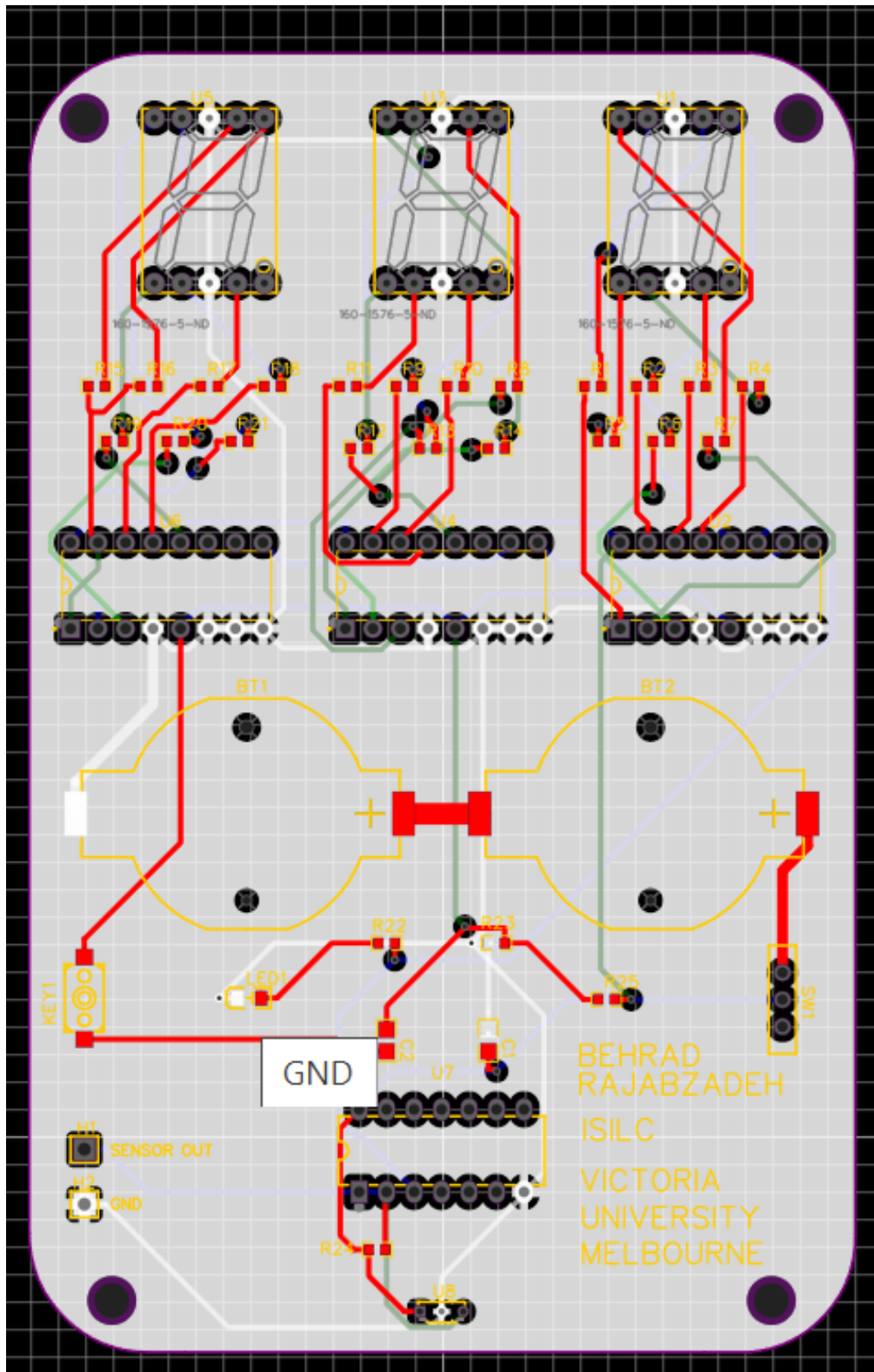
Figure 3.42. The grounding plain of the board highlighted in white.

3.3 Manufacturing

3.3.1 Printed Circuit Board (PCB)

Five PCBs with complete assembly were manufactured in JLC's factory number 1 in China. The base material of the board is made of an FR (Flame Retardant) - 4 with a standard glass transition temperature (TG) of 135 ºC -140 ºC. The final machined dimension of the board was 76.3 mm × 120 mm, which is almost the same as the original design. Electroless Nickel Immersion Gold (ENIG) was requested. This was intended for better performance and connectivity, specifically for the sensor and the sampling pins. The PCB has a thickness of 1.6 mm, and the vias were covered and filled with Epoxy. This was done to gain better structural integrity and add extra protection to the vias used in the circuit. This also improves the board's thermal and signal reliability while protecting the vias from water, moisture, and contamination. The board is also designed in a way that requires soldering SMD components almost directly over some of the vias, which would not be achievable without plating the vias. The outer copper weight was 1 oz, while the inner copper weight was set at 0.5 oz. Full flying probe test was performed on each board and the final products have Institute for Printed Circuits (IPC) Class 2 Standard, which is known to provide a balance between superior performance and lower cost within the industry, suitable for continuous and reliable usage. As seen in Chapter 2, four empty circles were drawn on the corners of the board. These were set for fixing the board where needed. The diameter of the circles was 3.2 mm so that they could be used for fastening the board with M3 screws which are very common and available through many outlets within Australia. Because of this, a board outline tolerance of 0.2 mm was requested from JLCPCB. The DFM analysis (Design for Manufacturability analysis) was evaluated without any issues. The only change made after sending the Gerber files was connecting the ON/OFF slide switch of the board to the ground on the off shorting. This was communicated to the manufacturing facility through email.

3.3.2 Components Assembly

A lead-free solder paste was used for SMT. The solder paste was a composition of Sn96.5%, Ag3.0% and Cu0.5%. The maximum reflow temperature (peak) used for the soldering oven was 260℃. All the parts were assembled on the top side of the board. To ease the ordering and reduce the costs, all boards were ordered with a Hall effect sensor soldered on U8. Ultimately, some of these sensors were removed from the board onsite in the Lab to be replaced with the Optical sensors. The removal was done by connecting all three pins of the installed sensor together by adding some solder to the area. Then the pool of solder was heated up by a wide soldering tip and the component was pulled out. The remaining of solder on the board was removed and cleaned using a 2 mm braid.

The Hall effect sensor used on the board (the manufacturing facility assembly) is a Through-Hole 3-Pin Texas Instruments DRV5023 Digital-Switch Hall Effect Sensor. This sensor is a current part released at the end of 2014. The part is also actively used in the automotive industry, however, there are several variants available, and not all are automotive grade. The part number of the sensor used on the board is DRV5023AJQLPG, providing an operating temperature range of -40℃ to +125℃, is a very common solution for magnetic sensing with excellent temperature stability, small package size, internal regulators and integral protection. The sensor works based on a threshold amount for magnetic flux density [19]. When the applied magnetic field exceeds the threshold amount, the sensor output goes low. This will stay low until the field is decreased to another threshold, which is mentioned as $B_{RP.}$ When this occurs, the output will go to a high impedance. The upper threshold mentioned earlier is labeled as B_{OP} in the datasheet of the sensor. The output state of the sensor based on B_{RP} and B_{OP} is shown in Figure 3.44.
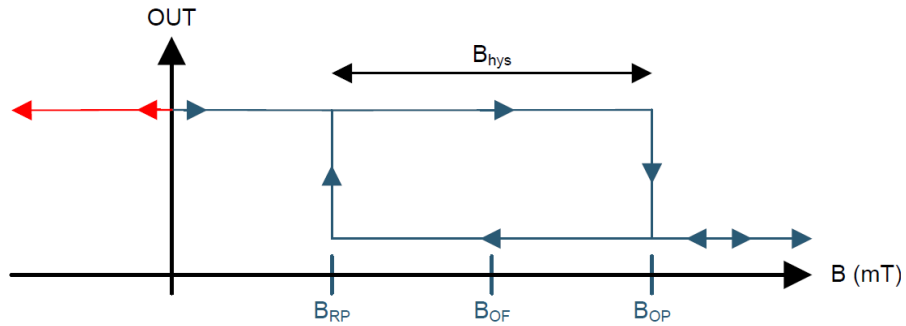
Figure 3.43. The output state of the DRV5023 sensor based on B_{RP} and B_{OP} [19].

The Functional Block Diagram of the sensor suggests the use of a resistor on the output and utilizing a capacitive component on the power supply connected to the VCC. Both of these suggestions are met without any alterations to the board. Figure 3.45 shows the Functional Block Diagram suggested by Texas Instruments.
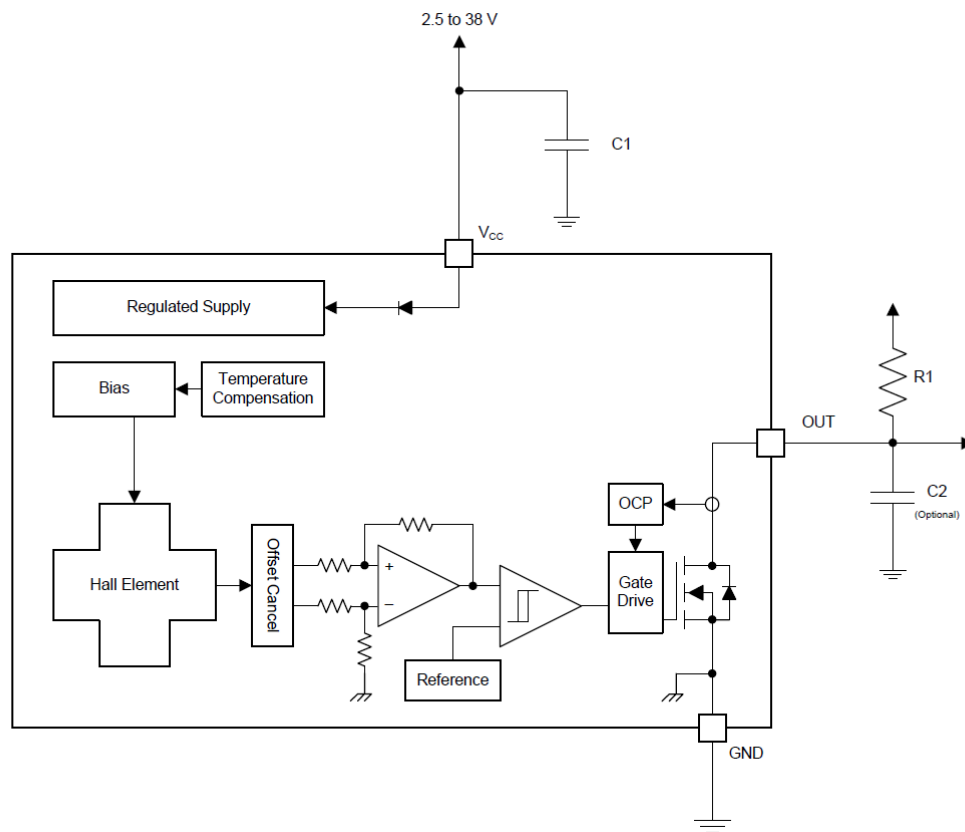
Figure 3.44. Functional Block Diagram of DRV5023 with Texas Instruments recommendations [19]

The field direction is important for the detection of the field by the sensor; however, in the tests conducted in the laboratory, it was observed that with high saturation and strong magnetic fields, the sensor will fail to react accordingly to the polarity of the magnetic field. In lower Gaus amounts, the positive and negative magnetic fields are defined as shown in Figure 3.46.
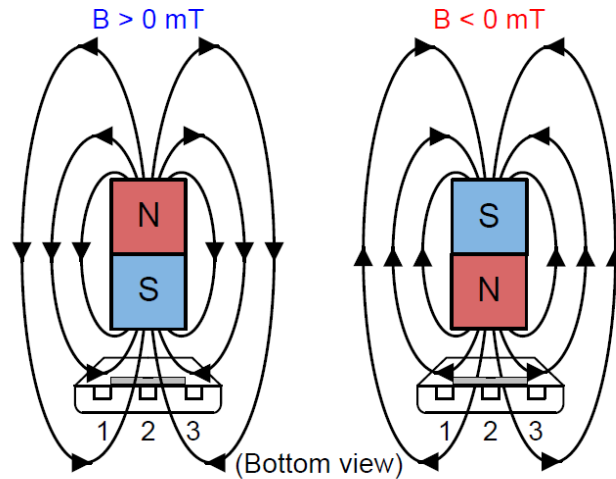
Figure 3.45. Positive magnetic field is a south pole near the marked side. [19]

This sensor does not exhibit ideal behaviour during power-on, as the output signal does not align with the intended output. The valid output is usually achieved shortly after the startup; however, this was mostly not an issue when integrated with the board. This behavior was not clearly visible using the oscilloscope available in the lab; however, it has been mentioned in the datasheet [19] for possible cases.

The other sensor mounted on the board (manually after manufacturing) is a KingBright phototransistor, purchased from Jaycar retail in Australia. The phototransistor is based on an NPN bipolar junction. The base is internal, exposed to the light. The two other pins connected to the board are the emitter, connected to the sensor output on U8 and the collector connected to the ground. The device exhibits analog behavior when exposed to light in the IR spectrum. The rise and fall times are both around 15 microseconds based on the information provided by the

manufacturer, and the operation temperature has a wide range of -40°C to +85°C if no infrared radiation is present. The component is not suitable for reflow soldering as the optical properties of the lens will be affected during the process. The installation of the phototransistor on the board was done manually with soldering iron.

A 3D object model of the Board was created for precise case design. The 3D model of the circuit board can be seen in Figure 3.47.

Figure 3.46. Circuit Board 3D modelling

3.3.3 The Case

With the help of the circuit board's 3D model and individual measurements, a case was designed to protect the components and the PCB. The design consisted of two separate parts sliding into each other. The circuit was securely held in place by using the M3 screw holes created on the board. The design was crafted by SketchUp software. The view of the case with the 3D object model of the board is shown in Figure 3.48.
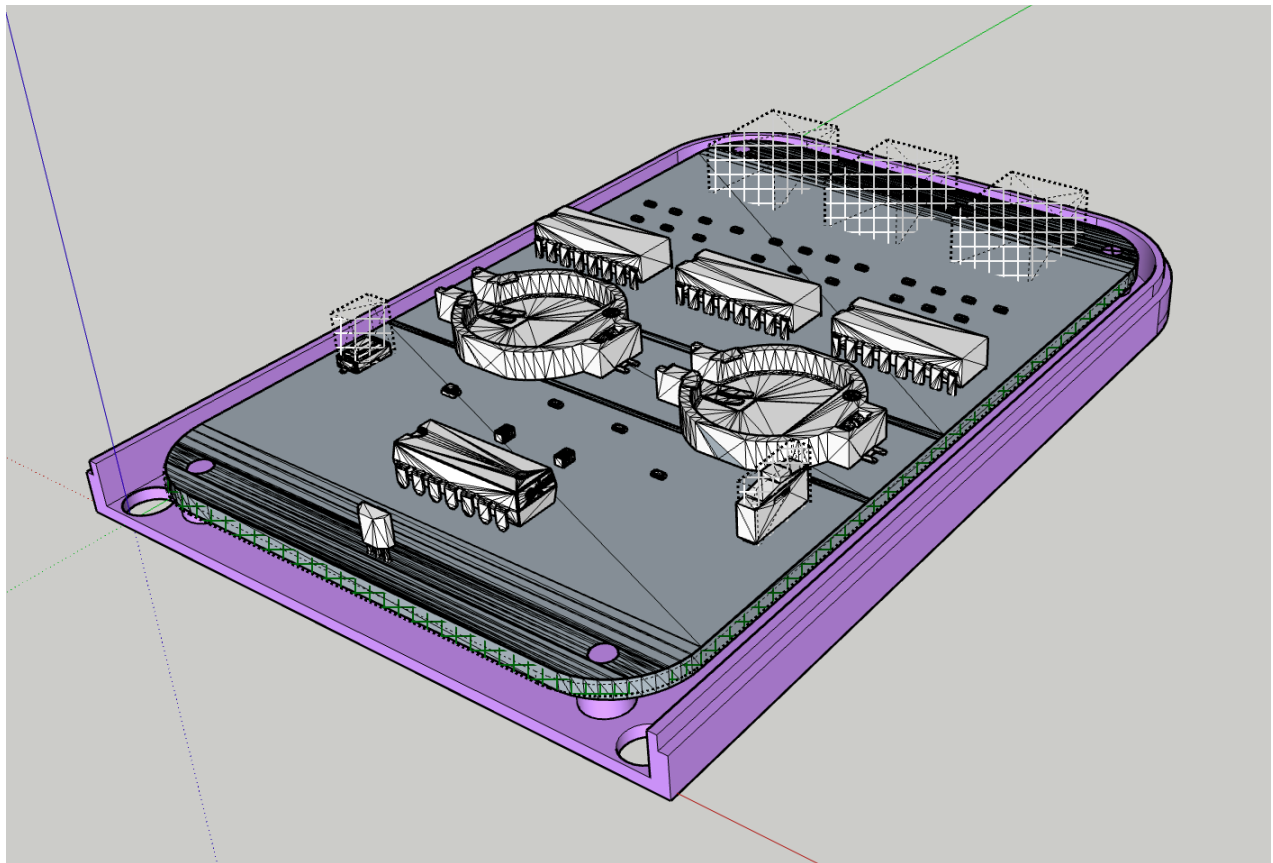
Figure 3.47. Modeling of the Electronic Circuit Board's Casing

The top part of the case was designed to avoid interference with the sensor, resulting in a visible cavity at the front of the case, as shown in Figure 3.49. Symmetrical dents were created over the button and switch to ensure accessibility. Additionally, a window was added for the indicator LED to enhance visibility.
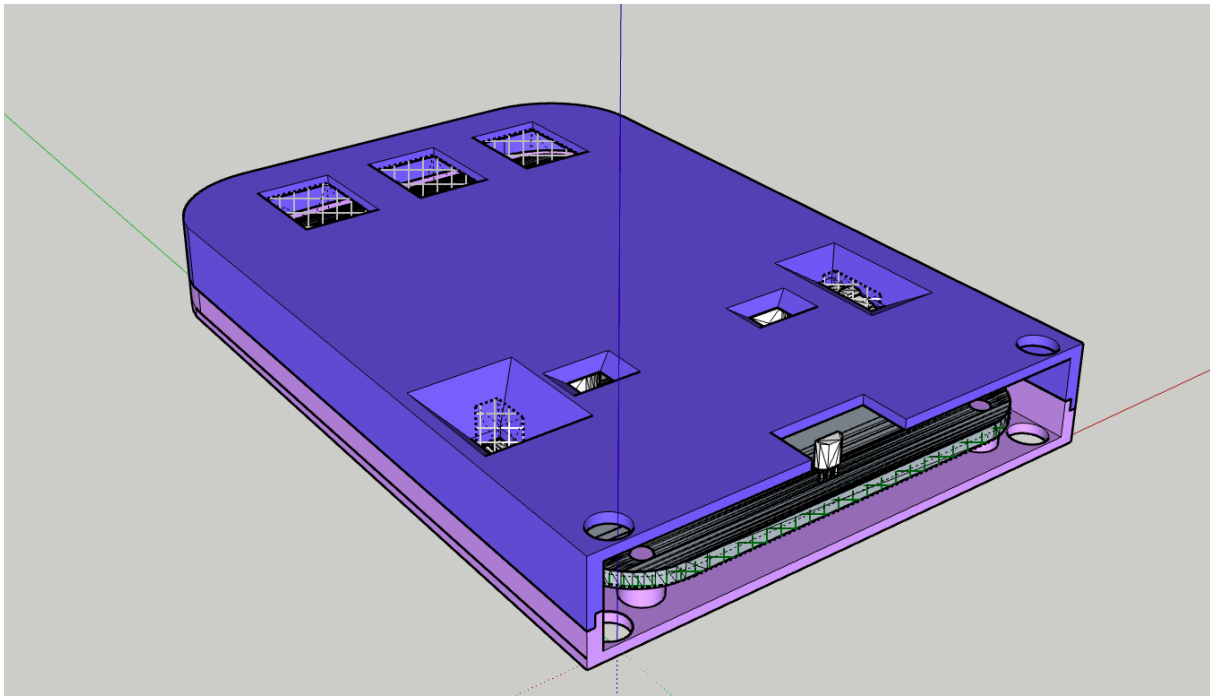
Figure 3.48. Case shielding designed by SketchUp

The case parts were printed by multiple 3D printers. The prototype was made by Creality Ender 3

Pro and had several assembly issues which were used as feedback to refine the design. The final

product was printed with a Stratasys F170 as shown in Figure 3.50.

Figure 3.49. Printed cases on Stratasys F170 plate. The case (grey) can be seen made of ABS
(Acrylonitrile Butadiene Styrene) plastic, on a white layer of QSR (Quick Support Removal)

The top part is assembled onto the bottom section and the circuit board. The circuit is fixed to the case only by four M3 stands, which extend to the top part of the case to support the assembly. Figure 3.51 shows the circuit board mounted on the bottom part of the case and the fully assembled case cover with the board.
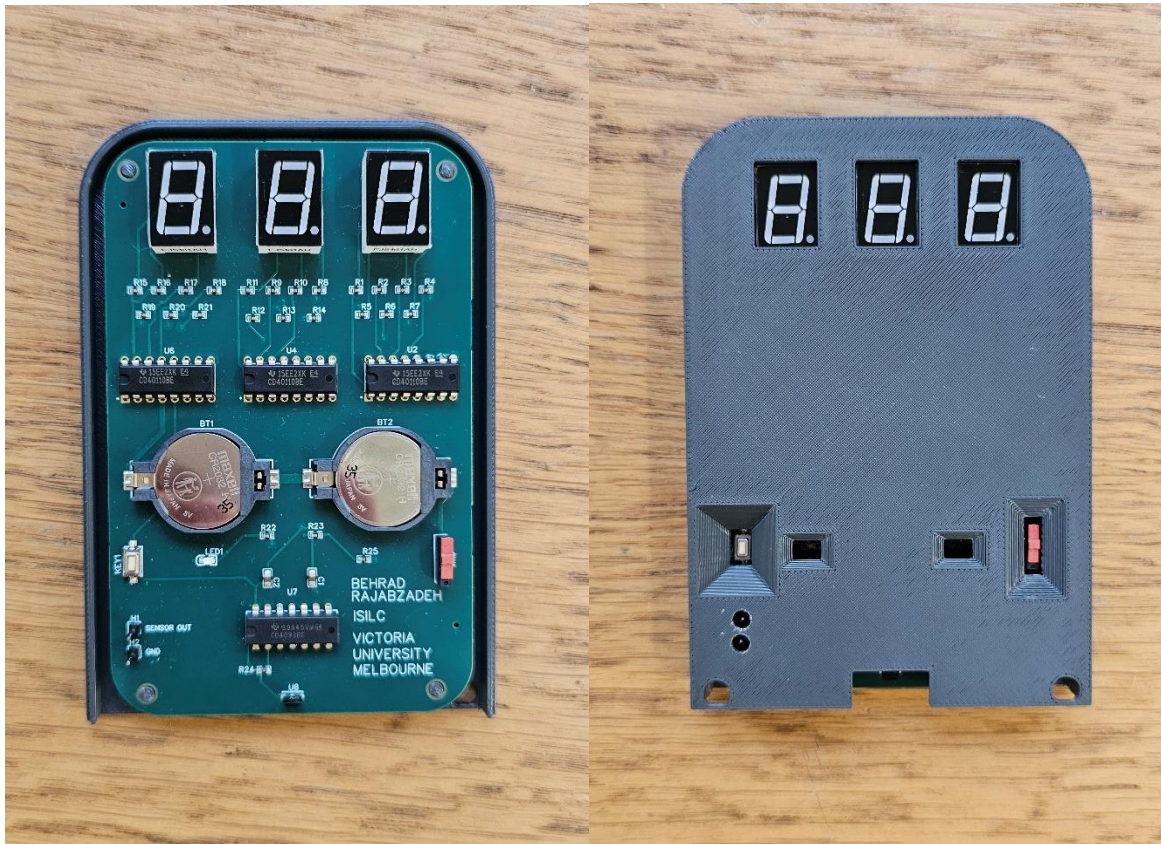
Figure 3.50. The Case Assembly.

The application of the case is to protect and shield the circuit and is used in the High-Speed integration of the system. To minimize the case's effect on the sensor's exposure, the bottom part does not have any surrounding walls. As seen earlier, there were some parts that did not have 3D models on the board. In this case, some of the parts were modeled and for other minor parts, the case was modified after 3D printing. The added modeled parts included the 7-segment displays, and post-manufacturing processing included the button accesses and sampling pinheader holes.

Chapter 4 : The Disk, Modelling and 3D Printing

The circuit board interacts with a Disk for rotation measurements. This interactive disk is responsible for:

- Safely housing magnets for coupling with Hall effect sensors.
- Including slits to act as a decoder for interaction with optical sensors.
- Withstanding high rotational speed for test conduction suitability.
- Being slim and lightweight for integration with various types of rotating systems.

To achieve the aforementioned characteristics and properties, several measures were taken into account, leading to a two-sectional design. This chapter explains some of the processes regarding the design and building considerations of this disk.

4.1 Disk Design and CAD Software

The disk is designed using the CAD software Onshape. Two parts of the disk were developed separately while ensuring perfect assembly and function. The sensor is supposed to be located at the bottom of the disk while it is spinning. Therefore, the bottom section of the disk had more technical considerations than the Top part and thus the design started with the Bottom part. The first consideration was the magnet's selection and housing. A market-available Rare-Earth magnet was selected before the design was initiated to ensure safe fitting and proper functionality. Multiple samples were purchased to test the application from different aspects, including safety, magnetic field strength, size and weight. The magnet selected for implementation was a 19 mm Rare Earth disk Neodymium magnet. The magnets used were purchased from the hardware retailer Bunnings and were ordered by EHI Australia under the brand name "Everhang". This magnet had a polarity assigned to each circular side of the disk. 3M adhesive sheets are attached to the magnet's north pole. Each magnet weighs around 10 grams, as measured on a pocket scale with a non-magnetic

plate. There were slight differences (approximately 1 gram) between the weights of the same magnets and it was endeavoured to select two magnets with the closest weights to keep the mass symmetry of the disk balanced. In the two-sectional design of the disk, the magnets were placed in the bottom section. To get optimal reading from the sensor interacting with the magnets in the disk, the bottom cap of the magnets was designed as thin as possible. The magnets are surrounded by thick walls attached to the bottom layer using chamfers and fillets. The housing of the magnet in the design can be seen in Figure 4.1.
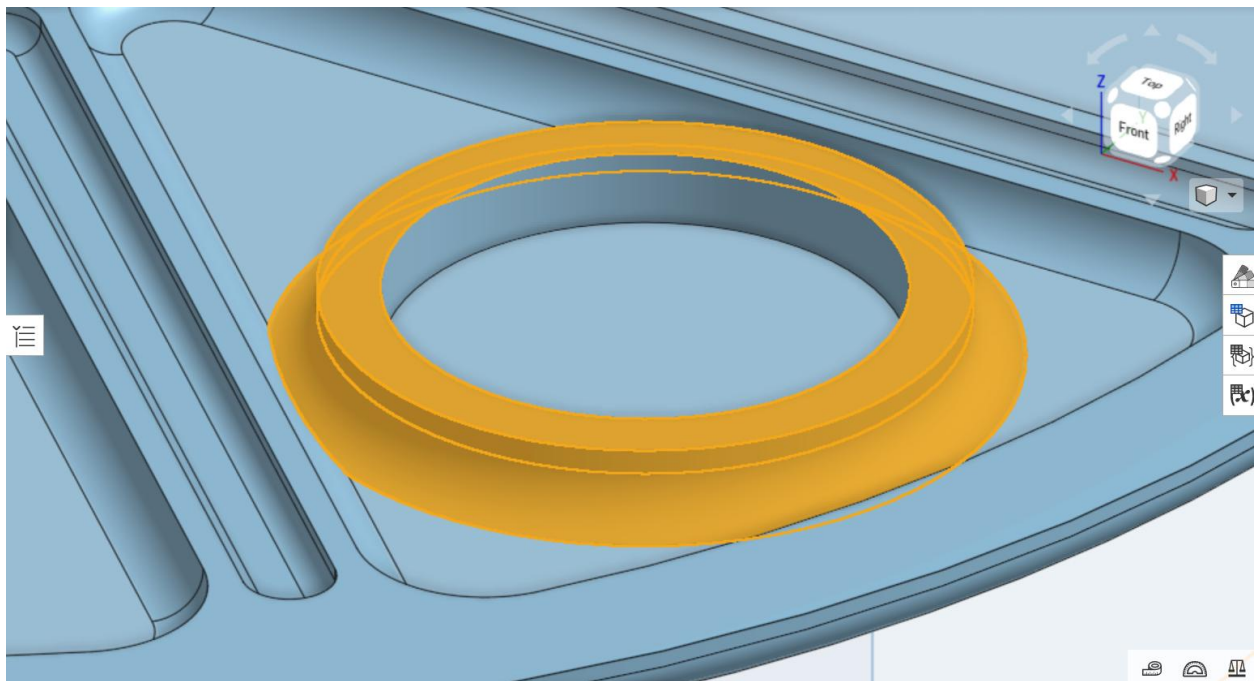
Figure 4.1. The housing of the magnet shown in the design. The outer surface of the magnet's shell is highlighted in yellow.

As can be seen, the disk is also characterized by triangular proportions. These portions have been dented and are filled with a raised segments when the top section of the disk is assembled on the bottom layer. There is a straight dent (bar dent) between each triangular portion. The total count of these straight dents is 8, only present in the bottom section of the disk, having multiple functions. The angular view of the bottom section design of the disk is shown in Figure 4.2.
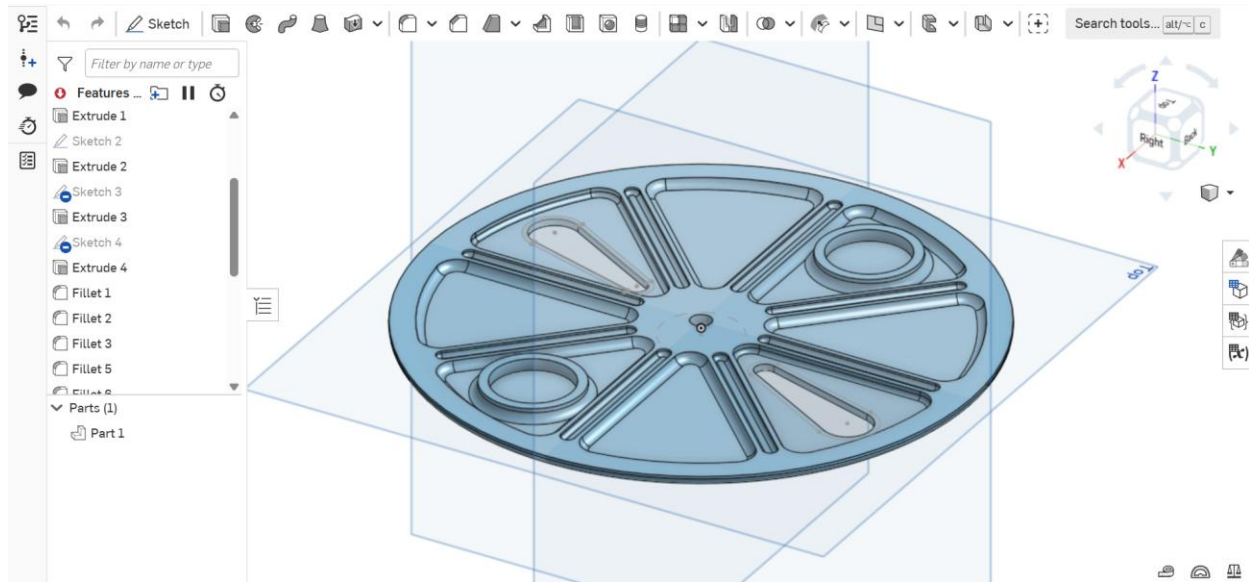
Figure 4.2. Angular view of the bottom section's design of the disk.

The bar dents increase the structural integrity of the disk by reducing and distributing the tensions caused by rotational movements. They also act as vents, flowing a controlled amount of air, preventing trapping and air pocket issues. The venting of these bar dents is discussed in the manufacturing process explanations, chapter 4.4 The Vents.

Since the disk is going to act as both a magnetic and an optical encoder, the slits have been added to the design with a special shape. The sections with slits are symmetrically in front of each other. To retain the symmetry of the encoder disk and to provide equal exposure for both magnetic and optical systems, the position of the line of the magnets and the slits have a circular/rotational difference of $\frac{\pi}{2}$ in reference to each other. The thin layer underneath the magnets does not pose any risks regarding the appropriate handling of the magnets by the disk. This is a result of forces that are going to affect the magnets in the rotational movements. Through spins, the sum of forces appearing on the magnets does not have a downward component. The force components are lateral and upward. Most of the lateral forces will be opposed by the circular walls surrounding the magnets. The upward forces can be hazardous and therefore, two measures have been

implemented. The first one is the adhesive sheet, fixing the magnet in place and the other one is the cap in the top section of the disk, as shown in Figure 4.3.
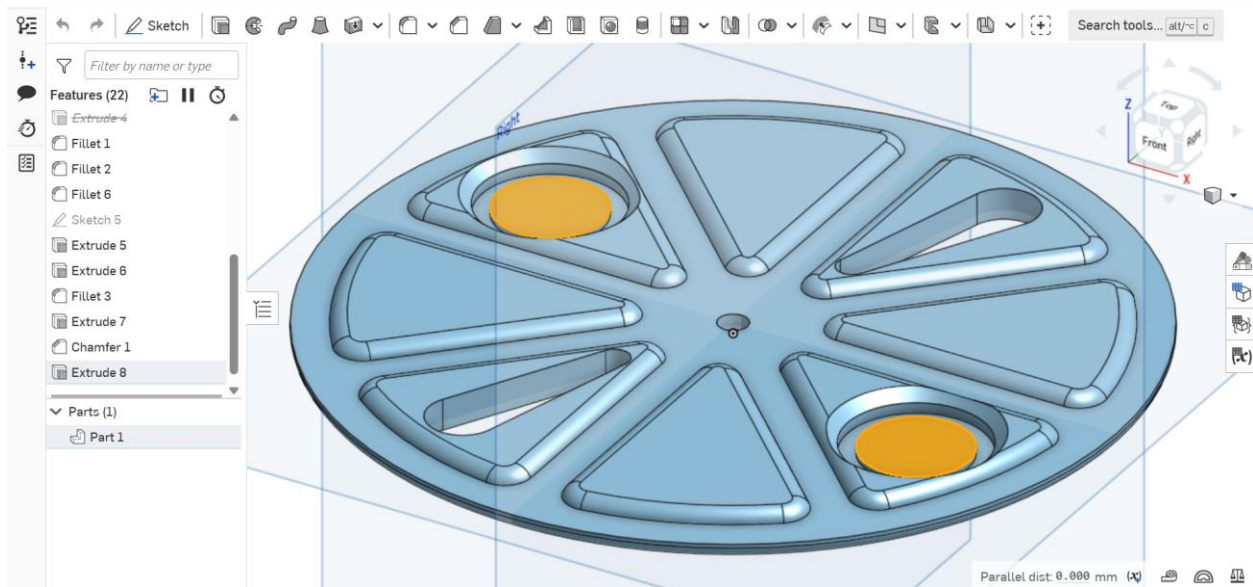
Figure 4.3. The top section design of the disk with the magnet holder caps highlighted in yellow.

All other parts of the top section are all convexed to fill the triangular concaves of the bottom section. The two separately designed parts were assembled virtually with the 3D models in the Onshape environment. Onshape has an assembly tool with different mating commands including Revolute, Fastened, Slider, Planar, Cylindrical and Tangent.

 Further modifications were made at this point to resolve assembly issues regarding mismatching dimensions, irregularities in the shapes, mismatched opposing chamfers and fillets, and gaps between the top and bottom sections.

The final gap between the parts is of utmost importance since the rotating part will be exposed to the flow and trapping of air where the gaps exist.

The assembled model of the disk is shown in Figure 4.4. The outer edges of both sections were equally filleted for safety, force distribution and better aerodynamics.
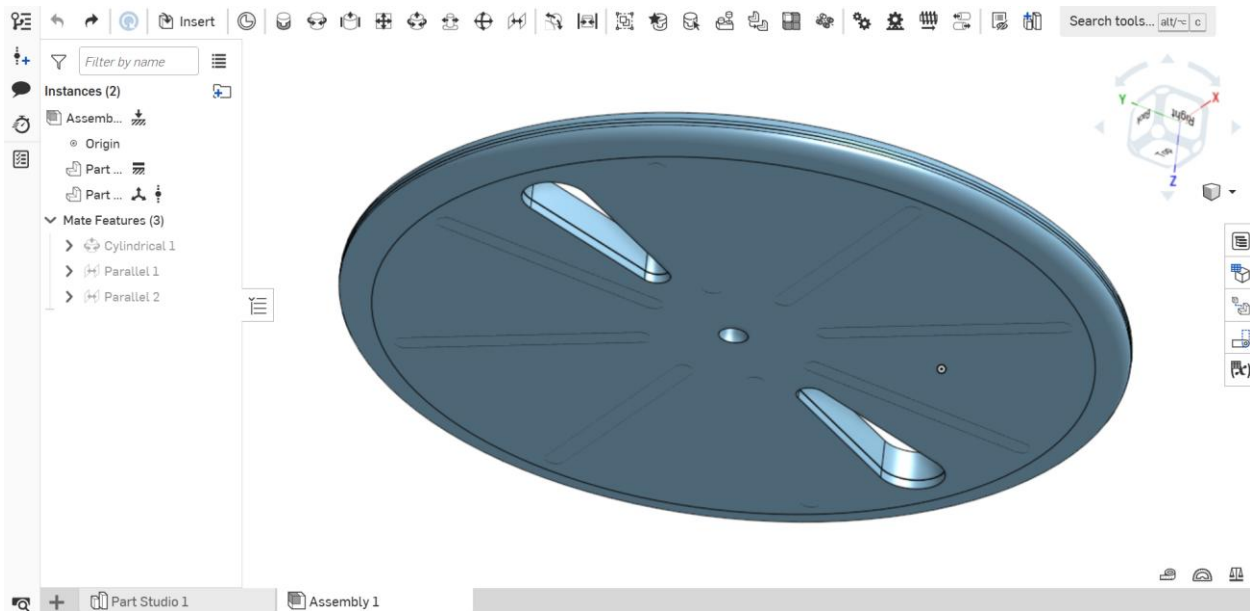
Figure 4.4. The two parts of the Disk design assembled.

The total thickness of the disk design was 7.36 mm, relatively thin and compact for an encoder disk, particularly considering its suitability for high-speed rotation and housing two large magnets.

4.2 Additive Manufacturing of the Disk

The disk was prototyped using various 3D printers, slicer programs, and materials (Filaments). The first attempt was using a Creality Ender 3 Pro. The printed product had multiple imperfections, making it unsuitable for any practical usage. As the next step it was decided to change the material and the settings on the same 3D printer. The chosen material was a PA (Polyamide, also known as nylon) reinforced with carbon fiber. The filament was ordered from China and although several attempts were made to change the setting of bed temp and the nozzle configuration, the manufacturing process failed. It was then decided to change the printer and an Ultimaker 3 was utilized. This time with the original filaments of the same brand being used to achieve better results. As shown in Figure 4.5, a sealed roll of Ultimaker Nylon Polyamide was used to print the

disk parts, but several issues appeared in the final product.

Figure 4.5. The filament used with Ultimaker 3

The most important issue was the excessive flexibility. The encoder disk needs a certain amount of rigidity for proper functionality when used in high-speed rotational settings. This is even more crucial when the integration of two magnets are intended. The other issue was the supports used for printing. Since the printer uses the same material for part printing and supports, the support and the parts were attached and the removal was not ideal. Various techniques were used to remove the support from the material efficiently. The best removal was achieved by making a small and sharp cut in the support and using the cut to expand it to the edges. The printer was also strung throughout the printing process, with unremovable strings remaining in the product. Brushing was used to remove the strings, but it could not remove them as needed. Figure 4.6 illustrates the support structure, the partial removal of the support using the previously explained technique and some of the stringing.
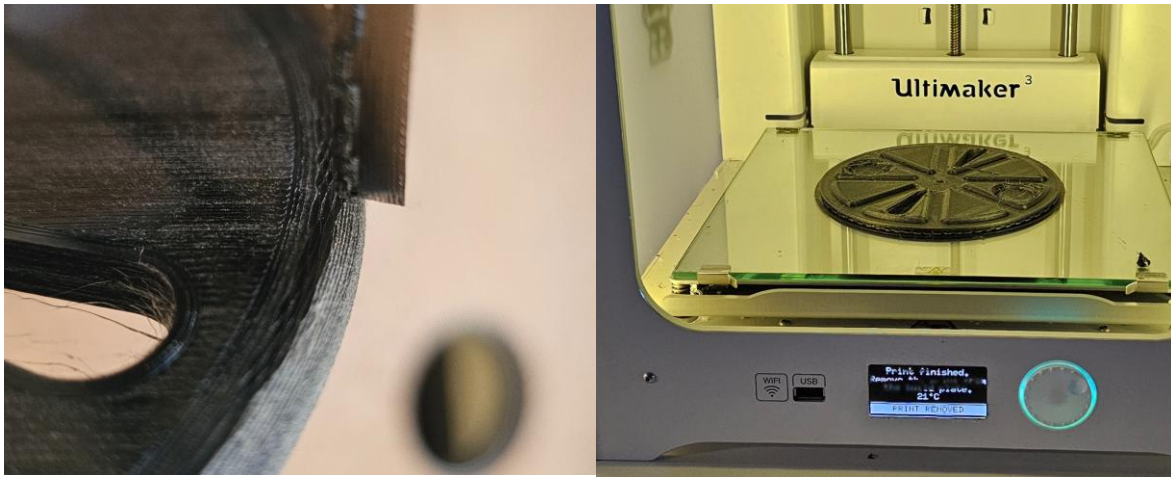
Figure 4.6. The support, the partial removal of the support with the explained technique and some of the stringing.

However, the disk was tested for high-speed rotation without the magnets and could withstand very high RPMs. This was mainly achieved by setting the infill density to 30% and using the Gyroid pattern. The Ultimaker slicer settings are shown in Figure 4.7.
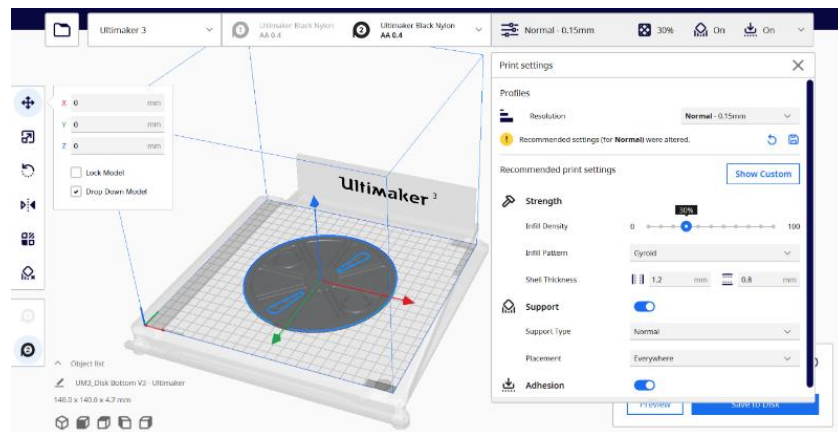
Figure 4.7. Slicer settings including the shell thicknesses aligned with the design characteristics

As the final attempt for disk additive manufacturing, a 3D printer with a controlled printing chamber and a separate support printing system was used. Stratasys F170 is a professional 3D printer device, used internationally for precise prototyping of parts. The printer has a climate chamber for a controlled printing environment. It uses two materials for support and part printing. The part is not directly printed on the printer's plate; instead, a precise support surface is printed

underneath the part. The settings of the F170 were fixed, as no modifications were permitted to be made to the system. Though the printing resolution was not high, benefiting from assistive technologies, the printed parts were of acceptable quality. The printed disk weighs around 87 grams. The goal was to keep the overall mass close to 100 grams with the magnets installed. Figure 4.8 shows the Stratasys F170 printing the disk parts and the bottom section of the printed disk.

Figure 4.8. The picture on the left shows F170 printing the disks. The printed bottom part of the disk is shown in the picture on the right.

The bottom part was only 32 grams while the top part weighed around 55 grams. This is a result of using the top section as a protective measure for holding and restricting the magnets in case of accidental detachment from the bottom section. With the upward forces summing on the magnets, it is crucial to make the top section with proper rigidity.

After printing the disk parts, the magnets were installed on the dedicated sections. After installing the magnets using the 3M adhesive sheets, the disk was fully assembled and rested for 24 hours. Then, a motor was used to spin the disk with the magnets starting from 500 RPM for the disk to get balanced. This was continued by rotating the disk for 15 minutes, using up to 2000 RPM to achieve equilibrium. After curing the disk with this method, the top part was dismounted to observe the disk, the internal structure and the magnets. No sign of damage, deformation, or tear was observed (Figure 4.9).
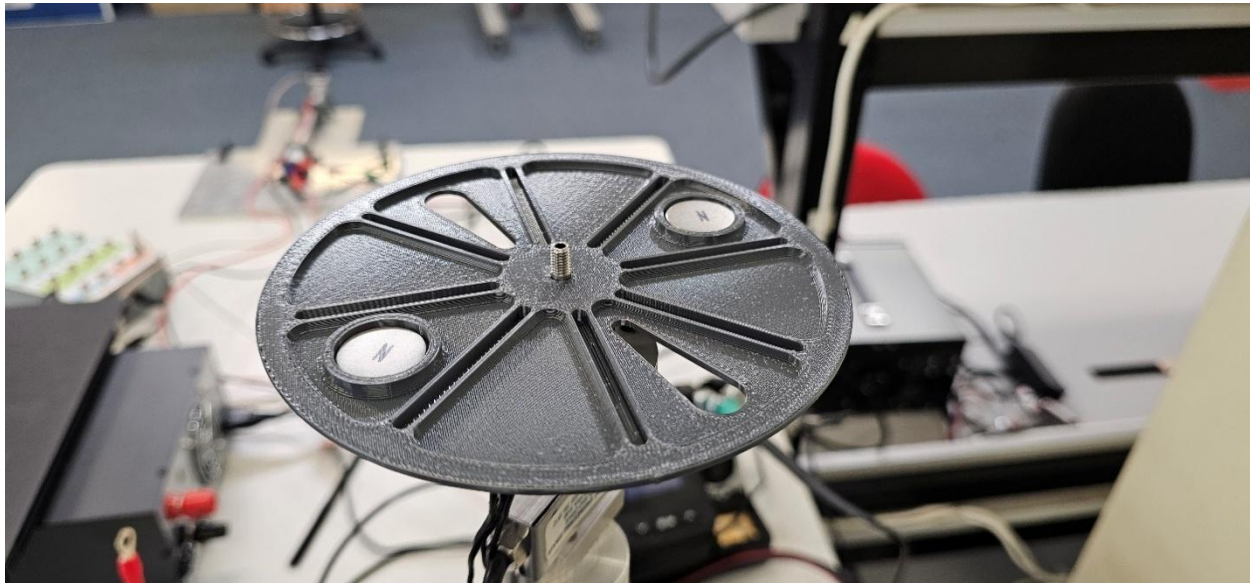
Figure 4.9. The disk's bottom section, after disassembling the top part it has come to a state of equilibrium after being cured and treated by high-speed rotations.

4.3 Ansys Simulation

The geometry was imported into Ansys Mechanical for analysis. The inner edge of the disk was selected for displacement. All the displacements except for the z-axis rotation were set to zero. The z-axis rotational displacement was set to "free" and the default of 6 modes was chosen for analysis. The natural frequencies of the disk are shown in Table 4.1.

Table 4.1. The natural frequencies of the disk obtained from the Ansys analysis.

Mode	Frequency (Hz)
1	626.43
2	1305.1
3	1349.4
4	1398.6
5	2428.5
6	2515.2

It can be seen that the first natural frequency is 624.43 Hz. To convert this to RPM, it should be simply multiplied by 60. Therefore, the first natural frequency of the disk will occur when the disk is rotating at 626.43 Hz × 60 = 37,585.8 RPM.

This is very efficient and proves that the disk will work optimally within rotating systems. This will ensure that with any RPM below 37.5K, the disk will not resonate. The deformation of the disk was also analysed (Modal).

The deformations at the start and also close to the first natural frequency (at 33.629 RPM) are illustrated in Figures 4.10 and 4.11.
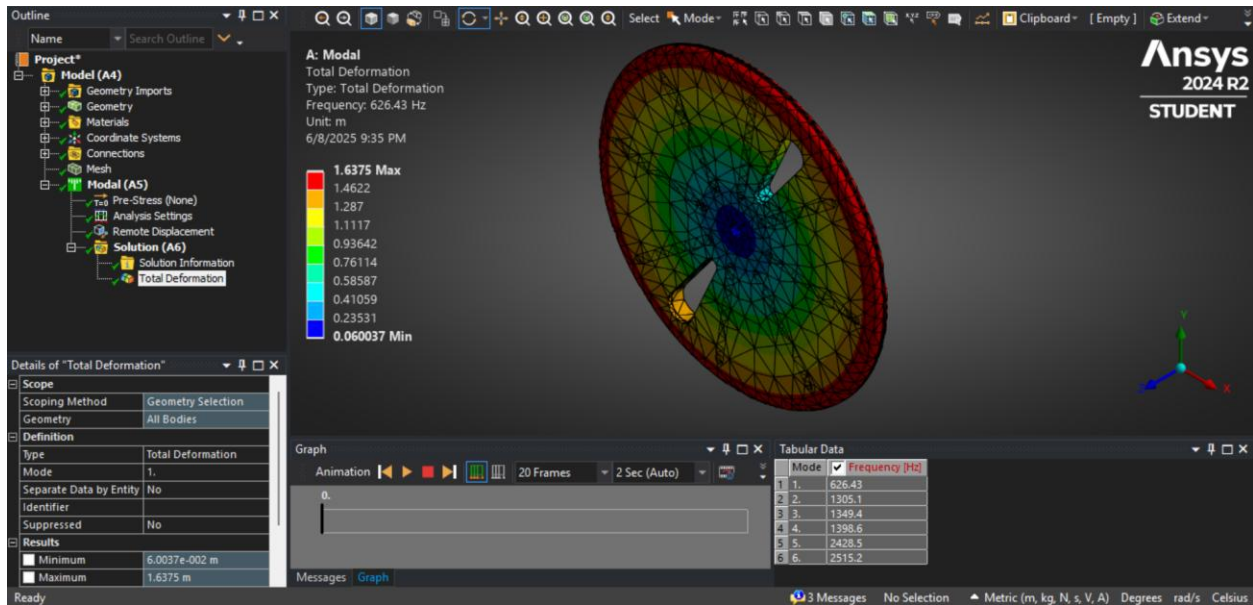
Figure 4.10. The deformation analysis of the disk initiating rotation.
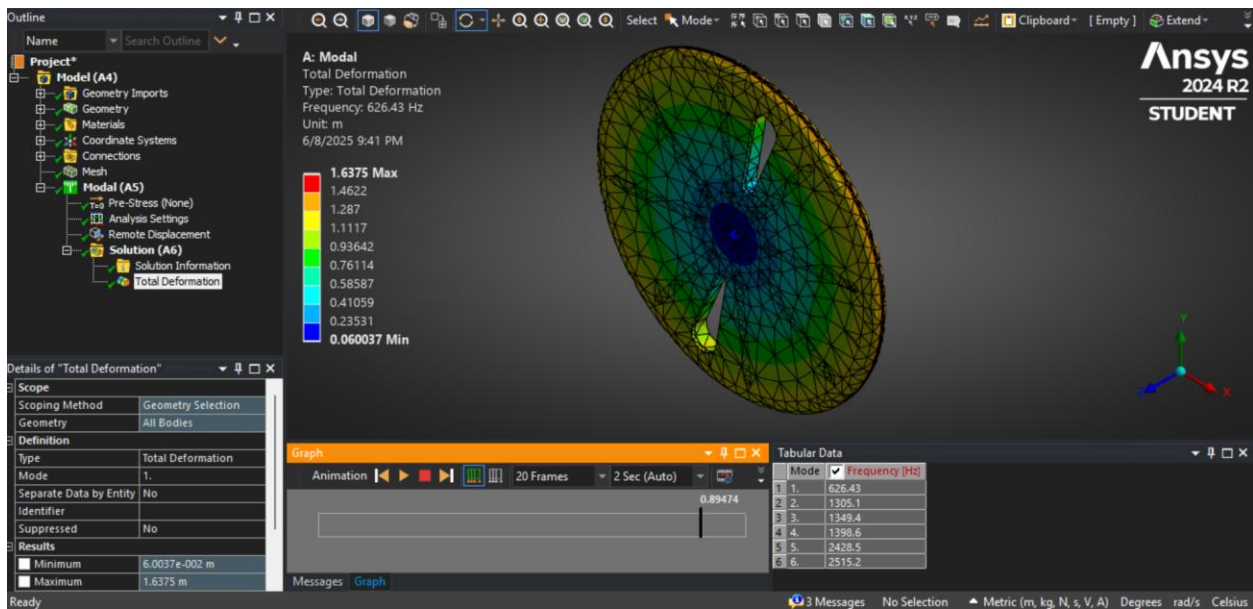
Figure 4.11. The deformation analysis of the disk rotating at 33.629 RPM, close to the first resonance frequency.

As shown, the disk's structure performs well in handling stress and deforming forces in rotational movements.

4.4 The Vents

The effect of air on the disk is significant since at high speeds the built-up pressure can damage the two-sectional disk. To avoid the formation of vacuums and trapped air pockets, multiple air vents have been created in the bottom section of the disk. To create these vents, the floor thickness of the bar cavities has been reduced to match the thickness of the solid formation of a single row of travel by the printer's nozzle. This results in accurate vents in different forms based on the location of the cavity bars with controlled airflow. Figures 4.12 – 4.14 illustrate these vent structures through microscopic shots.

Figure 4.12. Diagonal air vent patterns.
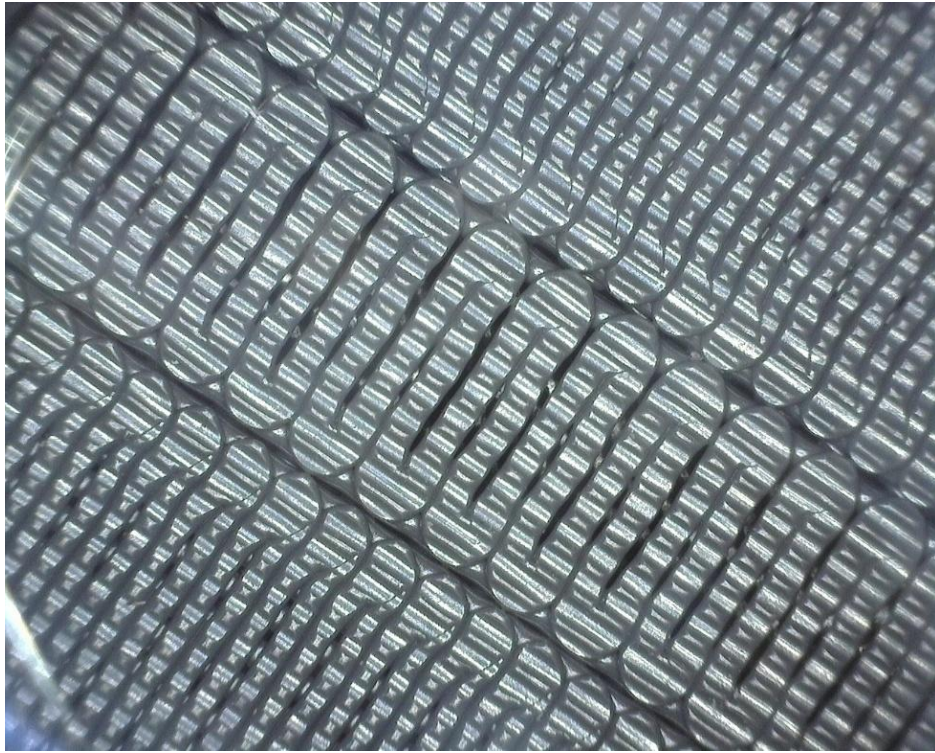
Figure 4.13. Vertical air vent patterns.
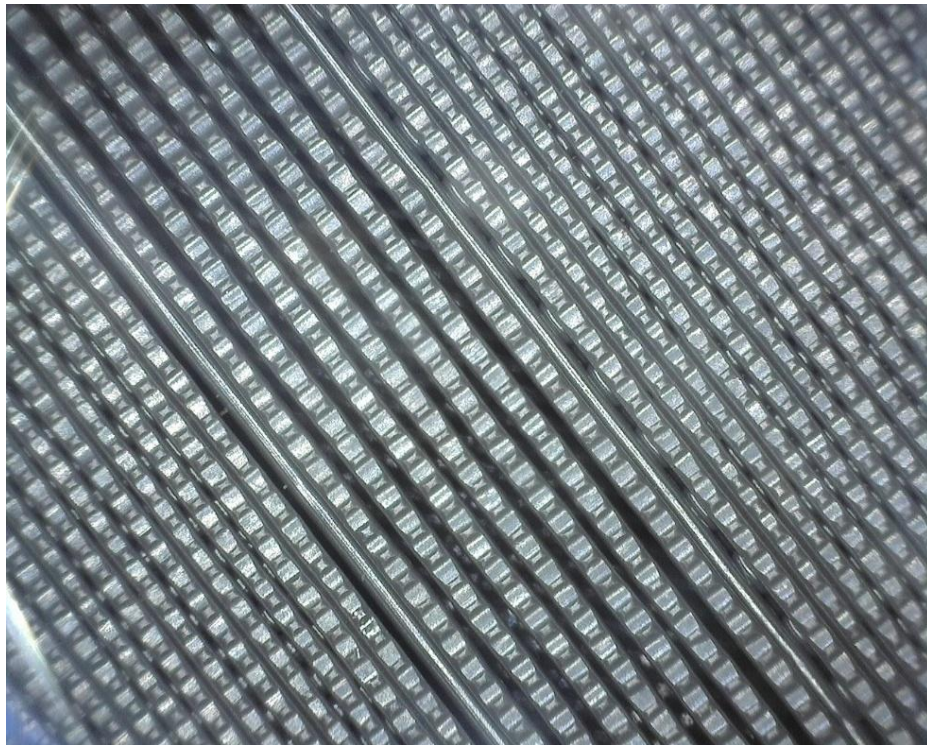
Figure 4.14. Horizontal air vent patterns.

Chapter 5 : Implementation, Tests and Experiments

A series of tests and experiments conducted on and with the designed system are discussed here. A number of remaining activities are mentioned on chapter 6.2 Future Work.

5.1 System Integration on a High-Speed Setup

A high-speed setup available at Victoria University's Footscray Park campus was chosen for system integration. The setup was primarily not working, and all the major parts were replaced. The movement of this setup is a T-Motor F60 Pro V KV1950. The mounting on the encoder disk was designed to match the titanium alloy shaft of this motor. An Aikon AK32 35A driver was connected to this motor to control the speed. The driver feeds from a B&K Precision 1694 DC Power Supply. The power supply was set to 18V without current limitation being set. For the experiment, the main outputs of the power supply on the back panel were used. The motor driver also receives a control voltage signal. A National Instruments NI USB-6009 data acquisition device generates this control signal. The whole setup is mounted vertically on a shaft, fastened with bolts.

The encoder disk, with a thickness of 7.36 mm, was mounted on the high-speed motor directly. The dimensions of the motor shaft were aligned with an M5 screw. To give the disk standard clearance for assembly, the disk housing had a 5.2 mm diameter. Two circuit boards were installed below the encoder disk, each with a different sensor. The optical and magnetic sensors were positioned within 90° relative to each other, aligned with the radian angular difference of the slits and the magnets on the disk. This hybrid sensing system is hereafter referred to as The Validist Encoder as shown in Figure 5.1. Additional information and details have been mentioned about the output process of the Validist Encoder at the end of chapter 5.1.
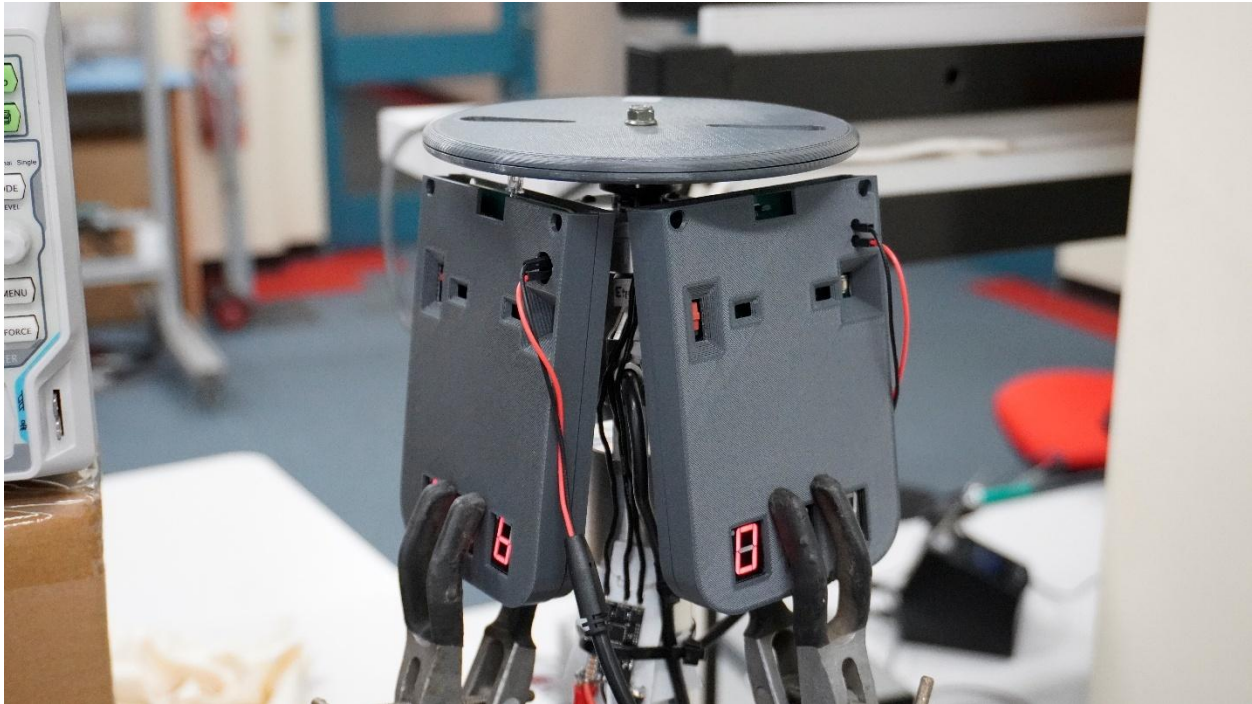
Figure 5.1. Validist Encoder System Implementation on the Highspeed setup.

The red and black cables connected to the circuit boards are connected to the channels of an oscilloscope. A cage was utilized to bound the rotating setup for safety and the boards were fixed with magnetic switch base clamps. A piece of a reflective tag was attached to the disk to be used for RS CT6 Tachometer for additional measurements. Some of the experiments were recorded using a crop sensor camera. The experiment apparatus and setup can be seen in Figure 5.2. The National Instruments 6009 was connected to a Windows computer running NI-DAQmx software, controlling the analog output (control voltage) of the channel used on the NI 6009. The oscilloscope was configured to show both activated channels on the display. Chanel One (Yellow) displays the Hall effect sensor output and the Blue graph (Channel Two) illustrates the output of the phototransistor. The oscilloscope also shows the calculated frequency value for each signal. The trigger setting was set to Rising Edge from the channel 1 source at 1.6V level.
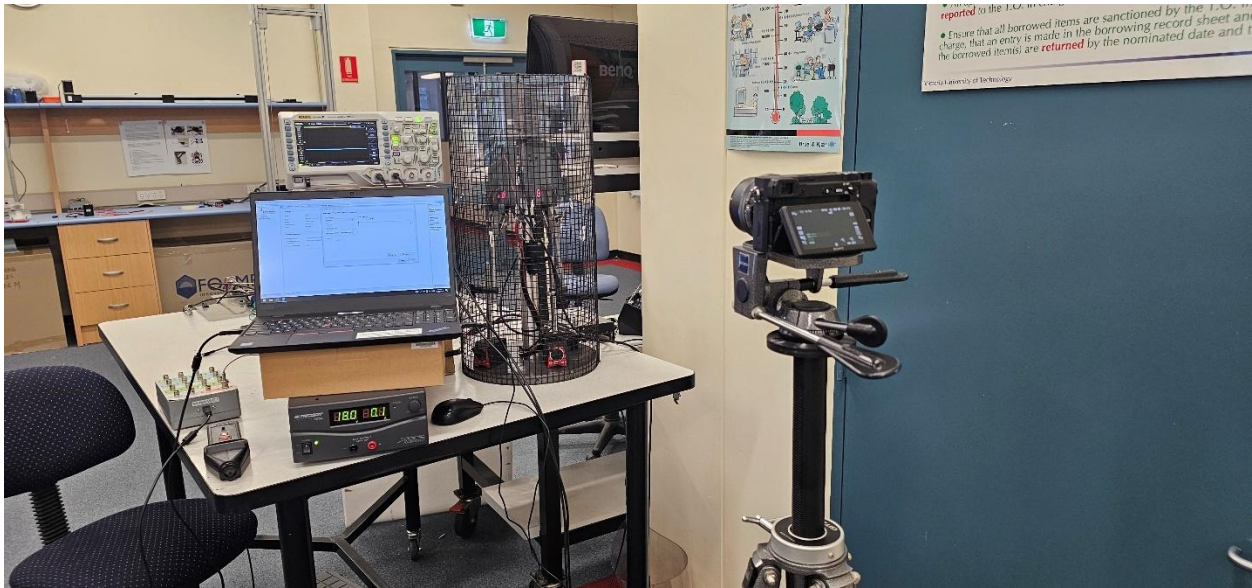
Figure 5.2. Highspeed test apparatus and setup.

To avoid extreme force concentration on the motor and the disk, the speed was increased gradually in multiple steps. This was done with precision, using a coaxial cable connecting the motor driver to NI 6009.

The control voltages applied through NI-DAQmx were accumulatively applied in small steps, starting from 0.3V, resulting in around 1300 RPM. The next step was only 0.1V increased and the RPM value increased to around 2100 RPM. This continued to achieve a speed exceeding 4000 RPM on the unit at the final stages, as shown in Figure 5.3.

To trigger the phototransistor, a light source was placed over the roof of the safety cage, illuminating the area above the sensor aligned with the slits on the disk.
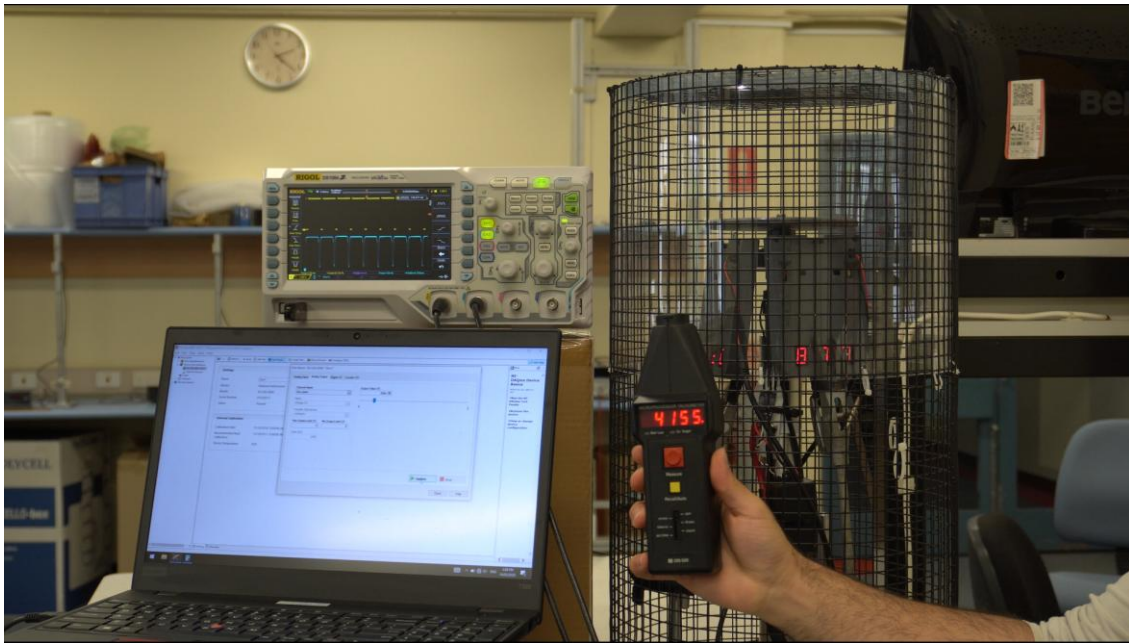
Figure 5.3. Final stages of the highspeed experiment. The tachometer showing a reading of 4155 RPM.

The speedup process reversed after the final stages with the same method to reduce speed until complete standstill of the disk and the motor. The sensor outputs when the rotation is decreasing to stop, can be shown in Figure 5.4 as no voltage is applied to the motor.
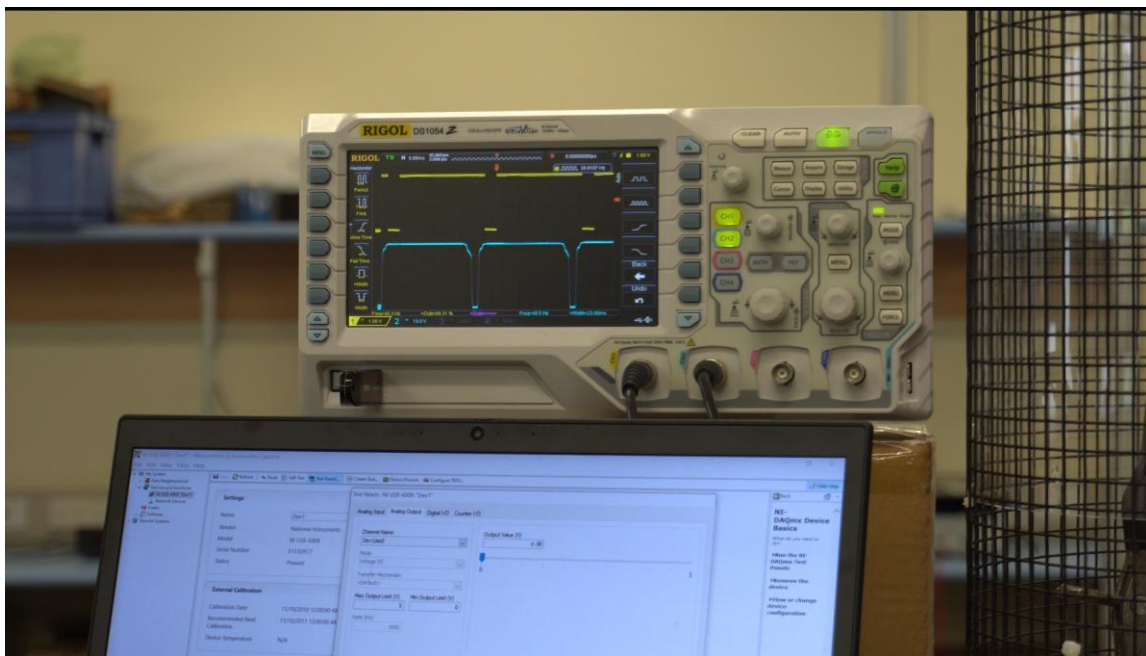
Figure 5.4. The output signals of the sensors decompressing as the control voltage is not applied and the motor's speed is reducing.

Signals shown in Figure 5.5, represent the system's activity at the highest speed reached. Since

the disk had two slits and two magnets, for each rotation (revolution) two exposures occur. To

convert the frequency (f) of the signals to RPM of the setup, Equation (5.1) is used.

$$RPM = \frac{f}{2} \times 60 \qquad\qquad (5.1)$$
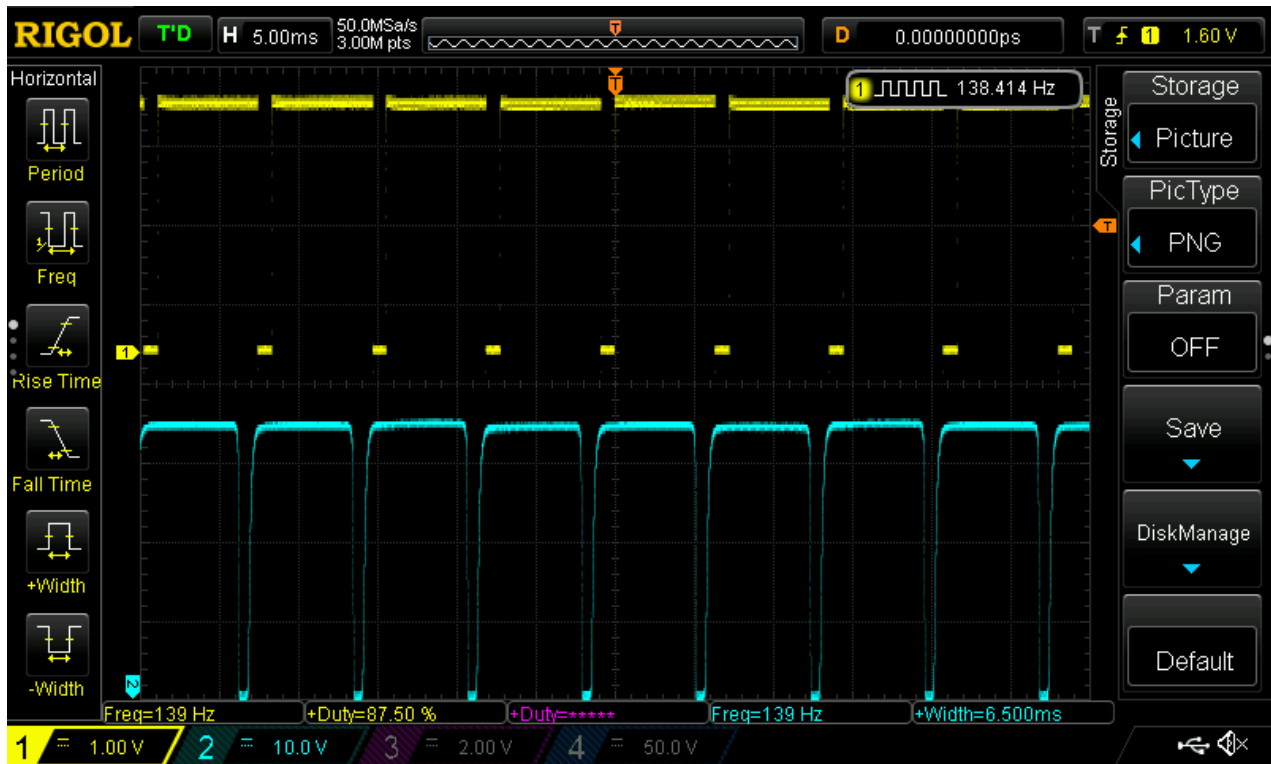
Figure 5.5. The system signals at the peak speed of the experiment.

Based on the equation, the RPM of the system is as shown below:

$$139_{(f)}/2 \times 60 = 4170 \text{ RPM}$$

Figure 5.6. The equivalent RPM based on the frequency (f) of the signals.

As illustrated in the signal graphs of the optical and magnetic sensors, the system behaves perfectly

in both methods, interacting with the encoder disk. The signals are in-phase and with the same

frequency, meaning that the system is very reliable. This unique system offers a hybrid encoding system that can be integrated with an AND logic gate between the two outputs, providing a very accurate measurement device for RPM in sensitive applications. Based on the application and usage, the outputs of the devices can be fed to an OR gate as, where false readings are essentially avoided. I have named this one-of-a-kind system The Validist Encoder, referring to its capability of validating the output based on the hybrid design and the gate used.

The experiment was also conducted with the disk made of Nylon. As discussed in Chapter 4, the nylon printed disk using Ultimaker 3 lacked rigidity and thus was not suitable for use on a hybrid system since magnets could not be installed safely for operation. However, without magnets the system was used with only optical exposure sensing, relying on the slits of the disk for measurements. It was successful at reaching a significantly higher RPM by virtue of the material, higher printing resolution and not housing magnets. The signals generated with this disk at the peak speed tested are shown in Figure 5.7.
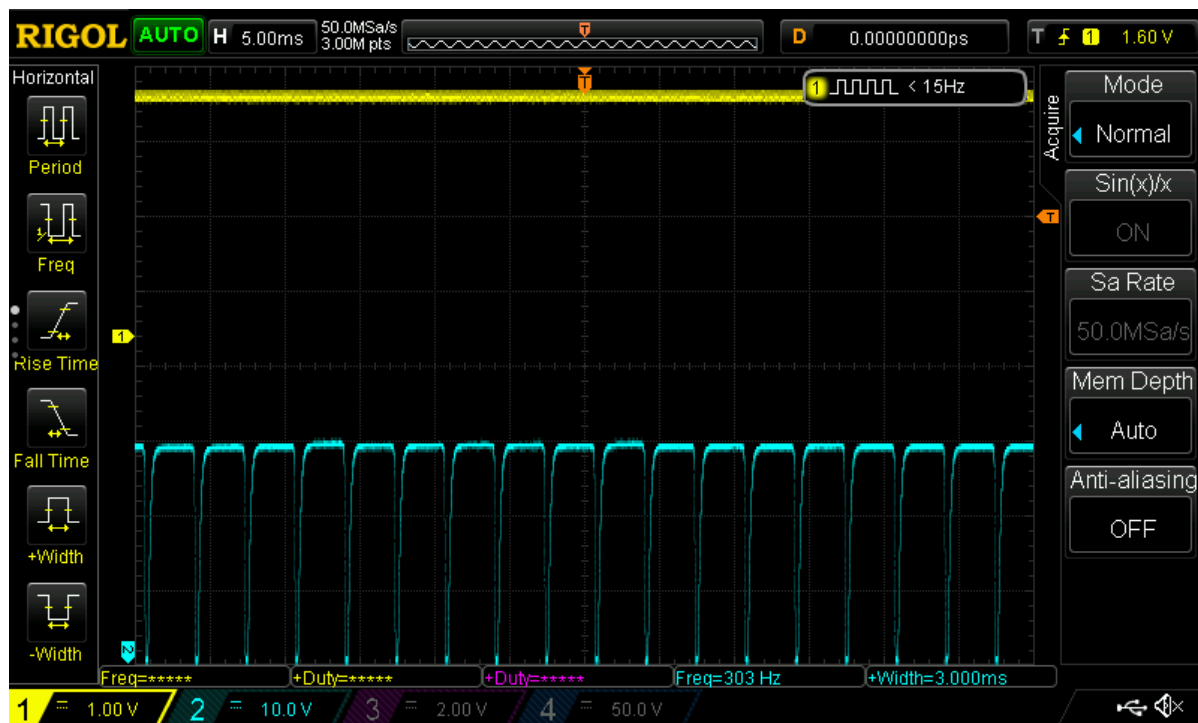
Figure 5.7. The signals generated by the Nylon disk without housing magnets.

As illustrated, the signal frequency is 303 Hz and based on the architecture of the disk (having two slits) converts to $\frac{303}{2} \times 60 = 9090\ RPM$ which is the same as the Highest RPM most cars can achieve.

5.2 Climate Chamber (The Temperature Test)

With the device's practical success in the high-speed experiment, additional testing was conducted to determine the system's reliability. The first test was performed using a custom-made climate chamber (Figure 5.7), changing the temperature of the circuit board while powered on by setting an extreme temperature alteration program.

Figure 5.7. The climate chamber.

The circuit board was placed on a piece of paper (Figure 5.9) to avoid shorting because of the metal mesh of the chamber. The board was temperature-probed through a machinery hole to measure the actual temperature of the circuit in depth. The circuit was powered on and a single exposure was made to keep the counter at 1.
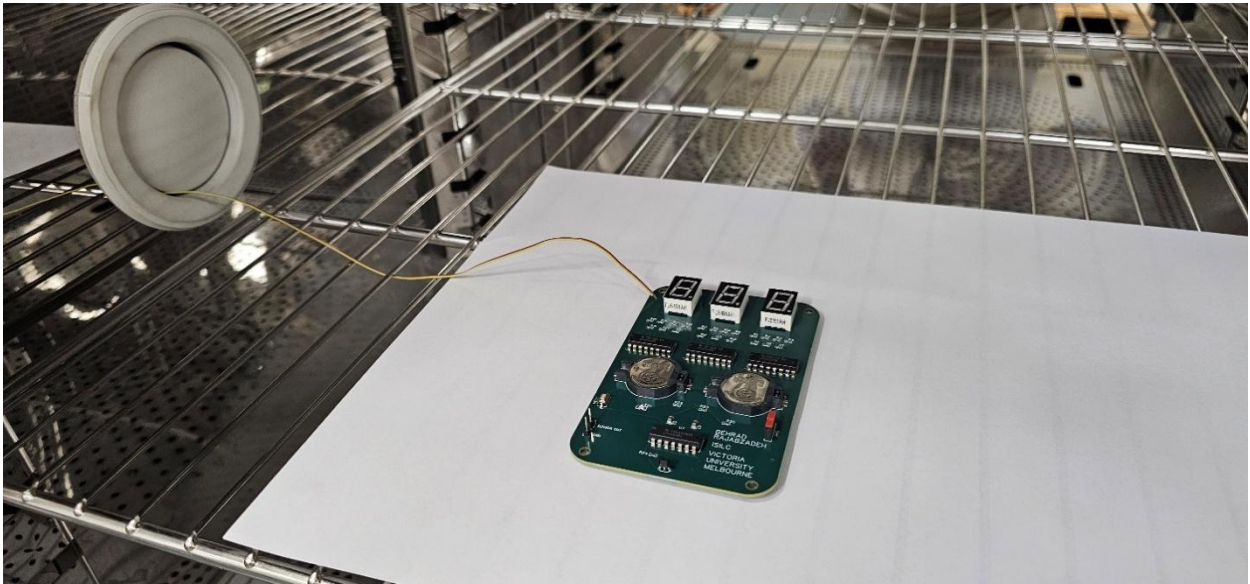
Figure 5.8. Placement of the circuit board in the climate chamber.

Program below (Figure 5.10) was used for the climate chamber.

Figure 5.9. Programming of the climate chamber.

Although several temperature interruptions were caused by the chamber's power supply issues, the overall goals were achieved. The lower limit of the temperature (-10°C) reached with no malfunctions observable on the system is shown in the Figure 5.11.

Figure 5.10. The lower temperature limit of the test.

The test continued with an increase in temperature until the chamber reached the program's upper limit, around 75°C. After equilibrium, the board temperature reached 73.7°C based on the measurements of the temperature probe as shown in Figure 5.12.
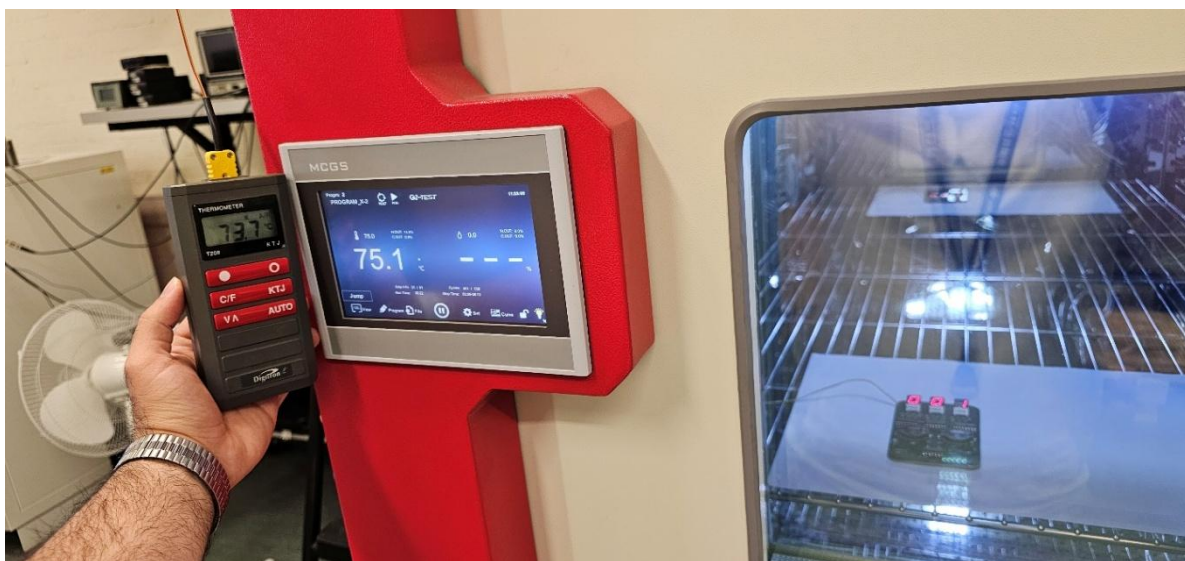
Figure 5.11. Chamber and board temperature.

The climate chamber was opened at this point and the sensor's temperature was measured using an IR noncontact thermometer with a recorded value of 72°C. The circuit board did not record any false exposure detections (The counter remained at 1) while it was fully functional at this point. The functionality of the circuit board was tested twice with two separate magnetic exposures, which were detected and recorded without any issues. The entire temperature curve of this experiment is shown in Figure 5.13.

Figure 5.12. Temperature curve of the experiment.

5.3 Power Consumption Test

To measure the power consumption of the system accurately, the copper track connecting the output of the battery to the main power switch was placed on the top layer of the circuit board at the circuit design stage. This was done to enable a power consumption test by scratching the mask

of the track, exposing the copper and creating a cut by removing a small amount of it in the middle of the connection. After cutting the exposed copper track, an ammeter was connected in series with the disrupted connection to measure the current in the track while the device was operating as shown in Figure 5.14.

Figure 5.13. The circuit's current measurement for power consumption assessment.

With 20.8 mA of current flowing through the main power track of the board, the power consumption can be evaluated based on the calculation below, since the maximum voltage of the series batteries is around 6V.

$$P = I \times V = 20.82 \text{ mA} \times 6 \text{ V} = 0.12492 \text{ W}$$

The maximum measured current was 23.26mA. With a 240mA nominal capacity for each of the batteries, **the device is capable of operating for more than 20 hours** by itself with the onboard batteries, as shown below.

$$(240 \text{ mAh} \times 2)/23.26 \text{ mA} = \mathbf{20.63 \text{ hours}}$$

5.4 Magnetic Exposures on Texas Instruments DRV5023

The Magnetic interference effect on each sensor is different and related to various factors. Since one of the uses of the developed system was to test the effect of influential factors on the sensors, some basic tests were conducted with the magnetic Hall effect sensor on the device. All the results were as expected, except one interesting finding on the behaviour of the Hall sensor. Despite the claims of the Datasheet regarding capabilities of the Hall switch to only react to the South pole of a magnet (defined as a south pole near the marked side of the sensor), it was observed that with the magnets north pole close to the backside of the sensor, DRV5023 reacted, and the switching occurred. In another case, with the magnet disk standing horizontally above the sensor with the south pole on the marked side, DRV5023 demonstrated the same behaviour. However, when the magnet disk was flipped, the sensor did not recognize it when it was directly placed above it and by any small displacement, the detection occurred simultaneously.

5.5 IR Exposures

With the use of the phototransistor in the system, severe vulnerability to external IR exposures was observed. The circuit indicated a saturated exposure when near sunlight, whether it was direct or not. This was not the only infrared interference detected, as the Lab lights were also affecting the sensor drastically. With the rapid PWM (Pulse Width Modulation) flickering of the lights used, the system started counting exposures since the light source had enough IR radiation density to simulate an encoder activity. Industrial environments are no exception when it comes to IR pollution, since there are various sources present. This can include:

- Visible light sources
- Sunlight
- Communication devices

- Proximity systems
- And any high-temperature object, etc.

Modulation in the sense of setting the signal conditioning circuit to only react to a particular pulse of the IR beam with a specific band of frequency is a highly practical solution, which will be discussed briefly in the conclusion and future work chapter.

5.6 Angular Errors

Both the magnetic and optical encoder systems are prone to displacements of the sensor and the encoder disk. This is more pronounced in optical systems, although many factors related to the sensing mechanism play significant roles. A domed epoxy lens was used in the packaging of the IR sensor used on the circuit board in this project. Due to this lens, the visibility of the sensor becomes peripheral. This tunnel visioning is mainly caused by the shape of the lens and can change drastically based on the type of sensor and the way it is manufactured. The sensor's tunnel vision comes with its pros and cons. Its advantages include less susceptibility to unwanted ambient IR radiations and a better range of view with focus. Contrarily, the sensing is more reliant on the precise alignment of the IR transmitter (source) and the sensor. This also caused issues if the encoder disk has any displacements, altering the vision of the sensor through tilted slits. These errors were observed in the Hall effect sensor system, but the effects were minimal.

Chapter 6 : Conclusions and Future Work

With each of the encoder systems having downfalls unique to their basis, hybrid encoder systems are a practical answer where precision is required. The best combination for this hybridization is achieved by choosing two frequently used methods for rotational speed measurements, which are magnetic and optical sensing. In professional practice, there have not been noticeable attempts to develop such systems, either for research or industry. The pre-existing models mostly exist as patent ideas with low to no practicality, causing drawbacks in turning these ideas into functioning models. In this project, a novel state-of-the-art system (The Validist Encoder) was fully designed, developed, implemented and tested (Figure 6.1), successfully from scratch.

Figure 6.1. The hybrid encoder system (Validist Encoder) with the optical sensing on the left and the magnetic sensing on the left.

6.1 Thesis summary and Conclusion

The thesis initiated by an introduction covering the necessary information for the reader to become familiar with the project, its significance and the methodology used. This was continued with an in-depth background familiarizing with the basics and advanced knowledge of sensors, sensing

and measurement systems finalized by a literature review capturing the closest research undertaken on the subject. As the developed system is comprised of two major parts, the following two chapters focus on the design, manufacturing and analysis of these two parts of the system. This is followed by system assembly, integration on a high-speed rotation setup and analysing the results. With the system developed being multi-functional and one of its functions providing a platform for investigation of the sensors and the influential factors affecting them, the following chapter also includes a series of tests and experiments discussing results and findings.

6.2 Future Work Considerations

There were several tests and experiments that could not be conducted due to the apparatus and testing equipment not being available within the timeline. As an essential simulation for the sensor's environment within a vehicle, the vibration effect is one of the critical tests. Using electro-dynamic shakers, exposing the sensor and the system to random and sinusoidal vibrations through a brief program would give valuable information regarding the effects of a vehicle environment. One of the functions of the designed system is to study and investigate the effect of different influential factors on various sensor and sensing system types used for RPM measurements. These investigations are among an area of opportunity for future work.

Other than the tests, several different designs were prepared. Integration of the hybrid system, use of other methods for sensing, and improved unique and novel designs were developed, which provide substantial opportunities for future work. A design with dentation and onboard light sourcing for an optical encoding system is shown in Figure 6.2.
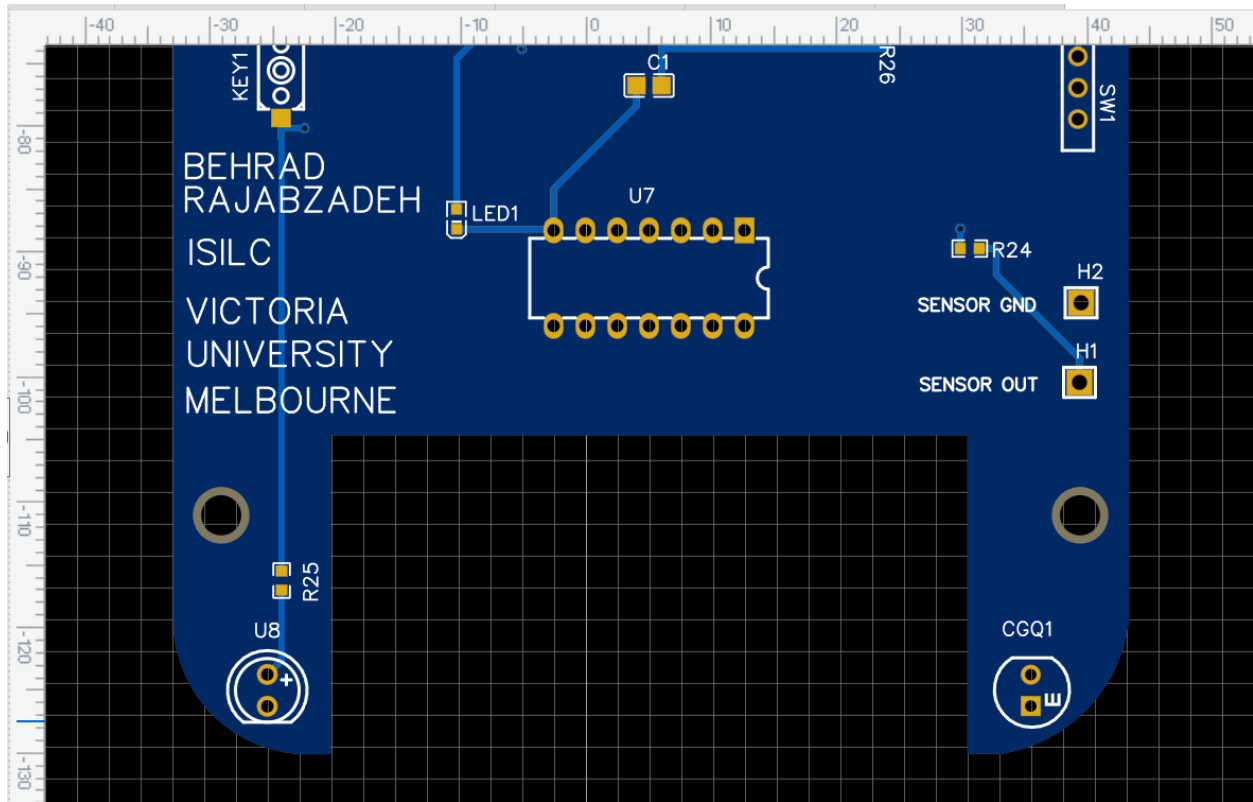
Figure 6.2. A circuit design indicating a dented circuit with the possibility of integration of the encoder component and on-board light source for optic-based RPM measurement.

There are various techniques and sensing systems that can be used in the designed system for exposure detection on encoding, such as ultrasonic and induction mechanisms.

6.2.1 Modulated IR Coupling

The other area for future work would be the modulation of the optical beams and the benefits it provides. These systems work based on two different mechanisms:

- RPM measurement based on detecting the frequency of interruptions in a continuous light beam. A steady, non-modulated light source shines through an encoder disk, and the receiver detects the periodic interruptions caused by the disk's rotation. The frequency of these interruptions corresponds to the rotational speed (RPM).
- Electronically modulating the optical transmitter and receiver on a fixed frequency for the elimination of similar wavelength interference.

The second method is vastly used recently. A use of this includes proximity sensing systems. Figure 6.3 shows a system of this type used on an Apple AirPod 4.

Figure 6.3. The proximity sensing system based on reflecting a modulated IR signal to detect if the Airpod 4 is worn by the user. The Activated IR beam is visible on the bottom right-hand corner of the black oval shape.

Although these systems can also be affected by interference, high reliability can be achieved by setting the right frequency on which the device works (transmitting and detecting). A temporary unit working on the same principle was assembled on a breadboard for this project to observe the behavior of the system. To implement the mentioned method, a 555 IC was utilized for modulation of the transmitted IR signal and a LM567 IC was used to decode and detect the frequency of the transmitted IR beam as shown in Figure 6.4.
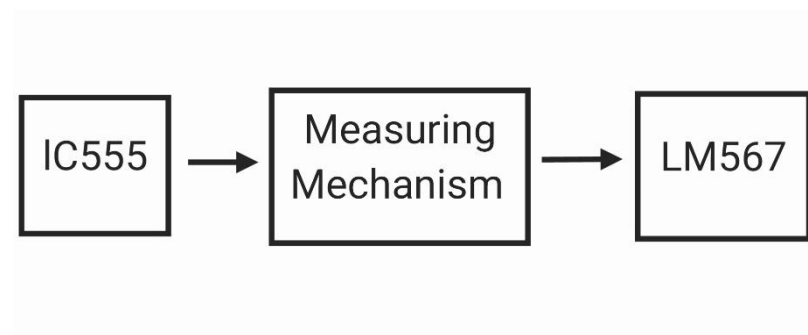

Figure 6.4. The diagram of the working principle of the test unit assembled on the breadboard.

The frequency of the ICs is determined by the external components connected to them. This is much more delicate on LM567, with much uncertainty for many frequency ranges. The assembled unit was designed with calculated values to work on 50Hz. As an unprecedented event, the flickering frequency of the lights used in the Lab was also 50Hz, interfering with the function of the test unit. This alone shows that even with precise limitation of the system frequency, there are still chances for interference. The assembled circuit on the breadboard is shown in Figure 6.5.
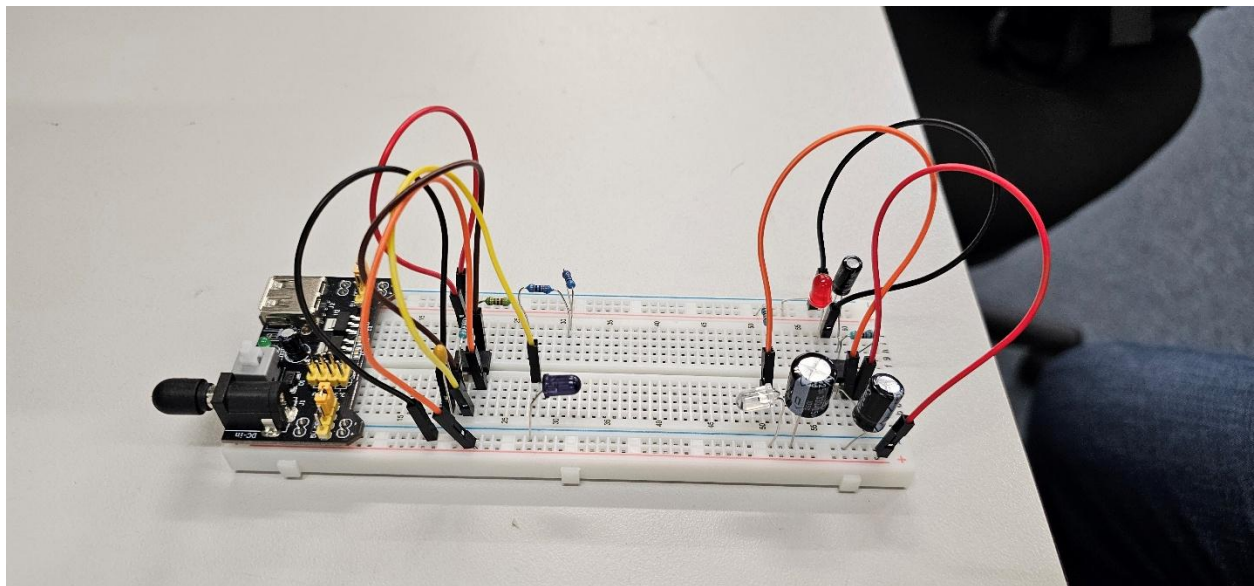
Figure 6.5. The assembled unit working on a 50Hz frequency signal.

It is worth noting that to achieve the desired result on setting the frequency as precisely as needed, a range of temperature-coherent resistors and capacitors were used on the assembly.

The calculations of the frequency coupling on the LM567, which is a commercial tone decoder, are extremely unpredictable and should not be relied on. Thus, practical testing is required to ensure functionality. The calculations used among the values for coupling this system are included briefly on the next page.

The two modulation-based mechanisms used for RPM measurement on encoders are major areas of future work.

For 555 IC:

$$f = \frac{1.44}{(R_1 + 2 \cdot R_2) \cdot C} \tag{6.1}$$

Values close to R1=88kΩ, R2=100 kΩ, C=100 nF would result in a frequency close to 50Hz as follows:

$$f = \frac{1.44}{(88{,}000 + 2 \cdot 100{,}000) \cdot 100 \times 10^{-9}} = 50 \text{ Hz}$$

For LM567:

$$f = \frac{1}{1.1 \cdot R_1 \cdot C_1} \tag{6.2}$$

With component values close to R1=12kΩ, C1=1.5µF and C2=100uF (Not involved but important) would result in a frequency close to 50Hz as follows:

$$f = \frac{1}{1.1 \cdot 12{,}000 \cdot 1.5 \times 10^{-6}} = \frac{1}{0.0198} \approx 50.5 \text{ Hz}$$

This combination would also result in a narrow and accurate bandwidth of approximately 6.7%, equivalent to 3,401 Hz in this configuration.

6.2.2 Mechanical Behavior of the Encoder Disks

As the last suggestion for future work, it is worth mentioning that in complex RPM encoder systems, the encoder disk becomes of great importance. In the hybrid encoder disks, such as those in this project, this importance becomes utmost. It is imperative to study the mechanical behaviors of the encoder disk and assess its impact on the applications and implementation. These studies can be done from different aspects, and one of them can be accomplished by utilizing a load cell

sensor in the rotating setup. Figure 6.6 shows an S-Type Load Cell Scale Sensor utilized in the system integration of the high-speed setup discussed in chapter 5.1. Unfortunately, there was not enough time to study the data generated by this S-Type Load Cell Scale Sensor for the hybrid encoder disks of this study. For future studies, however, an application-specific sensor with suitable sensitivity would be recommended, since the one used in the setup here was not chosen nor reviewed properly, as it was already available within the lab and utilized previously for a different project.

Figure 6.6. The S-Type Load Cell Scale Sensor installed in line with the hybrid Validist Encoder disk.

Such sensors will enable us to illustrate, record and study the mechanical behaviors of the encoder disks in practice, which are more practical compared to the simulations done by computer, such as the Ansys mechanical analysis done in chapter 4.3 of this thesis.

If he doesn't find himself immersed in the sea, to every wave he hangs a side he will see. Embrace Love.

Best,
Behrad Rajabzadeh, 18/09/2025

References

[1]   J. W. Creswell, *A concise introduction to mixed methods research*. SAGE publications, 2021.

[2]   J. S. Wilson, *Sensor technology handbook*. Elsevier, 2004.

[3]   Honeywell, "Hall Effect Sensing and Application."

[4]   R. M. Ramli, N. Mikami, and H. Takahashi, "Adaptive filters for rotational speed estimation of a sensorless DC motor with brushes," in *10th International Conference on Information Science, Signal Processing and their Applications (ISSPA 2010)*, 2010: IEEE, pp. 562-565.

[5]   D. Nemec, A. Janota, M. Hruboš, and V. Šimák, "Design of an electronic odometer for DC motors," *Transportation Research Procedia,* vol. 40, pp. 405-412, 2019.

[6]   E. Agamloh, A. Von Jouanne, and A. Yokochi, "An overview of electric machine trends in modern electric vehicles," *Machines,* vol. 8, no. 2, p. 20, 2020.

[7]   A. Ghayth and M. Şimşir, "Recent trends and challenges of electric motor technologies," *Int. J. Electr. Eng. and Sustain.,* pp. 21-28, 2023.

[8]   D. Rapos, C. Mechefske, and M. Timusk, "Dynamic sensor calibration: A comparative study of a Hall effect sensor and an incremental encoder for measuring shaft rotational position," in *2016 IEEE International Conference on Prognostics and Health Management (ICPHM)*, 2016: IEEE, pp. 1-5.

[9]   M. Taylor, "Gear fault detection using non-contact magnetic rotation position sensors," Queen's University, 2010.

[10]   L. Uniroyal Electronics Global Co., "Thick Film Chip Resistors." [Online]. Available: https://jlcpcb.com/partdetail/C25804

[11]   Texas Instruments, "CD4093BE." [Online]. Available: https://www.ti.com/lit/ds/symlink/cd4093b.pdf?ts=1738652234008&ref_url=https%253A%252F%252Fwww.google.com%252F

[12]   Maxell, "CR2032H Coin Type Lithium Manganese Dioxide Battery Data Sheet."

[13]   T. Yuden, "Multilayer Ceramic Capacitors JMK212BBJ107MG-TE." [Online]. Available: https://ds.yuden.co.jp/TYCOMPAS/ut/detail?pn=MSASJ21GBB5107MTCA01&u=M

[14]   LOTES, "Battery holder CR2032 SMD AAA-BAT-054-P06."

[15]   K. Hroparts, "TOGGLE SWITCH K3-1204D." [Online]. Available: https://en.krhro.com/Product-Details/247.html

[16]   K. Hroparts, "Tactile Switch K2-1107ST." [Online]. Available: https://en.krhro.com/Product-Details/80.html

[17]   Texas Instruments, "CD4011B."

[18]   TUOZHAN, "SMD LED TZ-P2-0805RTCS2-0.8T."

[19]   Texas Instruments, "DRV5023 Digital-Switch Hall Effect Sensor." [Online]. Available: https://www.ti.com/product/DRV5023/part-details/DRV5023AJQLPG

This page is intentionally left blank